Investigation of Actin-MRTF-A protein complexes in fibroblasts

Dissertation

for obtaining the academic degree

Doktor der Medizinischen Wissenschaften (Dr. rer. medic.)

for the subject area of “Molecular Medicine”

Submitted

to the Medical Faculty

at the Martin Luther University Halle-Wittenberg

von Marina Abd el Malek

Betreuer: Prof. Dr. Guido Posern

Gutachter:innen:

Prof. Dr. rer. nat. Stefan Hüttelmaier

Prof. Dr. rer. nat. Fred Schaper

Date of defense: 16.04.2024

PRESENTATION/SUMMARY

Fibrosis is a pathological condition which can occur after surgery or tissue damage due to the deregulation of the physiological function of fibroblasts. The myocardin-related transcription factor A (MRTF-A) is involved in the regulation of fibroblast proliferation, maturation, and protein expression during tissue regeneration. For this reason, different types of fibrosis have been linked to MRTF-A dysfunction. MRTF-A is activated upon release from an inhibitory complex with monomeric actin, but the events which lead to this dissociation are not fully understood. The aim of this work is to elucidate these molecular events in NIH 3T3 fibroblasts via different techniques. Using immunoprecipitation and mass spectrometry, Cobll1, Radil, Samhd1 and Ube3a were identified as possible MRTF-A competitors for actin binding. Further verification of their ability to influence MRTF-A during stimulation was tested by creating different knockdowns for each candidate and a quadruple knockdown for a possible synergistic effect. Although it was possible to obtain the knockdown for all candidates (with the exception of Radil), normal MRTF-A dissociation from actin was observed. Furthermore, the analysis of the spatio-temporal interaction dynamics between actin and the intrinsically disordered RPEL motifs of MRTF-A in the cytosol was investigated. In order to reach this goal, a newly developed FRET sensor containing the RPEL2 motif and the non-polymerizable mutant actin R62D was created to visualize events leading to actin-MRTF-A dissociation. Interaction dynamics of the complex were followed after serum addition and the influence of different modulators of MRTF activity was analysed. The FRET between RPEL and R62D actin decreased when cells were treated with serum and Cytocalasin D, whereas Latrunculin B increased FRET, consistent with their differential effect on MRTF-mediated transcription. Moreover, the inhibition of ROCK and the overexpression of a WH2

region, an RPEL competitor candidate, inhibited the normal FRET reduction after serum addition. By contrast, the MRTF inhibitor CCG-203971 did not impact the RPEL2-R62D dissociation, suggesting an inhibitory function outside the RPEL motif. In conclusion, our FRET sensor demonstrates that dissociation of the G-actin:RPEL complex can occur independently of actin polymerization and suggests the existence of as yet unidentified factors which repress the actin:MRTF complex upon signalling.

Abd el Malek, Marina: Investigation of Actin-MRTF-A protein complexes in fibroblasts, Halle (Saale), Univ., Med. Fak.; Diss., 79 pages, 2023

REFERAT/ZUSAMMENFASSUNG

Fibrose ist ein pathologischer Zustand, der nach chirurgischen Eingriffen oder Gewebeschäden aufgrund der Deregulierung physiologischer Funktionen von Fibroblasten auftreten kann. Der Myocardin-verwandte Transkriptionsfaktor A (MRTF-A) ist an der Regulierung der Proliferation, Reifung und Proteinexpression von Fibroblasten während der Geweberegeneration beteiligt. Aus diesem Grund wurden verschiedene Arten von Fibrose mit einer MRTF-A-Dysfunktion in Verbindung gebracht. MRTF-A wird aktiviert, wenn es aus einem Hemmkomplex mit monomerem Aktin freigesetzt wird. Die Ereignisse die zu dieser Dissoziation führen, sind nicht vollständig geklärt. Ziel dieser Arbeit ist es, diese molekularen Vorgänge in NIH 3T3-Fibroblasten mit verschiedenen Techniken aufzuklären. Mittels Immunpräzipitation und Massenspektrometrie wurden Cobll1, Radil, Samhd1 und Ube3a als mögliche MRTF-A-Konkurrenten für die Aktinbindung identifiziert. Zur weiteren Überprüfung ihrer Fähigkeit, MRTF-A während der Stimulation zu beeinflussen, wurden verschiedene Knockdowns für jeden Kandidaten und ein Vierfach-Knockdown für einen möglichen synergistischen Effekt durchgeführt. Obwohl es möglich war, den Knockdown für alle Kandidaten (mit Ausnahme von Radil) zu erreichen, wurde eine normale Dissoziation von MRTF-A von Aktin beobachtet. Darüber hinaus wurde die Analyse der räumlich-zeitlichen Interaktionsdynamik zwischen Aktin und den intrinsisch ungeordneten RPEL-Motiven von MRTF-A im Zytosol untersucht.

Um dieses Ziel zu erreichen, wurde ein neu entwickelter FRET-Sensor entwickelt, der das RPEL2-Motiv und die nicht polymerisierbare Aktin-Mutante R62D enthält, um Ereignisse sichtbar zu machen, die zur Dissoziation von Aktin und MRTF-A führen. Die Interaktionsdynamik des Komplexes wurde nach Zugabe von Serum verfolgt und der Einfluss verschiedener Modulatoren der MRTF-Aktivität wurde analysiert. Das FRET Signal zwischen RPEL und R62D-Actin verringerte sich, wenn die Zellen mit Serum und Cytocalasin D behandelt wurden, während Latrunculin B das FRET Signal erhöhte, was mit ihrer unterschiedlichen Wirkung auf die MRTF-vermittelte Transkription übereinstimmt. Darüber hinaus bewirkte die Hemmung von ROCK und die Überexpression einer WH2-Region, eines RPEL-Konkurrenten, die normale FRET-Reduktion nach Serumzugabe. Im Gegensatz dazu hatte der MRTF-Inhibitor CCG-203971 keinen Einfluss auf die RPEL2-R62D-Dissoziation, was auf eine hemmende Funktion außerhalb des RPEL-Motivs schließen lässt. Zusammenfassend zeigt unser FRET-Sensor, dass die Dissoziation des G-Actin:RPEL-Komplexes unabhängig von der Aktinpolymerisation erfolgen kann und deutet auf die Existenz noch nicht identifizierter Faktoren hin, die den Actin:MRTF-Komplex bei der Signalgebung unterdrücken.

Table of content

List of Figures

List of Tables

List of abbreviations

5-FU	5-fluorouracil
ABPs	Actin binding proteins
ADH1	Alcohol Dehydrogenase
APS	Ammonium persulfate
ARVC	Arrhythmogenic right ventricular cardiomyopathy
B1	Basic region 1
B2	Basic region 2
BiFC	Bimolecular fluorescence complementation
BSA	Albumin fraction from bovine serum
Cobll1	Cordon-bleu protein-like 1
Co-IP	Co-immunoprecipitatio
Cyt D	Cytochalasin D
DDM	n-Dodecyl β-maltoside
DMEM	Dulbecco's modified Eagle medium
DMSO	Dimethyl sulfoxide
DOC	Sodium Deoxycholate
Dox	Doxycyclin
ECL	Enhanced chemiluminescence
ECM	Extracellular matrix
EDTA	Ethylene-diamine-tetra-acetic acid
Em.	Emission wavelength
EV	Empty vector
Ex.	Excitation wavelength
FAK	Focal adhesion kinase
FASP	Filter-aided sample preparation
FBS	Fetal Bovine Serum
FDR	False discovery rate
FLIM	Fluorescence-lifetime imaging microscopy
FRET	Förster resonance energy transfer or Fluorescence resonance energy transfer
GBD	GTPase binding domain
HEPES	4-(2-Hydroxyethyl)piperazine-1-ethanesulfonic acid
HSC	Hepatic stellate cells
IAA	Iodoacetamide

IEG	Immediate-early genes
JMY	Junction mediating and regulatory protein
KCl	Potassium chloride
KH_2PO_4	Monopotassium phosphate
L9Hx3	Ribosomal protein-based linker
Lat B	Latrunculin B
LFQ	label-free quantitation
LZ	Leucine-zipper
MAPK	Mitogen-activated protein kinase
MMC	Mitomycin-C
MS	Mass spectrometry
NA	Sodium acetate
Na_2HPO_4	Sodium phosphate dibasic
NaCl	Sodium chloride
NLS	Nuclear Localization Signal
PASEF	Parallel accumulation serial fragmentation
PCR	Polymerase chain reaction
PIP2	Phosphatidylinositol 4,5-bisphosphate
PPI	Protein-protein interaction
PTM	Post-translational Modifications
Q	Glutamine-rich region
R62D	Non-polymerizable G-actin mutant with a point mutation in position 62
Radil	Ras-associating and dilute domain-containing protein
ROCKs	Rho-associated protein kinases
RPEL2(P133A)	RPEL2 sequence with point mutation in position 133
RPxxxEL	Arginine-proline-X-X-glutamic acid-leucine
rSAP	Shrimp alkaline phosphatase
Samhd1	Deoxynucleoside triphosphate triphosphohydrolase
SAP	SAF-A/B, acinus, PIAS
SDS	Sodium dodecyl sulfate
siRNAs	Small interfering RNAs
SMCs	Smooth muscle cells
SRF	Serum responsive Factor
TAD	Transcriptional activation domain

TCF	Ternary complex factors
TCSPC	Time correlated single photon counting
TEMED	N,N,N,N-Tetra-methyl-ethylene-diamine
TFA	Trifluoroacetic acid
TMT	Tandem mass tag
TCEP	Tris (2-carboxyethyl)phosphine
Ube3a	Ubiquitin-protein ligase E3A
VCA	Verprolin; central, acidic domain
WB	Western blot
WH2	WASP-Homology 2, or Wiskott-Aldrich homology 2
WT	Wild type
λ	Half-life
τ	Fluorescence lifetime

1. Introduction

1.1. The family of MRTF transcription coactivators

1.1.1. MRTF regulation by actin-mediated signalling

All living organisms including their cells, need to be able to adapt to the surrounding environment. Different cellular processes must be regulated in both time and space for this to occur. This can be achieved by tight regulation of protein expression or Post-translational Modifications (PTM) specific to the cellular functions. Thus, cells must be able to receive, transduce and respond to different stimuli. One of the most important features that the cell has to regulate is the structure of the cytoskeleton. Actin is the main protein of the cytoskeleton. It is, also, one of the most abundant proteins inside cells and plays essential roles for cell shape, adhesion, migration and transcription. The pathways regulating these cellular processes require interaction with many different actin binding proteins (ABPs). Among the ABPs, the myocardin related transcription factors (MRTF-A and B) are involved in the regulation of gene expression in response to many different stimulations.

In order to control its transcriptional activity, MRTF shuttles between the cytosol and the nucleus, going from its inactive to its active state (Fig. 1). Specifically, MRTF is kept inactive in the cytosol as a result of its binding to actin monomers. When a signal is received by the cell, the Rho-GTPase signaling pathway is activated and induces the dissociation of MRTF-A from actin, whilst actin polymerizes to form actin filaments. In the unbound state, the free MRTF exposes its Nuclear Localization Signal (NLS) and is able to translocate into the nucleus via the binding to importin α/β (Pawlowski et al. 2010). Once inside the nucleus, MRTF binds to the Serum responsive Factor (SRF), which then induces gene transcription. Moreover, actin binding to MRTF can relocate MRTF into the cytosol via Crm1 (Vartiainen et al. 2007).

SRF can also be activated by binding to another class of co-transcription factor, the ternary complex factors (TCF) to which belong Elk-1, Net and Sap-1. This second class of co-transcription factors are activated via the mitogen-activated protein kinase (MAPK) signalling pathway. Thus, after binding to either MRTF or the TCF, SRF binds to a specific DNA motif, the $CC(A/T)_6GG$ sequences called the CArG box (Taylor et al. 1989; Treisman 1986). The CArG box has been demonstrated to be present and responsible for the transcription of two different classes of genes: the immediate-early genes (IEG) and cytoskeletal related genes. Their expression regulates cell growth and cell migration or adhesion. These two cellular functions are regulated by TCF or MRTF activation, respectively, although some regulated genes have been shown to be regulated by both co-transcription factors (Knoll 2011; Gualdrini et al. 2016).

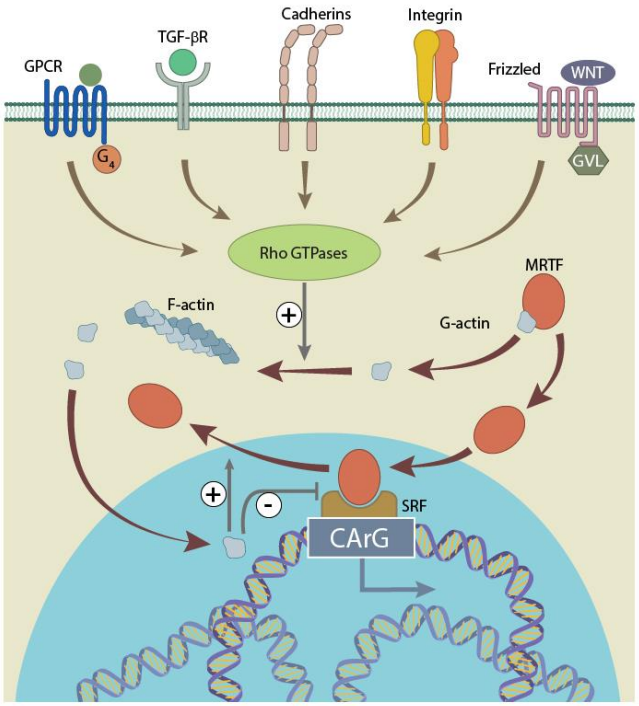

Figure 1: Schematic overview of regulation of Myocardin related transcription factors (MRTFs). MRTFs are kept in their inactive state via the interaction with monomeric actin. Upon stimulation, Rho-dependent pathways induce its dissociation from actin and thereby activates MRTF-dependent transcription in the nucleus (adapted from Olson & Nordheim, Nature Rev. Mol. Cell. Biol. 2010).

1.1.2.Domain structure of MRTF-A

MRTF is formed by different domains devoted to the binding of different protein partners for their regulation. On the N-terminus, MRTF-A presents an intrinsically disordered region, called the RPEL region, involved in the binding to G-actin (Fig. 2).

The RPEL region is formed by three RPEL motifs and two spacers between RPEL1/PREL2 and RPEL2/RPEL 3; each of these sequences can bind one monomeric actin, thus forming a final pentameric actin-RPEL complex (Fig. 2A) (Mouilleron et al. 2011). The RPEL sequences are characterized by the conserved motif arginine-proline-X-X-glutamic acid-leucine (RPxxxEL), except for RPEL1, which has a non-canonical RPEL sequence with RR instead of RP. In this complex, the monomeric actins present a different orientation compared to the actins present in the filaments, thus avoiding the binding of other actins to the MRTF-actin complex. Moreover, the G-actin binding keeps MRTF in the cytosol and prevents its activation by covering the NLS (B2 and B3). It was demonstrated that if the RPEL region is deleted, MRTF loses its ability to bind to actin and it is constitutively active in the nucleus (Miralles et al. 2003). Due to its intrinsically disordered feature, the structure of RPEL region was solved only after actin binding (Fig. 2B). The study of the crystal structures of actin with other ABPs has demonstrated the same mode of actin binding by WH2 (WASP-Homology 2, or Wiskott-Aldrich homology 2) region as by RPEL

(Fig. 2C) (Mouilleron et al. 2008). The WH2 region, which is also intrinsically disordered, has already been shown to affect the RPEL:actin complex (Weissbach et al. 2016).

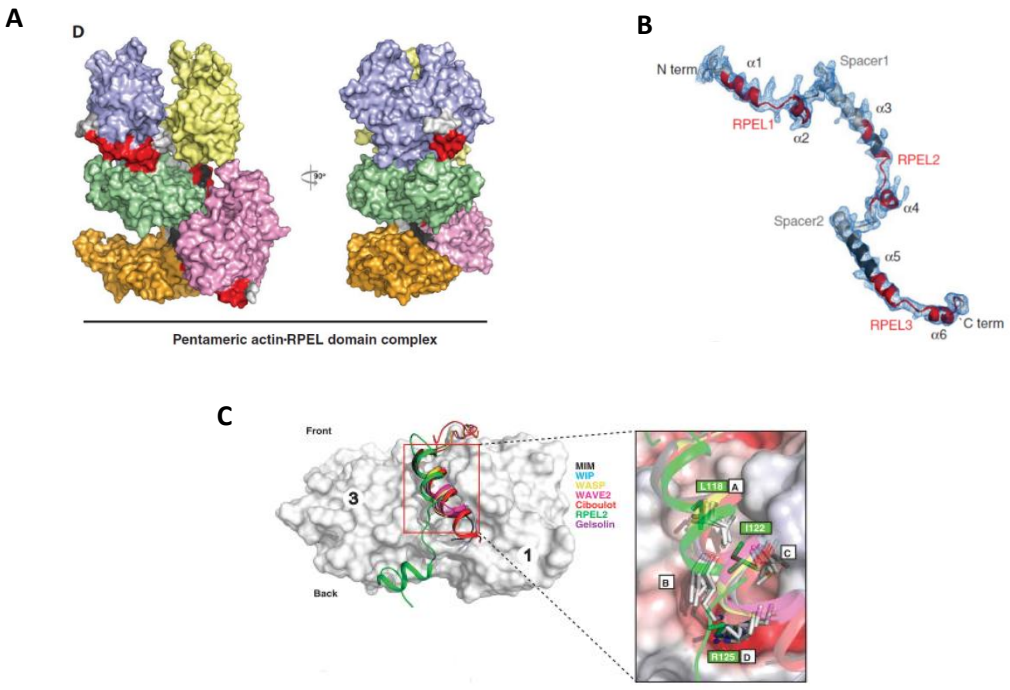

Figure 2: Structural analysis of RPEL:actin complex . A) Pentameric complex formed by five actin proteins binding to a single RPEL motif and the spacers. The different actins are indicated in purple, yellow, green, orange and pink; the RPEL sequences are indicated in red and the spacers of the RPEL motif in black. B) Isolated crystal structure of RPEL motif obtained from RPEL:actin pentameric complex. C) Comparison of different ABPs bound to the hydrophobic cleft of actin. Figures taken from Mouilleron (Mouilleron et al. 2011; Mouilleron et al. 2008).

Following the RPEL motif, an additional basic region (B1) exists, which is not only involved in nuclear translocation, but it is mainly involved in the SRF binding together with the glutamine-rich region (Q). The function of the successive SAP (SAF-A/B, acinus, PIAS) motif is still unclear. The hypothesis is that it is involved in DNA binding or that it allows MRTF-dependent gene transcription independently of SRF (Reed et al. 2021). Subsequently, MRTF homo- and heterodimerization occurs via the leucine-zipper (LZ) domain (Reed et al. 2021). Lastly, in the C-terminus MRTF displays a transcriptional activation domain (TAD) which activates the transcription of genes.

MRTF is expressed in two different isoforms, A and B. Experiments on mice have demonstrated that MRTF A and B expression is time-regulated. In fact, MRTFA knockout mice showed a normal development, but female mice were not able to breast feed the pups due to an abnormal acini formation in the mammary glands (Li et al. 2006). Yet, a MRTFB knockout causes embryonic lethality due to impairments in the development of cardiovascular organs (Wei et al. 2007). Both

MRTF-A and B are part of the myocardin family, to which myocardin and OTT-MAL proteins also belong (Fig. 3). All of the myocardin family members share the same domains with a very high sequence similarity. This allows to coordinate the function of myocardins proteins in time, and the different sequences guarantees a specific function in the cell or in different tissue.

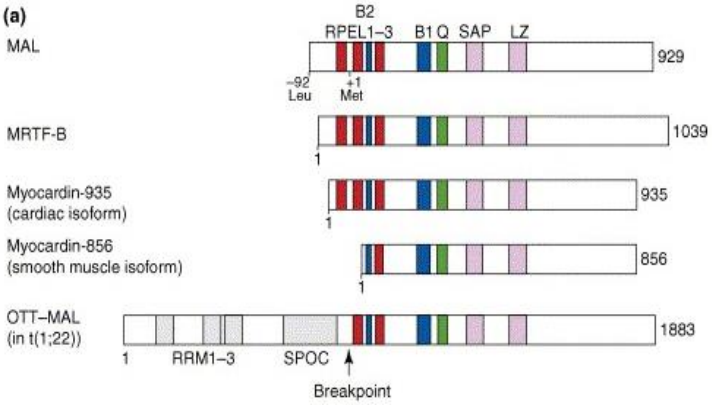

Figure 3: Scheme of distribution of myocardin family protein domains from N- to C-terminus. In red are indicated the RPEL sequences, in blue the basic regions (B1 and B2), in green the glutamine-rich region (Q) and in pink the SAP (SAF-A/B, acinus, PIAS) and leucine-zipper (LZ) domains. Figure taken from Posern (Posern and Treisman 2006).

1.1.3.MRTF activation and repression

MRTF is an important checkpoint of the cells, since many different mechano-chemical stimuli and many different compounds can activate or inhibit MRTF (Fig. 4).

The actin status is the main MRTF regulator. It has been demonstrated that an increased amount of cytoplasmic G-actin inhibits MRTF translocation (Posern et al. 2004). This was achieved through either an overexpression of a non-polymerizable actin mutant, by inhibiting the Rho pathway, or by the addition of drugs, such as Latrunculin B (Lat B) (Fig.5) (Gau and Roy 2018; Wakatsuki et al. 2001). By contrast, the addition of Cytochalasin D (Cyt D) inhibits actin polymerization and simultaneously activates MRTF (Wakatsuki et al. 2001). Increased amount of F-actin can be also achieved via mechanical stresses when the matrix stiffness increases. This pathological condition has severe consequences, since cells are not able to maturate and to respond to any further mechanical stimulus in this condition (Reed et al. 2021).

Due to regulation of MRTF by nuclear actin, different factors, which control nuclear actin polymerization status, also affect and regulate MRTF transcriptional activity. For example, Filamin A, which induces actin polymerization, has been demonstrated to activate MRTF transcriptional activity (Kircher et al. 2015).

As a part of MRTF regulation by actin, other factors can influence MRTF transcriptional activity. Phosphorylation has been proven to influence both positively and negatively MRTF-actin binding

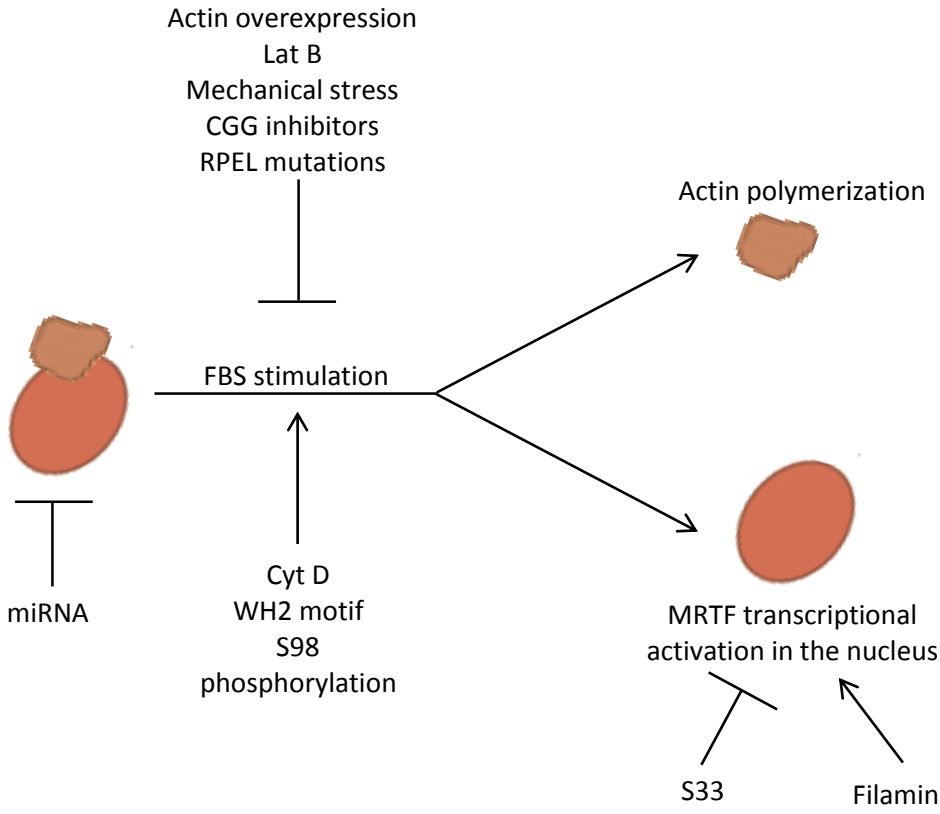

Figure 4: MRTF regulating factors during cellular development. Upstream, MRTF activity can be blocked by reducing its protein expression when specific miRNAs are expressed. A second level of MRTF activity control consists in its association-dissociation status from actin in the cytosol. Here different factors can inhibit its dissociation, such as actin overexpression, Lat B, mechanical stresses given by the environment, CGG inhibitors or by introduction of point mutations in the RPEL sequences. On the other hand, MRTF dissociation can be induced by Cyt D or by overexpression of WH2 containing proteins, and can be prevented by phosphorylating Ser98 of MRTF. Finally, MRTF transcriptional activity in the nucleus can be prevented by Ser33 phosphorylation, inducing MRTF export, or induced via Filamin overexpression.

and transcriptional activity (Panayiotou et al. 2016). Additionally, MRTF activity can be regulated in time by regulating its expression. One way of regulating MRTF abundance is by expressing miRNA (Holstein et al. 2020). In this case, expression of specific inhibitory miRNAs reduces MRTF protein abundance, allowing the differentiation of myotubes.

As described above, modulation of RPEL:actin interaction is essential for MRTF activity. Mutation in the conserved motif (RP-xxx-EL) of the prolin to an alanine, or of the arginine to an aspartic acid in each RPEL sequence, has been demonstrated to prevent binding to actin (Miralles et al. 2003). These mutants have shown a constitutive nuclear localization and the same results were achieved if the entire RPEL motif was deleted. Additionally, RPEL:actin interaction can also be impaired by competition with the WH2 domain, which has been proven in fibroblasts (Weissbach et al. 2016). Indeed, the expression of different WH2 domains from different actin nucleation-promoting factors, such as N-WASP and WAVE2, induced an increased MRTF-SRF

luciferase activity compared to the control. Moreover, the overexpression of N-WASP and WAPE2 induced a nuclear relocalization of the endogenous MRTF.

New novels MRTF inhibitors have been recently identified. For example, several CCG compounds have been recently developed for MRTF/SRF transcription pathway inhibition, but for many of them, the exact mechanism is still unknown or speculated.

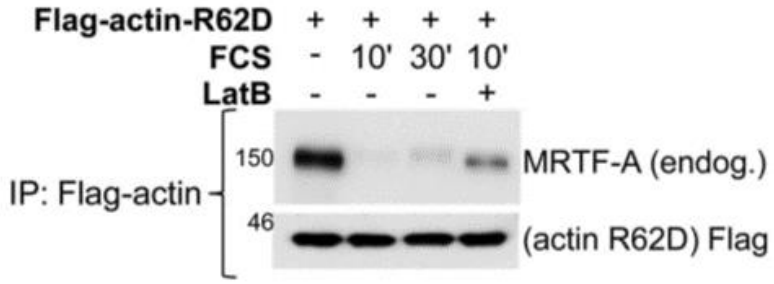

Figure 5: Analysis of MRTF dissociation after stimulation. Endogenous MRTF-A after immunoprecipitation detected with western blot in NIH 3T3 expressing Flag-R62D actin. Addition of FBS to the samples induce MRTF dissociation from actin after 10 minutes, with a slow recovery after 30 minutes. Addition of 5 µM Lat B partially inhibits MRTF dissociation. Figure taken from Weissbach (Weissbach et al. 2016).

1.1.4.Medical impact

Although MRTF has an important physiological role, its de-regulation can lead to a pathological condition. MRTF regulates the expression of many cytoskeletal and extracellular matrix (ECM) proteins, some of which are also implicated in fibrosis. In fact, it is well known that MRTF deregulation induces and is involved in fibrosis after injury or surgery in many different organs. In this scenario, MRTF transcriptional activation induces fibroblasts proliferation and maturation into myoblasts and induces the expression of different connective tissue proteins (Crider et al. 2011). The accumulation of both fibroblasts and connective tissue in the injured area causes fibrosis, which can lead to organ failure (Wynn 2008; Velasquez et al. 2013).

An occurrence of fibrosis in the eye can lead to vision loss. Cytotoxic antimetabolites mitomycin-C (MMC) and 5-fluorouracil (5-FU) (Yu-Wai-Man et al. 2017) are currently used as clinical treatments. Unfortunately, both MMC and 5-FU have many side effects due to their unspecificity, which leads to an increasing need for new treatments targeting fibroblast migration and maturation controlled by MRTF activity.

MRTF activity has been demonstrated to play a major role in kidney fibrosis, but its mechanism is still not fully understood, with many studies still ongoing (Miranda et al. 2021).

The liver is another important organ where fibrosis is induced by MRTF (Al-Hetty et al. 2022). In this case, it has been demonstrated that MRTF is crucial for the transdifferentiation of hepatic stellate cells (HSC) into myofibroblast-like cells (Fig. 6) (Shimada et al. 2010).

Moreover, MRTF function has been associated with other diseases, such as tumour metastasis (Minton 2021), arrhythmogenic right ventricular cardiomyopathy (ARVC) (Dorn et al. 2018) and many others (Ito et al. 2020; An et al. 2019).

Given the central role of MRTF in many different pathological scenarios, many *in vivo* and *in vitro* models have been developed for the analysis of MRTF function. Different knockdown and knockin mice have been obtained and analysed. For example, in MRTF-A null mice a reduced fibrosis after treatment with Angiotensin or myocardial infarction was observed (Small et al. 2010; Rejmontova et al. 2016). NIH 3T3 mouse fibroblasts have been widely used as an *in vitro* model not only for the study of fibrosis event, but also for proliferation, adhesion and migration studies (Rejmontova et al. 2016). Double knockdown of MRTF A and B in NIH 3T3 cells has shown to influence normal cell cycle control (Shaposhnikov et al. 2013).

Thanks to the establishment of these different MRTF triggered diseases, it is possible not only to perform MRTF studies *in vitro* and *in vivo*, but also to identify novel MRTF inhibitors for the disease treatment. The recently developed MRTF inhibitors CCG-1423, CCG-222740 and CCG-203971 have been proven to reduce both the expression of pro-fibrotic genes and scar formation in *in vitro* and *in vivo* experiments in all the organs mentioned above. Although they have a promising fibrosis inhibition effect, their mechanism of action is still not well understood. Consequently, many efforts have been undertaken to elucidate their mechanism of action in the hope of producing a possible alternative therapy.

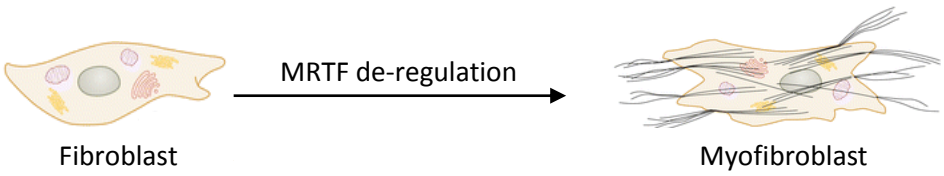

Figure 6: MRTF function in fibroblasts. MRTF activation is a crucial step for fibrosis progression. Different growth factors and mechanical tension present in the environment induce activation of MRTF via the Rho GTPases pathway. This, in turn, induces expression of smooth muscle cells (SMCs), fibrosis and collagen genes. Figure adapted from (Small 2012).

1.2. Mass spectrometry

Over time, different techniques have been developed and employed for the study of protein structure and protein identification. Mass spectrometry is one of the most widely used techniques for deep analysis of the proteome, the identification of new protein-protein interactions and stoichiometric studies. Many different mass spectrometers have been developed, but they work on the same principle where molecules are identified based on their mass to charge ratio. Mass spectrometers are formed by three main parts: an ionization source,

a mass analyser, and an ion detection system. Briefly, in the ionization source, molecules are vaporized and ionized, which allows molecules to separate based on their mass to charge ratio. This is accomplished by accelerating and deflecting the trajectory of molecules using an electric or magnetic field in the mass analyser, and subsequently identifying them using the detection system. The Orbitrap mass analyser utilizes the most recent technology, providing higher resolution and high mass accuracy (Fig. 7).

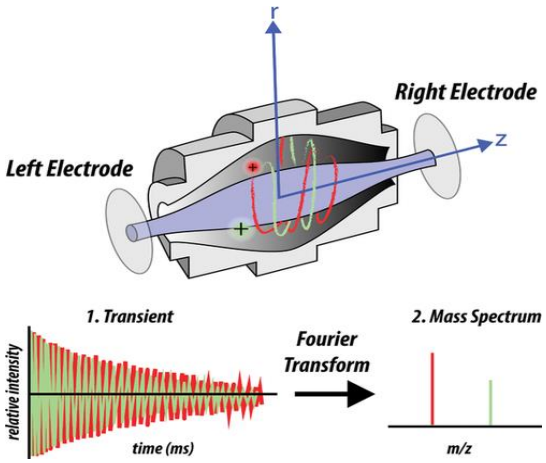

Figure 7: Orbitrap working principle. Selected ions are injected into the Orbitrap. Ions present different oscillation frequencies along the vertical and horizontal axes of the Orbitrap, which are due to different mass to charge ratios (m/z). In order to obtain a mass spectrum, the frequencies recorded in time are transformed using the Fourier Transformation. Picture taken from (Savaryn et al. 2016).

Mass spectrometry has been applied to analyse purified proteins and samples derived from cell culture and from tissues. Different labeling strategies have been established for comparing amounts of proteins derived from different samples applied to both *in vitro* and *in vivo* experiments. Labeling the samples allows the identification of possible new PTMs or different protein interactions. One labeling technique widely used is the tandem mass tag (TMT). The TMT labeling is a powerful tool to analyse 6 to 16 samples in a single MS mix (Fig. 8). This allows for a direct comparison of protein abundance between the different samples with reduced variability. Here, each sample is labeled with the same compound that have the same nominal mass, but different isotopes, which can be identified only after peptide fragmentation.

Label-free MS experiments are also widely performed, which present numerous advantages. They allow for a higher number of identified proteins and peptides in the sample (Patel et al. 2009). Moreover, sample preparation is less complicated and less expensive compared to labeling MS methods (Lai et al. 2013).

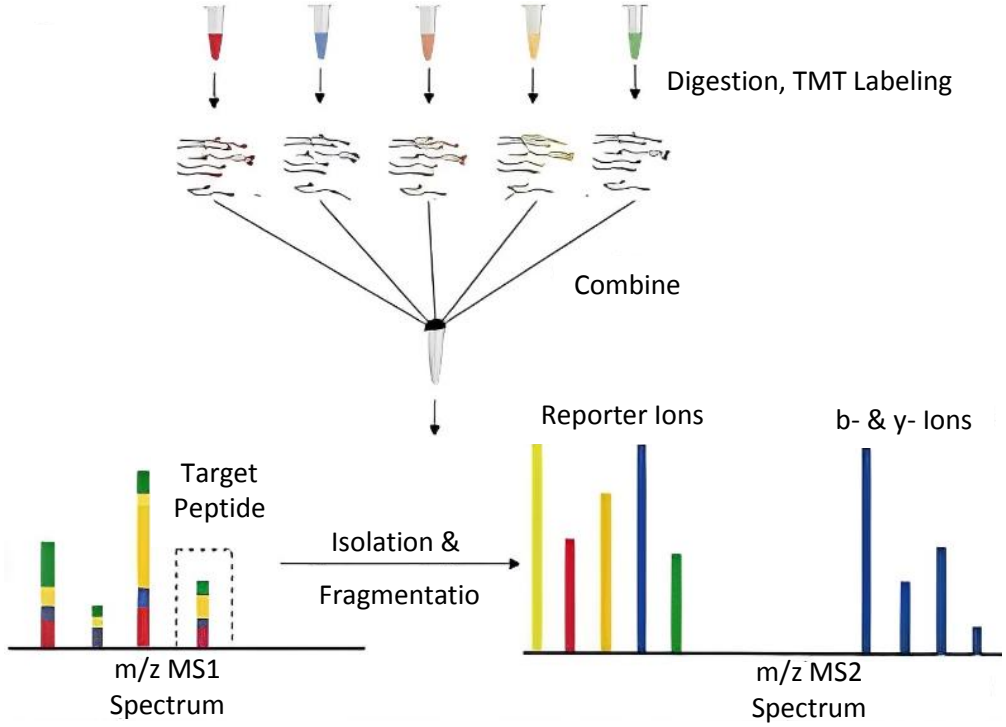

Figure 8: Scheme of TMT labeled sample analysis. Different isotopes of the same structure are used to label different samples and combined in a single sample. Inside the mass spectrometer, the peptides are separated and, subsequent to fragmentation, the amount of the reporter ions are obtained and linked to the amount of the peptide in the different samples. Figure taken from (Gupta et al. 2018).

1.3. FRET

One frequently used method to study protein-protein interactions is the analysis of Förster resonance energy transfer or Fluorescence resonance energy transfer (FRET). FRET is the physical non-radiative transfer of energy from an excited donor fluorophore to an acceptor fluorophore. For the occurrence of FRET, the fluorophores must fulfil certain requirements. First of all, donor and acceptor must be in close proximity. Thereby, the Förster radius defines the distance at which the donor is still able to transfer 50% of their energy to its acceptor. For fluorescent proteins, depending on the FRET pair, Förster radii can be around 5-6nm. Distances above >10nm vastly abolish FRET, rendering this method as a useful tool for studying interactions of biomolecules like proteins. Second, the emission spectrum of the donor has to overlap with the excitation spectrum of the acceptor. This is generally achieved by the selection of a suitable FRET pair, which gives rise to a spectral overlap of at least 30% (Fig. 9). Thus, it is possible to study the interaction dynamics of two proteins of interest when they are bound to the donor or the acceptor. FRET has also been used for a variety of protein studies, such as protein folding analysis where the folding of the protein of interest brings the two fluorophores in close proximity (Liu et al. 2020); and for proteolytic enzyme activity analysis, where

compartmentalization and influence (Zadran et al. 2012) on a protein are due to changes in the cellular environment (such as pH variation, calcium etc.) (Esposito et al. 2008; Mank et al. 2006). Compared to other protein interaction validation techniques like Bimolecular fluorescence complementation (BiFC), the interaction between the fluorophores in FRET technique is reversible. This makes it possible to analyse protein interaction in time and space, and in different conditions. Moreover, FRET technique gives the chance for in-depth analyses of the inhibitory or activation activity and of the influence of different compounds on a specific protein complex, as well as possible competition effects from other proteins. Many different fluorophores and many different biosensors have been developed (Bajar et al. 2016), each of which has been designed for the specific condition to be analysed and for the system used. As an important step of FRET sensor optimization, the donor and the acceptor fluorophore pairs have to be chosen so that the energy transfer is maximized and the fluorescent pair is suitable for the system in use. Lastly, the selection of the proper linker between the different counterparts inside the biosensor is crucial (Komatsu et al. 2011).

FRET causes several changes in the properties of the donor and acceptor fluorescence which allow it to be monitored via different FRET techniques (Broussard and Green 2017). On the one hand, in the presence of FRET, the donor fluorescence is largely reduced (donor quenching). This phenomenon can be used in acceptor photobleaching experiments to specifically detect FRET. On the other hand, during donor excitation, the acceptor emits light whose energy is a result of energy transfer (FRET), but not from its own excitation. This fluorescence emission of the acceptor is called sensitized emission and can also be used to measure FRET. This is achieved by either a ratiometric analysis for donor and acceptor fluorescence, or by a precise correction of the acceptor fluorescence to isolate the FRET-induced sensitised emission component. The FRET to donor ratio is obtained with the corresponding excitation and emission wavelength. The closer the acceptor is to the donor, the more donor emission decreases (donor quenching) and acceptor emission increases (sensitized emission). Consequently, an increased FRET to donor ratio is obtained. Since all the signals are measured, corrections for the bleed-through and for the background have to be performed before analysis. Although ratiometric FRET analysis is an easy technique, is used in a wide variety of systems, and allows the analysis of quick reactions in live-cell imaging, it has some disadvantages. Its major disadvantage is its sensitivity to protein concentration. This requires the calculation of the noise of the donor into the acceptor channel and vice versa. This phenomenon is called cross talk and can be obtained from samples expressing only the donor or only the acceptor. For this reason, the cross talk leads to a high

level of noise. This cross talk, however, can be corrected to isolate the pure sensitised emission (corrected FRET).

Another technique used to overcome the SE disadvantages is fluorescence lifetime imaging microscopy (FLIM). When the donor is excited, a photon is emitted upon return to its electronic ground state. However, not all donor molecules fall back to the ground state and emit photons at the same time, this rather represents an exponential decay process. The rate of relaxation determines the speed of the fluorescence decay, which can be expressed in a fluorophore characteristic value: the fluorescence lifetime (τ). τ is the time that the fluoresce decay needs to fall to the fraction of 1/e (~36.8%) of its initial fluorescence. Thereby, τ is a time value somewhat similar to the half-life (λ, decay to 50%) of a radioactive decay processes; however, fluorescence decay usually occurs within nanoseconds. In the case of FRET, a large fraction of the energy of the excited state is transferred to the acceptor. This offers a second and faster rate of relaxation, causing the lifetime to be reduced depending on the efficiency of the FRET. In this technique, the noise is reduced since only the donor fluorescence is measured, which is not affected by protein concentration.

Many other FRET techniques have been developed and used depending on the working system: for example, if protein-protein interaction is performed in purified proteins or in living cells; on the sub-cellular localization of the protein; on the kind of analysis (protein-protein interaction analysis, protein conformational changes etc.). FRET is widely applied for protein studies due to its versatility.

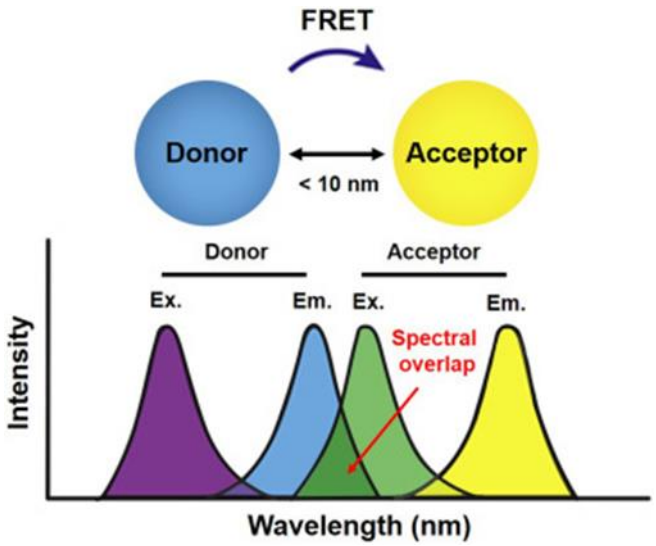

Figure 9: Representation of FRET mechanism. Donor fluorophore at a minimum of 10 nm distance to the acceptor fluorophore transfers energy when excited. The donor has to be excited with a specific excitation wavelength (Ex.) and its resulting emission wavelength (Em.) has to overlap the excitation wavelength of the acceptor for at least 30%. Figure taken from Chen (Chen et al. 2019).

2. Aim of this study

Despite significant efforts to understand MRTF regulation, MRTF dissociation events from actin during stimulation and under different conditions are still not clear and awaits further study. Here I aimed to identify candidates which compete with MRTF-A for actin binding and to visualize events resulting in the dissociation of actin and the intrinsically disordered RPEL motifs of MRTF-A. For the identification of MRTF competitors, isobaric labelling and label-free mass spectrometry approaches were applied after co-immunoprecipitation experiments. For the visualization of the events that lead to MRTF dissociation from actin, I aimed to generate a new FRET sensor. The FRET sensor needed to be characterized and validated. For this, the previously demonstrated effects of the FBS and of various MRTF interfering compounds over time were utilized. In particular, the influence of Latrunculin B, Cytochalasin D, Y-27632 (a ROCK inhibitor) and the overexpression of WH2 motif were followed over time after adding FBS. Furthermore, the action of CCG-203971 was investigated. This work intended to analyse and visualize the events that influence MRTF activation in the cytosol.

3. Materials and methods

3.1. Material

3.1.1. Devices and reagents

Table 1: Equipment

Use	Device	Manufacturer
Ice machine	ice machine CB640	Brema
PCR equipment	PCR System T 3000 Thermocycler	Biometra
Centrifuges	Centrifuge 5417C	Beckman Coulter
	Centrifuge 5417R	Eppendorf
	Sprout Mini-Centrifuge	Biozym
	Universal 320	Hettich
	Allegra 6KR Centrifuge	Beckman Coulter
Mixer and shaker	Lab dancer	IKA
	Magnetic Stirrer Model L-71	Labinco
	Magnetic Stirrer R1000	Carl Roth GmbH
	MR Hei-Standard	Heidolph
	Vortex-Genius 3	IKA
	Duomax 1030	Heidolph
	RM 5	CAT
	Rotamax 120	Heidolph
	Thermomixer comfort	Eppendorf
pH meter	LE409	Mettler Toledo
Microscope	EVOS XL Core Microscope	Thermo Scientific
	EVOS FL Microscope	Carl Zeiss Jena GmbH
	Axio Observer 7	
	Microscope with Apotome	Zeiss
	Confocal laser scanning microscope	Nikon A1R
	Cage incubator	Okolab
	Argon laser	Melles Griot, Germany
	PMT/GaAsP detector unit	Nikon
	Time-Correlated Single Photon Counting (TCSPC)	PicoHarp300 (Pcoquant)
	Pulsed laser source	PDL 828 Sepia II (Picoquant)
Voltage sources	Consort EV261	Peqlab

	peqPOWER	Peqlab
Spectrophotometer	Nanodrop 2000c	Thermo Scientific
Vacuum pumps	Mini-Vac eco 90-6030	Peqlab
Gel documentation	Gel Stick	Intas Science Imaging
Western blotting detection	ODYSSEY CLx ChemiDoc MP Imaging System	LI-CORE BIO-RAD
PAGE equipment	Mini-PROTEAN Tetra System	BIO-RAD
Scales	Kern ABS Kern 572	Kern&Sohn GmbH Kern&Sohn GmbH
Incubator and cell culture equipment	HERAcell 150 HERAsafe Water bath Incubator	Thermo Scientific Thermo Scientific GFL Memmert
Mass spectrometer and MS instruments	Orbitrap Fusion Lumos Tribrid Mass Spectrometer SpeedVac	Thermo Fisher Scientific Savant, Thermo Fisher Scientific

Table 2: General chemicals

Chemical/reagent	**Manufacturer**
Agar-Agar, bacteriological grade	Carl Roth GmbH
Agarose Standard	Carl Roth GmbH
2-amino-2-(hydroxymethyl) propane-1,3-diol (Tris)	Carl Roth GmbH
Ethylene-diamine-tetra-acetic acid (EDTA)	Carl Roth GmbH
Ethidium bromide, 1% solution	Promega
Sodium acetate (NA)	Sigma-Aldrich
Sodium dodecyl sulfate (SDS), 20%	Carl Roth GmbH
Triton X-100	Carl Roth GmbH
Tween 20	Carl Roth GmbH
Paraformaldehyde	Sigma-Aldrich
Potassium chloride (KCl)	Sigma-Aldrich
Sodium chloride (NaCl)	Carl Roth GmbH
Monopotassium phosphate (KH_2PO_4)	Sigma-Aldrich
Sodium phosphate dibasic (Na_2HPO_4)	Sigma-Aldrich
Albumin fraction from bovine serum (BSA)	Carl Roth GmbH

Ethanol	Sigma-Aldrich
Sodium Deoxycholate (DOC)	Sigma-Aldrich
n-Dodecyl β-maltoside (DDM)	Merck-Sigma
2-Mercaptoethanol	Sigma-Aldrich
Acrylamide/Bis solution	Carl Roth GmbH
Glycerol, 87%	Carl Roth GmbH
Ammonium persulfate (APS)	Sigma-Aldrich
N,N,N,N-Tetra-methyl-ethylene-diamine (TEMED)	SERVA
Isopropanol	Sigma-Aldrich
Non-fat milk powder	Carl Roth GmbH
Glycine	Carl Roth GmbH
Methanol	Sigma-Aldrich
Tryptone	Carl Roth GmbH
Yeast Extract	Carl Roth GmbH
Agar-Agar, bacteriological grade	Carl Roth GmbH

Table 3: Standards

GeneRuler 100 bp DNA ladder	Thermo Scientific
GeneRuler 100 bp Plus DNA ladder	Thermo Scientific
GeneRuler 1 kb DNA ladder	Thermo Scientific
Precision Plus Protein Standards	BIO-RAD

Table 4: Cell culture reagents and chemicals

cOmplete, Mini, EDTA-freier Protease-Inhibitor-Cocktail	Merck/Sigma-Aldrich
Dulbecco's modified Eagle medium (Gibco DMEM), high glucose	Invitrogen
DMEM, high glucose, no glutamine, no phenol red	ThermoFisher
Fetal Bovine Serum (FBS)	Gibco
Antibiotic-Antimycotic (100X)	Gibco
Sodium Pyruvate (100X)	Gibco
L-Glutamine (100X)	Gibco
Dimethyl sulfoxide (DMSO)	Sigma-Aldrich
0,5% Trypsin-EDTA	Thermo Scientific
Doxycyclin	Thermo Scientific
Opti-MEM reduced serum medium (Gibco)	Thermo Scientific

X-tremeGENE 9 DNA Transfection Reagent	Roche
ANTI-FLAG M2 magnetic beads	Sigma-Aldrich
Dynabeads Protein G	Invitrogen
DharmaFECT 1 Transfection Reagent	Dharmacon
CCG-203971	Tocris Bioscience
Cytochalasin D	Calbiochem
Latrunculin B	Calbiochem
Y-27682	Sigma/ Merck
Ampicillin	Carl Roth GmbH
Kanamycin	Sigma-Aldrich

Table 5: Enzymes and Reagents used in Molecular Cloning

QIAGEN Plasmid Maxi Kit	Qiagen
QIAGEN Plasmid Mini Kit	Qiagen
QIAquick MinElute Gel Extraction Kit	Qiagen
QIAquick MinElute PCR Purification Kit	Qiagen
CutSmart Buffer	New England Biolabs
Deoxy nucleotides, Solution Mix	New England Biolabs
Shrimp Alkaline Phosphatase	New England Biolabs
Q5 High-Fidelity DNA Polymerase	New England Biolabs
Q5 High-Fidelity Reaction Buffer (10x)	New England Biolabs
T4 DNA Ligase	New England Biolabs
T4 DNA Ligase buffer	New England Biolabs
Taq DNA Polymerase	New England Biolabs
Thermo Pol Reaction Buffer (10x)	New England Biolabs
Gel loading dye, purple (6X)	New England Biolabs
PacI	New England Biolabs
KpnI	New England Biolabs
HindIII	New England Biolabs
NheI	New England Biolabs
XhoI	New England Biolabs
BCA analysis	Thermo Fisher Scientific

Table 6: Consumables

Name	**Manufacturer**
Nitrocellulose blotting membranes, roll, pore size 0,2 µm	GE Healthcare
Immobilon-FL PVDF membrane	Merck Millipore
Ibidi µ-Slide 8 well	Ibidi
Cryotube	VWR
Menze Microscope Coverslips	Sigma-Aldrich
Serological pipettes (5, 10, 25 ml)	Greiner BIO-ONE
Plastic goods	Greiner BIO-ONE
Parafilm	Carl Roth GmbH
Eppendorf LoBind Microcentrifuge Tubes: Protein	Fisher scientific
Amicon® Ultra-0.5 Centrifugal Filter Devices	Millipore
Immu-Mount	Epredia

Table 7: Mass spectrometry reagents and chemicals

Name	**Manufacturer**
Sequencing Grade Modified Trypsin	Promega
ProteaseMax	Promega
4-(2-Hydroxyethyl)piperazine-1-ethanesulfonic acid (HEPES)	Roth
Iodoacetamide (IAA)	Applichem
TMT10plex Mass Tag Labeling Kits	Thermo-Scientific
Alcohol Dehydrogenase (ADH1)	Sigma- Aldrich
Trifluoroacetic acid (TFA)	Sigma-Aldrich
Urea	Applichem
Sodium chloride (NaCl)	Grüssing
Acetonitrile (LC-MS Grade)	VWR
Tris(2-carboxyethyl)phosphine (TCEP)	Carl Roth GmbH

3.1.2.Common buffers and solutions

Table 8: Buffers and solutions

Purpose of use Name	**Composition**
SDS GEL	
TAE-Puffer (10x)	400 mM Tris base 10 mM EDTA 50 mM sodium acetate
Lysis buffers	
RIPA buffer	50 mM Tris-HCl 150 mM NaCl 2 mM EDTA 1% (v/v) Triton X-100 0.5 % (v/v) DOC 0.1% (v/v) SDS
DOC buffer	50 mM Tris-HCl 150 mM NaCl 2 mM EDTA 1 % (v/v) DOC
DDM	50 mM Tris-HCl 150 mM NaCl 2 mM EDTA 0.1/0.5/1 % (v/v) DDM
TBS buffer (1X) pH 7.5	20 mM 150 mM Tris-HCl NaCl
Lysis buffer with single inhibitor addition	Lysis buffer 1X AEBSF 1X Leupeptin 1X Antipain 1X Pepstatin 1X Aprotinin

7X complete Protease-Inhibitor-Cocktail	1.5 ml Lysis buffer 1 complete Protease-Inhibitor-Cocktail tablet
Western blot solutions	
TBS-T buffer	0.1% (v/v) Tween 20 in TBS
Phosphate Buffer Saline (PBS, pH 7,4)	2.7 mM KCl 137 mM NaCl 10 mM Na_2HPO_4 1.8 mM KH_2PO_4
Running Gel (PAGE) pH 8.8	8-14% Acrylamide/Bis 375 mM Tris-HCl 0.1% (v/v) SDS 0.1% (v/v) APS 0.1% (v/v) TEMED
Stacking Gel (PAGE) pH 6.8	5% Acrylamide/Bis 127 mM Tris-HCl 4.5% (v/v) Glycerol 0.1% (v/v) SDS 0.1% (v/v) APS 0.1% (v/v) TEMED
Blocking solution	5% non-fat milk powder in TBS-T
Transfer Buffer (PAGE)	25 mM Tris base 192 mM Glycine 20% (v/v) Methanol 0.05% (v/v) SDS
Mammalia cells culture medium	
Complete DMEM Medium	DMEM 1X Antibiotic-Antimycotic (100x) 1X L-Glutamin (100x) 1X Sodium pyruvate 10% (v/v) FBS

Complete DMEM Medium - AA	DMEM 1X L-Glutamin (100x) 1X Sodium pyruvate 10% (v/v) FBS
Starvation DMEM Medium	DMEM 1X Antibiotic-Antimycotic (100x) 1X L-Glutamin (100x) 1X Sodium pyruvate 0.5 % (v/v) FBS
Freezing medium	45% (v/v) DMEM 50% (v/v) FBS 5% (v/v) DMSO
Bacteria culture medium	
Lysogeny broth (LB)	5 g yeast extract 10 g tryptone/peptone 10 g NaCl per 1 l 100 µg/ml ampicillin or 30 µg/ml kanamycin
Solid medium	Lysogeny broth (LB) 1.5% agar-agar
Trypsin digestion solutions	
UA	0,1 M Tris-HCl (pH 8,5) 8 M Urea 10 mM TCEP
UB	0,1 M Tris-HCl (pH 8,5) 8 M Urea
IAA	0,05 M Iodacetamid in UB

3.1.3.Antibodies

Table 9: Primary antibodies

Reagent	**Description**	**Source**	**used in**
Anti- Myc	Mouse, monoclonal, clone 4A6	Millipore Cat. 05-724	IF: 1:1000
Anti-MRTF-A/B	Rabbit polyclonal serum	Homemade (Sina Pleiner)	IF 1:1000 WB 1:1000
Anti-FLAG	Rabbit polyclonal	Sigma-Aldrich Cat. F7425	WB 1:2000
Anti-α-tubulin	Mouse monoclonal IgG1, clone DM1A	Sigma-Aldrich Cat. T9026	WB 1:2000
Anti-GFP	Rabbit polyclonal	Sigma-Aldrich Cat. G1544	IF 1:200 WB 1:1000

Table 10: Secondary antibodies

Reagent	**Source**	**used in**
Alexa 488-goat anti-mouse IgG	Molecular Probes Cat. A11001	WB-F 1:200
Alexa 546-goat anti-mouse IgG	Molecular Probes Cat. A11030	WB-F 1:200
Anti-mouse IgG, HRP-linked Antibody	Cell signalling Cat. 7076S	WB-C 1:5000
Anti-rabbit IgG, HRP-linked Antibody	Cell signalling Cat. 7074S	WB-C 1:5000

3.1.4.Oligonucleotides

Table 11: Oligonucleotides for cloning

Amplicon	Name	Sequence
RPEL	RPEL forward	TATTAATTAAATGAGGAACCCCAATTTACCTCC
	RPEL reverse	ATGGTACCTTGCTGGACTCCACAGGCAG
RPEL1	RPEL 1 forward	ATTAATTAAATGCTTAGTGAGCGGAAGAATGTGCT
	RPEL 1 reverse	AAGGTACCGCTTTTCAAAGGCGGCATGATC
RPEL2	RPEL 2 forward	TTAGCTCTAGAATGCGGGCCAGGACCGAGGACTATTTGAAAC
	RPEL 2 reverse	AAGGTACCAGCCGAGGTCTCTTCCAGAAT
RPEL3	RPEL 3 forward	ATTAATTAAATGAGAGCCAGGCTGGCTGATG
	RPEL 3 reverse	AAGGTACCGCTGGACTCCACAGGCAG
RPEL(P133A)	RPEL(P133A) forward	ATTAATTAAATGAGAGCCAGGCTGGCTGATG

	RPEL(P133A) reverse	AAGGTACCGCTGGACTCCACAGGCAG
Actin	Actin forward	CGCGCTAGCATGGATGATGATATCGCCGCGCTCG
	Actin reverse	CGGAAGCTTCTAGAAGCATTTGCGGTGGAC
WH2	WH2 forward	AAACTCGAGATCTGAGTCCGGCCGGACTTGTACAGCTCGTCCATGCC
	WH2 reverse	AAAGCTAGCGCCACCATGGTGAGCAAGG

Table 12: siRNA oligonucleotides

Name	**Catalog N.**	**Manufacturer**
ON-TARGETplus Mouse Radil (231858) siRNA - SMARTpool, 5 nmol	L-057913-01-0005	Dharmacon
ON-TARGETplus Mouse Samhd1 (56045) siRNA - SMARTpool, 5 nmol	L-065589-01-0005	Dharmacon
ON-TARGETplus Mouse Ube3a (22215) siRNA - SMARTpool, 5 nmol	L-047237-01-0005	Dharmacon
ON-TARGETplus Mouse Cobll1 (319876) siRNA - SMARTpool, 5 nmol	L-051032-01-0005	Dharmacon
ON-TARGETplus Non-targeting Control Pool	D-001810-10-05	Dharmacon

3.1.5. Plasmids

Table 13: Pre-existing plasmids

Name	Description	Reference
pEF Flag actin R62D without 3' UTR	pEF-Flag plink containing human β-actin R62D	(Posern et al, 2002)
pEF Flag actin WT without 3' UTR	pEF-Flag plink containing human β-actin	(Sotiropoulos et al, 1999)
pEF Flag empty vector	pEF plink vector containing only Flag tag sequence	from Richard Marais EFplink from MLV plink (Dalton & Treisman, 1992; Mizushima & Nagata, 1990)
pTriEx-RhoB- ΔPKN1	pTriEX vector expressing a RhoB-ΔPKN1 FRET sensor constituted by:	(Reinhard et al, 2016)

	RhoB, mVenus, L9Hx3, Cerulean3 and ΔPKN1.	
pTriEx-RhoA- ΔPKN1	pTriEX vector expressing a RhoA-ΔPKN1 FRET sensor constituted by: RhoA, mVenus, L9Hx3, Cerulean3 and ΔPKN1.	(Reinhard et al, 2016)
LeGO-C2 mCherry	pLentiLox3.7 vector expressing mCherry protein.	Plasmid #27339 from Addgene
pEGFP-C1 mCerulean	pLentiLox3.7 vector expressing mCherry protein.	Plasmid #15214 from Addgene
pEGFP-WH2 A (JMY)	pEGFP-C2 carrying the first isolated WH2 domain (A; AS 846-882) of mouse JMY with additional (GS)5 linker between GFP and WH2 domain	from franzi M. M. Kessels (Ahuja et al., 2007)

Table 14: Created plasmids

pTriEx-RPEL-YFP-CFP-R62D	RPEL sequence was amplified using RPEL forward and revers primers containing PacI and KpnI restriction sequence respectively. R62D actin was amplified using Actin forward and reverse primers containing NheI and HindIII restriction sequence respectively. Both RPEL and R62D amplified sequences were inserted in pTriEx-RhoB- ΔPKN1 instead of ΔPKN1and RhoB respectrively.
pTriEx-RPEL-YFP-CFP-WT	RPEL sequence was amplified using RPEL forward and revers primers containing PacI and KpnI restriction sequence respectively. Wild type (WT) actin was amplified using Actin forward and reverse primers containing NheI and HindIII restriction sequence respectively. Both RPEL and R62D amplified sequences were inserted in pTriEx-RhoB- ΔPKN1 instead of ΔPKN1and RhoB respectrively.
pTriEx-RPEL1-YFP-CFP-R62D	RPEL1 sequence was amplified using RPEL1 forward and revers primers containing PacI and KpnI restriction sequence respectively. R62D actin was amplified using Actin forward and reverse primers containing NheI and HindIII restriction

	sequence respectively. Both RPEL1 and R62D amplified sequences were inserted in pTriEx-RhoB- ΔPKN1 instead of ΔPKN1and RhoB respectrively.
pTriEx-RPEL1-YFP-CFP-WT	RPEL1 sequence was amplified using RPEL1 forward and revers primers containing PacI and KpnI restriction sequence respectively. Wild type (WT) actin was amplified using Actin forward and reverse primers containing NheI and HindIII restriction sequence respectively. Both RPEL1 and R62D amplified sequences were inserted in pTriEx-RhoB- ΔPKN1 instead of ΔPKN1and RhoB respectrively.
pTriEx-RPEL2-YFP-CFP-R62D	RPEL2 sequence was amplified using RPEL2 forward and revers primers containing PacI and KpnI restriction sequence respectively. R62D actin was amplified using Actin forward and reverse primers containing NheI and HindIII restriction sequence respectively. Both RPEL2 and R62D amplified sequences were inserted in pTriEx-RhoB- ΔPKN1 instead of ΔPKN1and RhoB respectrively.
pTriEx-RPEL2-YFP-CFP-WT	RPEL2 sequence was amplified using RPEL2 forward and revers primers containing PacI and KpnI restriction sequence respectively. Wild type (WT) actin was amplified using Actin forward and reverse primers containing NheI and HindIII restriction sequence respectively. Both RPEL2 and R62D amplified sequences were inserted in pTriEx-RhoB- ΔPKN1 instead of ΔPKN1and RhoB respectrively.
pTriEx-RPEL3-YFP-CFP-R62D	RPEL3 sequence was amplified using RPEL3 forward and revers primers containing PacI and KpnI restriction sequence respectively. R62D actin was amplified using Actin forward and reverse primers containing NheI and HindIII restriction sequence respectively. Both RPEL3 and R62D amplified sequences were inserted in pTriEx-RhoB- ΔPKN1 instead of ΔPKN1and RhoB respectrively.
pTriEx-RPEL3-YFP-CFP-WT	RPEL3 sequence was amplified using RPEL3 forward and revers primers containing PacI and KpnI restriction sequence respectively. Wild type (WT) actin was amplified using Actin

	forward and reverse primers containing NheI and HindIII restriction sequence respectively. Both RPEL3 and R62D amplified sequences were inserted in pTriEx-RhoB- ΔPKN1 instead of ΔPKN1and RhoB respectrively.
pTriEx-RPEL2(P133A)-YFP-CFP-R62D	RPEL(P133A) sequence was amplified using (P133A) forward and revers primers containing PacI and KpnI restriction sequence respectively. Amplified (P133A) sequences was inserted in pTriEx-RPEL2-YFP-CFP-R62D instead of RPEL2.
pmCherry-WH2 A (JMY)	mCherry fluorophore sequence was amplified using mCherry forward and reverse primers. After double digestion with NheI and XhoI of the PCR protduct and pEGFP- WH2 A (JMY) vetor, mCherry was inserted instead of EGFP protein sequence.

3.1.6. Cell lines

Table 15: Bacterial strains

Name	**Description**	**Source**
E. coli DH5α	F- ϕ80/lacZ ΔM15 Δ (lacZYA-argF) U169 deoR recA1 endA1 endA1 hsdR17(rK-, mK+) phoA supE44 thi-1 gyrA96 relA1 λ-, chemically competent	Invitrogen

Table 16: Mammalian cell lines

Cell line	Description	Source
NIH 3T3	*National Institutes of Health,* Swiss embryonic mouse fibroblasts, spontaneously immortalized (Todaro & Green, 1963)	R. Treisman, Cancer Resaerch UK (London)
NIH 3T3 TR-TO-R62D	Momoclonal *National Institutes of Health,* Swiss embryonic mouse fibroblasts, spontaneously immortalized (Todaro & Green, 1963) expressing Flag-R62D with Tet-inducible expressing system from pcDNA4.TO vector in the NIH pcDNA6.TR	Made by A.Descot.

3.2. Methods

3.2.1. Cloning

3.2.1.1. PCR

For the amplification and creation of new DNA fragments to insert into the plasmid, polymerase chain reaction (PCR) was performed using Q5 High-Fidelity DNA Polymerase for a low-error amplification. For each reaction the different components were added:

5x Q5 Reaction Buffer	8 µl
10 mM dNTPs (final concentration 200 µM)	1 µl
Q5 High-Fidelity DNA Polymerase	0.5 µl
10 µM Forward primer (final concentration 0.5 µM)	2.5 µl
10 µM Reverse primer (final concentration 0.5 µM)	2.5 µl
plasmid DNA (final concentration 0.3-1 µg)	x µl
H_2O	Up to 40 µl
Total volume	40 µl

The reaction was carried out in the T 3000 Thermocycler and cycles were established as follows:

Step	**Temperature**	**Time**
Initial denature	98°C	3 min
Denaturation	98°C	30 sec
Primer annealing	Calculated from primer melting temperature	30 sec
Q5 polymerization	72°C	30 sec for 1 Kb
Final extension	72°C	2 min
Program ending	4°C	∞

Steps 1 to 4 were repeated 30 cycles before proceeding to the further steps.

For the purification and analysis of the amplified fragment, 6 x loading dye was added to the PCR mix and loaded into 1% agarose gel (1 g agarose per 100 ml 1 x TBE buffer) electrophoresis, together with biorad precision plus protein dual color standards for molecular weight determination. For UV light DNA detection, a 0.01% (v/v) of DNA-intercalating ethidium bromide was added to the agarose gel for visualization of nucleic acids by UV light. Gel was let it run for 40 minutes at 90 V and 400 mA and DNA visualization was performed with Intas Science Imaging system at 312 nm. Thereafter, QIAquick MinElute Gel Extraction Kit was performed, and purified DNAs were stored at -20°C.

3.2.1.2. DNA digestion and fragment ligation

Plasmid vector or PCR amplified fragment were digested using restriction endonucleases (NEB). The reaction was carried out as follows:

DNA (1 µg plasmid vector or 26 µl of the PCR amplified fragment)	x µl
Restriction enzyme I	0.5 µl
Restriction enzyme II	0.5 µl
CutSmart Buffer	3 µl
H_2O	Up to 30 µl
Total volume	30 µl

For both PCR amplified fragment and vector digestion, the reaction was carried out at 37°C for 1 hour. In order to avoid vector relegation by de-phosphorylating the 5´ ends, 1 µl of shrimp alkaline phosphatase (rSAP) was added to the reaction solution and incubated for an additional hour at 37°C. An agarose gel electrophoresis and QIAquick MinElute Gel Extraction Kit were used for digested vector purification, whereas, for digested PCR fragment only QIAquick MinElute Gel Extraction Kit was used.

For the introduction of the PCR fragment into the digested vector, a ligation reaction was performed with 1:3 vector to insert molar ratio. In detail, the ligation mix was as follows:

10 x T4 DNA Ligase Buffer	2 µl
T4 DNA Ligase	1 µl
DNA (3 digested PCR fragment : 1 digested vector) DNA (3: 1 molar ratio of digested PCR fragment to digested vector)	x µl
H_2O	Up to 20 µl
Total volume	20 µl

Reaction was carried out at 16°C overnight.

3.2.1.3. Transformation of Chemically Competent DH5α Cells

E. coli DH5α cells were transformed with the ligated solution for the amplification of the new plasmid or with 1 µl of pre-excisting plasmid for normal re-transformation. Briefly, the entire ligation mix was used with 50 µl of chemically competent DH5α cells and left for 30 minutes on ice. A heat shock was induced for 45 seconds at 42°C and then DH5α cells were re-positioned on ice for 3 minutes. 450 µl of pre-warmed LB-medium were added and kept for 1 hour at 37°C with 450 rpm constant shaking. To concentrate the bacteria pellet in a small volume, transformed DH5α cells were centrifuged for 3 minutes at 2000 rpm and ~ 420 µl were carefully

removed. Bacterial pellet was then gently re-suspended and plated on LB-agar 10 cm dish plates containing the appropriated antibiotic for bacterial selection. DH5α cells were then let to grow overnight at 37°C.

3.2.1.4. Colony PCR

For the verification of colonies successfully transfected with the new plasmid, colony PCR was carried out. Each isolated colony was picked and re-suspended in 10 µl of water; from this mix, 3 µl were used for the PCR reaction. The other components were added as follows:

Taq DNA Polymerase (1.25 U/50 µl)	0.2 µl
10 mM dNTPs (final concentration 200 µM)	0.5 µl
10 x Thermo Pol Reaction Buffer (final concentration 1 x)	2 µl
10 µM Forward primer (final concentration 0.5 µM)	0.5 µl
10 µM Reverse primer (final concentration 0.5 µM)	0.5 µl
Transformed DH5α colony	3 µl
H2O	13.3 µl
Total volume	20 µl

The reaction was carried out in the T 3000 Thermocycler and cycles were established as follows:

Step	**Temperature**	**Time**
Initial denature	95°C	3 min
Denaturation	95°C	30 sec
Primer annealing	Calculated from primer melting temperature	30 sec
Q5 polymerization	68°C	1 min for 1 Kb
Final extension	68°C	5 min
Program ending	4°C	∞

Steps 1 to 4 were repeated 30 cycles before proceeding to the further steps.

The resulting PCR amplified fragments were analysed via 1% agarose gel as previously described. The bacterial colonies that displayed the correct PCR fragment size were then incubated overnight on the shaker (150 rpm) at 37°C in 4 mL of LB-medium with the appropriate antibiotic.

3.2.1.5. Mini-prep and DNA sequencing

The day after the incubation of the positive colonies, QIAGEN Plasmid Mini Kit was used for DNA purification following manufacturer's instructions, and DNA concentration was determined by using Nanodrop 2000c at 260 nm and 280 nm absorption.

Subsequently, 1200 ng of the newly prepared DNA was put in 15 µl volume of water and sent for Sanger sequencing to Microsynth SeqLab (Goettingen, Germany).

Once the correct sequence of the positive colonies was confirmed via sequencing, the colony was inoculated in 200 µl LB-medium with the appropriate antibiotic and incubated overnight as previously. The following day QIAGEN Plasmid Maxi Kit was carried out as manufacturer's instructions.

3.2.2.Cell culture

NIH3T3 cells were cultured in complete DMEM medium and kept in the incubator at 37°C and 5% CO_2 . For cell splitting, one pre-warmed PBS wash was performed before Trypsin was added and kept for 5 min in the incubator. Cells were split every 2-3 days. Thereafter, complete DMEM medium was added and 1/10 was then transferred into a new flask filled with complete medium. A manual count was carried out via neubauer improved 0,100 mm in order to determine cell number. For long cell storage, cells were centrifuged and re-suspended in freezing medium (50% complete DMEM medium and 50% DMSO) after splitting. Re-suspended cells were transferred into CryoTube™ vials and kept for 24 hours at -80°C and then moved to -150°C. Thawing was performed via warming the CryoTube™ vial at 37°C for two or three minutes and then transferring the cells into the flask.

3.2.3.Transfection of plasmid DNA

X-tremeGENE 9 (Roche) transfection kit was followed according to manufacturer's instructions for plasmid transfection 24 hours after seeding (Table 17). For the expression of FRET constructs, transfection medium was changed to starvation medium after 6 hours in order to reduce cell stress. Further analyses were performed 24 hours post transfection.

Table 17: Plasmid amount used

Plate	Final plasmid amount
10 cm dish	5 µg (2.5 µg empty vector + 2.5 µg Flag-R62D)
12 well plate	0.5 µg
8 ibidi slide	0.15 µg (0.075 µg WH2-mCherry + RPEL2-R62D FRET sensor)

3.2.4.FLAG-R62D actin induced expression in stable cell line

Doxycyclin (Dox) was added to medium to a final concentration of 1 µg/ml and kept for 24 hours to induce Flag-R62D actin expression in the stable cell line TR-TO-Flag-R62D NIH3T3.

3.2.5.Co-Immunoprecipitation and western blot

For monomeric actin binding protein isolation, co-immunoprecipitation was performed into Flag-R62D expressing cells. Briefly, cells were moved on ice and medium was aspirated by tilting the plates and lysis buffer (500 µl and 200 µl for 10 cm dish and 6 well plate, respectively) with inhibitors being added immediately after and incubated for 10 minutes. Cells were scraped off the wall and transferred into a pre-chilled Eppendorf which was then centrifuged at 14000 rpm for 15 minutes at 4°C. Meanwhile, M2 magnetic beads anti-FLAG (25 µl for 10 cm dish and 20 µl for 6 well plate) were prepared through three 1X TBS washes using a magnetic beads separations (Invivogen, DYNAL) to keep the beads attached to the Eppendorf wall. After 1X TBS washes, magnetic beads were then kept in the same lysis buffer that was used to lyse the cells before usage. For magnetic beads anti-Myc, 25 µl of Dynabeads Protein G beads were used. After the removal of the liquid with a magnetic beads separations, 200 µl of PBS with 2.5 µl of anti-Myc antibody were added and incubated for 10 minutes on the rotator at room temperature. Once the centrifuge was over, 15 µl or 30 µl of the supernatant was used for the input analysis for 10 cm dish and 6 well plate, respectively, and 15 µl of 3X LD were added and boiled at 95°C for 5 minutes, whereas the rest of the supernatant was added to the beads after solution removal. Magnetic bead and the supernatant were then incubated at 4°C for 2 hours on the rotator. Three washes with 500 µl pre-chilled lysis buffer were carried out in order to remove unspecific proteins and then the sample was either stored at -20°C after the addition of the lysis buffer or prepared for western blot analysis by adding 25 µl 3X LD and boiled at 95°C for 5 minutes.

3.2.6.Western blot

Boiled samples were loaded into a 1% SDS-PAGE separation gel and it was let it run at 130 V for 1.1 hour. Proteins on the gel were then transferred on the membrane (PVDF for fluorescence, WB or Nitrocellulose for chemiluminescent) at 100V for 1.3 hours followed by a blocking step of 1 hour with blocking solution. Membrane were then cut at the desired molecular weight and incubated over night at 4°C with primary antibody diluted in blocking solution. The next day, 3 TBS-T washes were performed before 1 hour secondary antibody (Alexa for fluorescence WB, HDP for chemiluminescent WB). Final 3 TBS-T washes were carried out before membrane

visualization. LiCor's Odyssey CLx system and ChemiDoc MP Imaging System were used for fluorescence or chemiluminescent WB respectively.

3.2.7.TMT 10 plex mass spectrometry

Frozen samples were kept on ice to slowly thaw. Half of the co-immunoprecipitated sample was loaded on the Amicon filter (MWCO 10 kDa), 20 pmol of ADH1 were added directly to the sample and a centrifugation of 10 minutes at 14000g at 4°C was carried out. For reduction, 250 µl of UA buffer were added to the filter two times, and thereafter an alkylation step was followed with 100 µl of IAA solution. Two washes with 200 µl of UB buffer were performed with an additional two washes with 200 µl of Hepes in order to remove urea. When solutions were added to the filter, beads were slowly re-suspended and centrifuged for 10 minutes at 14000g at 4°C.

For sample digestion, Trypsin (final conc. 0.05 µg/µl) and ProteaseMAX Surfactant (final conc. 1%) were incubated for 3 hours at 37° C at 12000 RPM in the Thermo Shakers. The digested sample was then collected in a new amicon microcentrifuge tube and in all the further steps, solutions were added directly to the flow-through. TMT10plex Mass Tag Labeling Kits were thawed 10 minutes before usage and each TMT label was quickly spun before being dissolved in 82 µl of Acetonitrile 100%. 26 µl of each TMT label was combined with the corresponding sample (Table 18, vertical columns) and incubated at room temperature for 1 hour. To quench the reaction, 3 µl of Hydroxylamine 5% were added and incubated for 15 minutes and, after that, 5 µl 50 % TFA trifluoroacetic acid (TFA) were added in order to acidify the solution to block trypsin activity. The solution was vortexed and span down and the pH was checked and adjusted to approximately 2 -3.

Half of each sample was then mixed with the proper sample combination for the preparation of the three biological replicates (Table 18, horizontal columns: A, B and C in the I, II and III mix respectively).

Samples' volume was reduced in a SpeedVac system. When necessary, volume was brought to 200 µl with 0.1% TFA and 15 µl of it were mixed to 110 µl of 0.1% TFA. In the first run, only 15 µl to 20 µl of each replicate were used for MS analysis.

Table 18: Schema of the sample mixed for the labeling experiment. (EV = empty vector; Dox = doxycycline; A, B and C = different replicates)

TMT^{10}-127C	**TMT^{10}-128N**	**TMT^{10}-128C**	**TMT^{10}-129N**	**TMT^{10}-129C**	**TMT^{10}-130N**	**TMT^{10}-130C**	**TMT^{10}-131**	
Stable - Dox - FBS	Stable - Dox + FBS	Stable + Dox - FBS	Stable + Dox - FBS	Transient EV - FBS	Transient EV + FBS	Transient Flag-R62D - FBS	Transient Flag-R62D + FBS	**I (A)**
Stable - Dox - FBS	Stable - Dox + FBS	Stable + Dox - FBS	Stable + Dox - FBS	Transient EV - FBS	Transient EV + FBS	Transient Flag-R62D - FBS	Transient Flag-R62D + FBS	**II (B)**
Stable - Dox - FBS	Stable - Dox + FBS	Stable + Dox - FBS	Stable + Dox - FBS	Transient EV - FBS	Transient EV + FBS	Transient Flag-R62D - FBS	Transient Flag-R62D + FBS	**III (C)**

Table 19: Specific reporter ion isotopic distribution

TMT^{10}-127C	TMT^{10}-128N	TMT^{10}-128C	TMT^{10}-129N	TMT^{10}-129C	TMT^{10}-130N	TMT^{10}-130C	TMT^{10}-131
127.131	128.128	129.134	129.131	129.138	130.135	130.141	131.138

3.2.8.Label-free mass spectrometry

Samples were first transferred in an 0.5 mL centrifugal filter units (30 kD cutoff, Sigma Aldrich, Darmstadt, Germany) and an adapted FASP (filter-aided sample preparation) (Wisniewski et al. 2009) protocol was carried out for LC/MS analysis. Two washes with 8 M urea in 50 mM, pH 8.5, 10 mM TCEP and centrifuged at 14000x g for 10 min. Subsequentially, alkilation was carried out in the dark with 50 mM iodoacetamide in 8 M urea, 50 mM HEPES, pH 8.5 at RT for 20 min followed by two washes with with 50 mM HEPES, pH 8.5 (10 min at 18,000× g each). Between all previous steps, samples were centrifuged for solution removal. Sample digestion was performed by adding to the filter 1 µg trypsin in 50 mM HEPES, pH 8.5 at 37 °C overnight. The next day, digested samples were acidified with TFA (final conc. 0.5 % (v/v).

3.2.9. Mass spectrometry data analysis

PEAKS Studio software (version 10, Bioinformatics Solutions Inc.) was applied for processing the LC-MS/MS raw data for label-free samples, whereas for the labeled samples proteome discoverer software was used. For database search, PASEF scans with same precursor masses and same mobility and retention profiles were merged. For protein identification, the obtained

data were searched against the Uniprot *mus musculus* database (version 01/28/22, 17,027 entries). For precursor ions, a maximum mass deviation of 15 ppm was applied, wheras for product ions, max. 25 ppm were allowed. Carbamidomethylation of cysteines was set as fixed modification, while oxidation of Met and acetylation of protein N-termini as variable modifications. Two missed cleavage sited per peptide were considered. Peptide quantification was carried out via LFQ (label-free quantitation).

3.2.10. Nano-HPLC-MS/MS

Nano-HPLC-MS/MS on an UltiMate 3000 RSLC nano-HPLC system (Thermo Fisher Scientific) coupled to a timsTOF Pro mass spectrometer equipped with CaptiveSpray source (Bruker Daltonik) was used for the analysis of proteolized samples. Trapping of the peptides was carried out on a C18 precolumn (Acclaim PepMap 100, 300 µm × 5 mm, 5 µm, 100 Å, Thermo Fisher Scientific) and separated on a µPAC 50-cm column (PharmaFluidics). Afterwards, with a concave 240-min gradient from 3% (v/v) to 35% (v/v) CAN peptides were separeted. Subsequentially, a flow rate gradient ranging from 900 to 600 nl/min in 15 min, followed by a constant flow rate of 600 nl/min was employed for elution. All LC separations steps were performed at room temperature.

Parallel accumulation serial fragmentation (PASEF) method for standard proteomics was performed for the MS analysis with the timsTOF Pro mass spectrometer. Mobility-dependent collision energy ramping values were set to 59 eV at an inversed reduced mobility (1/k0) of 1.6 V s/cm2 and 20 eV at 0.6 V s/cm2. Collision energies were linearly interpolated between these two 1/k0 values. Merging of TIMS scans was not performed. Per individual PASEF precursor, target intensity was set to 20,000 with an intensity threshold of 2,500. A scan range between 0.6 and 1.6 V s/cm2 with a ramp time of 100 ms was set. 10 PASEF MS/MS scans were triggered per cycle (1.17 s) with a maximum of three precursors per mobilogram. For fragmentation, precursor ions in the m/z range between 100 and 1700 with charge states ≥2+ and ≤5+ were selected. Active exclusion was enabled for 0.4 min (mass width 0.015 Th, 1/k0 width 0.015 V s/cm2).

3.2.11. siRNA

150000 NIH 3T3 TR-TO-R62D cells were seeded in 6 well plate and, after 24 hours, transfection of siRNA was performed according to the manufacturers. Briefly, 10 µl of 5 µM siRNA was diluted in 190 µl of Opti-MEM in one tube, whereas in a separate tube, 6.7 µl of DharmaFECT reagent were diluted in 193.3 µl of Opti-MEM. The two tubes were gently mixed and incubated for 5

minutes at room temperature. The contents of the two tubes were combined and incubated for another 20 minutes. Finally, 1.6 mL of Complete DMEM Medium – AA was added to the mix and the resulting 2 ml were added to the 6 well plate after medium removal. 24 hours from siRNA transfection, Doxycyclin (final conc. 1 μg/ml) was added for induction of Flag-R62D actin expression, and the next day the medium was changed to starvation medium. Thus, 72 hours from transfection, Co-IP was then performed (see section 3.2.5) for protein analysis.

3.2.12. Cell fixation

NIH 3T3 cells were seeded and transfected on a coverslip in a 12 well plate. Cells were transfected the next day. After 6 hours from transfection, the medium was changed to starvation medium in order to reduce cell stress and kept for another 18 hours. Fixation was then performed to stimulated and unstimulated samples by removing medium and adding paraformaldehyde (3.7% in PBS) for 15 minutes at room temperature. Thereafter, 3 PBS washes were performed for PFA removal and cells were covered with the Immu-mount reagent.

3.2.13. Live FRET analysis

In an 8 ibidi-slide 12000 NIH 3T3 cells were seeded per each cumber, and FRET sensor expression was induced (see transfection section 3.2.3). A minimum of 15 cells per condition were measured on at least three different days as independent biological replicates.

For the analysis of protein-protein interaction via the FRET sensor, three different signals where measured: the FRET signal (excitation wavelength of the donor: 420 nm; emission wavelength of the acceptor: 525 nm); the donor signal (mCerulean: excitation wavelength: 420 nm; emission wavelength: 475 nm) and the acceptor signal (mVenus: excitation wavelength: 515 nm; emission wavelength: 525 nm).

After data collection from ZEISS Microscope, images and data analysis were performed with ImageJ and Microsoft Excel2010.

For FRET ratio calculation, the following formula was applied:

$$R_{FRET} = I_F / I_D$$

Where I_D is the emission of the donor and I_F is the FRET-derived emission of the acceptor.

For the donor bleed-through-correction (β), only donor expressing cells were measured and the donor signal detected in the acceptor channel was calculated (~ 60%) and removed from the I_F to obtain the corrected value (I_{corr}) as follows:

$$I_{corr} = I_F - (\beta * I_D)$$

Thus, the final FRET ratio was calculated as:

$$R_{FRET} = I_{corr} / I_D$$

Before FRET and donor signal measurements in ImageJ, background was removed (Reinhard et al. 2016; Pertz et al. 2006; Heemskerk et al. 2016).

For experiments performed with the confocal microscope, NIS-Elements digital imaging software (Nikon, Tokyo, Japan) was used for image processing and FRET index was calculated as follows:

$$\text{FRET index} = 100\% * (DA - \alpha DD - \beta AA)/DD$$

DA was the FRET image and DD and AA were donor and acceptor images, respectively. DD and AA were multiplied with correction factors for donor crosstalk (α) and for the acceptor (β) for the bleed-through into the FRET channel (DA image). For all images, correction for the background was performed before analysis.

Fluorescence lifetime was determined using time correlated single photon counting (TCSPC). The donor, Cerulean3 was excited using a pulsed laser source (PDL 828 Sepia II, Picoquant, Berlin, Germany) with a repetition rate of 20 Mhz. Intensity of laser excitation was adjusted to 2,000 kcps as maximum count rate to avoid pile-up effect. Single photons and their arrival times were recorded and stacked for each timeframe using the Picoharp detection system (Picoquant, Berlin, Germany). SymPhoTime 64 software (Picoquant, Berlin, Germany) was used for the analysis of the fluorescence decay profiles using a 2-exponential reconvolution model and a calculated instrumental response function (IRF). The average amplitude weighted lifetime of the 2-exponential reconvolution fit is shown in diagrams.

All imaging analysis were performed at 60X object (plan apo lambda, Nikon, numerical aperture=1.4). For the creation of FRET index images, corrected FRET images were normalized to the corresponding intensity of the donor following the formula:

$$FRET_{index} = 100\% * (DA - \alpha DD - \beta AA)/DD).$$

3.2.14. Calculation and Statistics

Calculations and statistics were performed using Microsoft-Office Excel 2010. Unpaired one sample Student's t-test was carried out to verify significance level between different cells. P-values lower than 0.05, 0.01 and 0.001 are indicated with *, ** and *** respectively. For each condition, a minimum of 15 cells were analysed.

4. Results

4.1. Identification of putative MRTF competition via mass spectrometry

4.1.1. Overview of co-immunoprecipitation/ mass spectrometry experiments

The regulation of MRTF-A, remains an important area of research with many unanswered questions. MRTF-A is activated upon dissociation from a complex with G-actin. Despite numerous studies, the mechanisms underlying the formation and dissociation of the MRTF:actin complex after stimulation are not fully understood.

Recent research has revealed that MRTF-A can also be activated by other proteins, particularly those containing WH2 domains (WASP-Homology 2, or Wiskott-Aldrich homology 2), such as N-WASP and WAVE2, which compete with MRTF-A for binding to G-actin. This competition leads to the release of MRTF-A from G-actin, allowing for its nuclear translocation and subsequent activation of gene transcription. Notably, this activation of MRTF-A by N-WASP, WAVE2, and other proteins can occur independently of actin polymerization, suggesting a distinct mechanism for MRTF-A activation that is separate from actin dynamics. However, only a limited number of proteins are known to directly bind to G-actin and release MRTF-A from it.

Therefore, the aim of this study is to investigate MRTF regulation during FBS stimulation and identify potential candidates that compete with MRTF-A for binding to G-actin. To achieve this goal, a non-polymerizable G-actin mutant (R62D) was expressed in cells, and monomeric actin-binding proteins were collected via co-immunoprecipitation (Co-IP) experiments. Subsequently, mass spectrometry (MS) experiments were performed to identify these proteins in collaboration with the group of Prof. Dr. Andrea Sinz (Fig. 10).

To investigate proteins that exclusively interact with monomeric actin, the R62D actin tagged with a flag-tag was expressed in NIH 3T3 mouse fibroblasts. Proteins from both FBS-stimulated and unstimulated cells were then purified using Co-IP with anti-Flag magnetic beads, facilitated by the Flag-tag. The purified samples were subjected to mass spectrometry analysis to identify and compare the interactors of G-actin. This approach allowed for the specific analysis of proteins that interact with monomeric actin, providing insights into the regulation of MRTF-A during FBS stimulation.

For this study, NIH 3T3 cells were seeded in a 10 cm dish and induced for Flag-R62D actin expression using doxycycline, as the cells were expressing R62D actin under a Tet-on promoter. Stable NIH 3T3 Flag-R62D cell line was created by A.Descot (as mentioned in 3.1.6.). As an alternative, Flag-R62D actin expression induced via transfection was also analysed (Fig 10A). After 24 hours of seeding, the medium was changed to starvation medium (0.5% FBS) and incubated for an additional 24 hours. Subsequently, FBS stimulus was added to the experimental

sample, while the control sample remained unstimulated. Cells were then lysed, and Co-IP with Flag magnetic beads was performed to verify the dissociation of MRTF-A. Western blot (WB) analysis was used to confirm the reduction of MRTF-A after FBS stimulation, which was observed in three independent replicates (Fig. 10B). Quantitative MS was conducted for further data analysis (Fig. 10C).

Several different steps had to be established and adapted for our specific goal in order to successfully identify and characterize potential MRTF competitors.

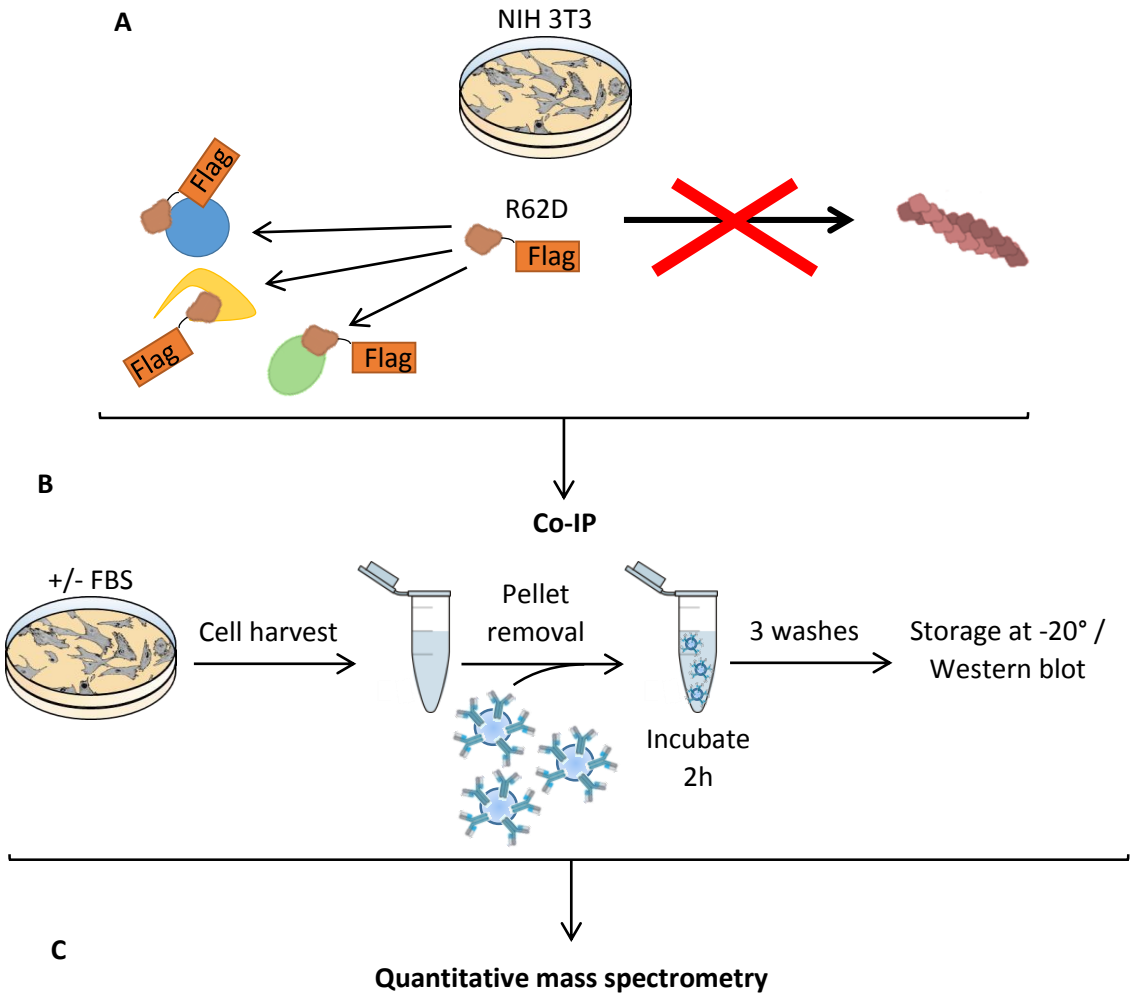

Figure 10: Schematic representation of Co-IP/MS experiment workflow. A) After 1 million NIH 3T3 mouse fibroblasts cells were seeded in a 10 cm dish, the expression of a flag-tagged non-polymerizable mutated actin (flag-R62D) was induced. B) Cells were then kept in starvation medium (0.5% FBS) for 24h and subsequently a co-immunoprecipitation experiment was performed to stimulated and unstimulated cells (+/- FBS). Co-IP was performed using magnetic beads anti-Flag for the specific Flag-R62D actin pull-down and 3 washes were performed for removal of unspecific binding proteins. C) Finally, quantitative mass spectrometry was performed to identify the different monomeric binding proteins in the two conditions.

4.1.2. Optimization of the conditions for co-immunoprecipitation

4.1.2.1. Lysis buffer content

One million cells were seeded in a 10 cm dish to establish the appropriate cell density for the experiment. Next, Co-IP conditions were determined in NIH 3T3 transiently expressing Flag-R62D. Previous studies had used the standard RIPA buffer for Co-IP experiments (Miralles et al. 2003; Posern et al. 2004). However, due to the incompatibility of Triton X-100 and SDS with mass spectrometry, a new lysis buffer was required. As an alternative to Triton X-100, n-Dodecyl β-maltoside (DDM), a well-known detergent for Co-IP/MS experiments was selected and tested for its suitability.

In order to establish the most suitable lysis buffer for the study, MRTF-A abundances after immunoprecipitation were compared using different detergents for cell lysis. Immunoblotting was performed to compare the amounts of MRTF-A pulled down using lysis buffers containing 0.1%, 0.5%, and 1% DDM, as well as RIPA and DOC 1% buffers (Fig. 11A). This comparison aimed to determine the optimal lysis buffer for subsequent experiments, considering the compatibility of the detergents with mass spectrometry and the effectiveness of MRTF-A pull-down.

As a result of the lysis buffer optimization, it was found that 0.5% DDM showed the highest amount of MRTF pulled down (Fig. 11A, top), indicating minimal interference with the MRTF-actin interaction. Moreover, the effect of salt concentration on the MRTF:actin complex was also assessed, with 150 mM and 600 mM salt concentrations tested (Fig. 11B). Immunoblotting analysis showed that the MRTF:actin complex had a stronger interaction with 150 mM salt concentration compared to 600 mM. To ensure specificity of the co-immunoprecipitation signal, anti-Myc beads were used as a control (Fig. 11B on the right), and no MRTF or Flag signal was detected in the immunoprecipitated samples using anti-Myc beads, confirming the specificity of the co-immunoprecipitation.

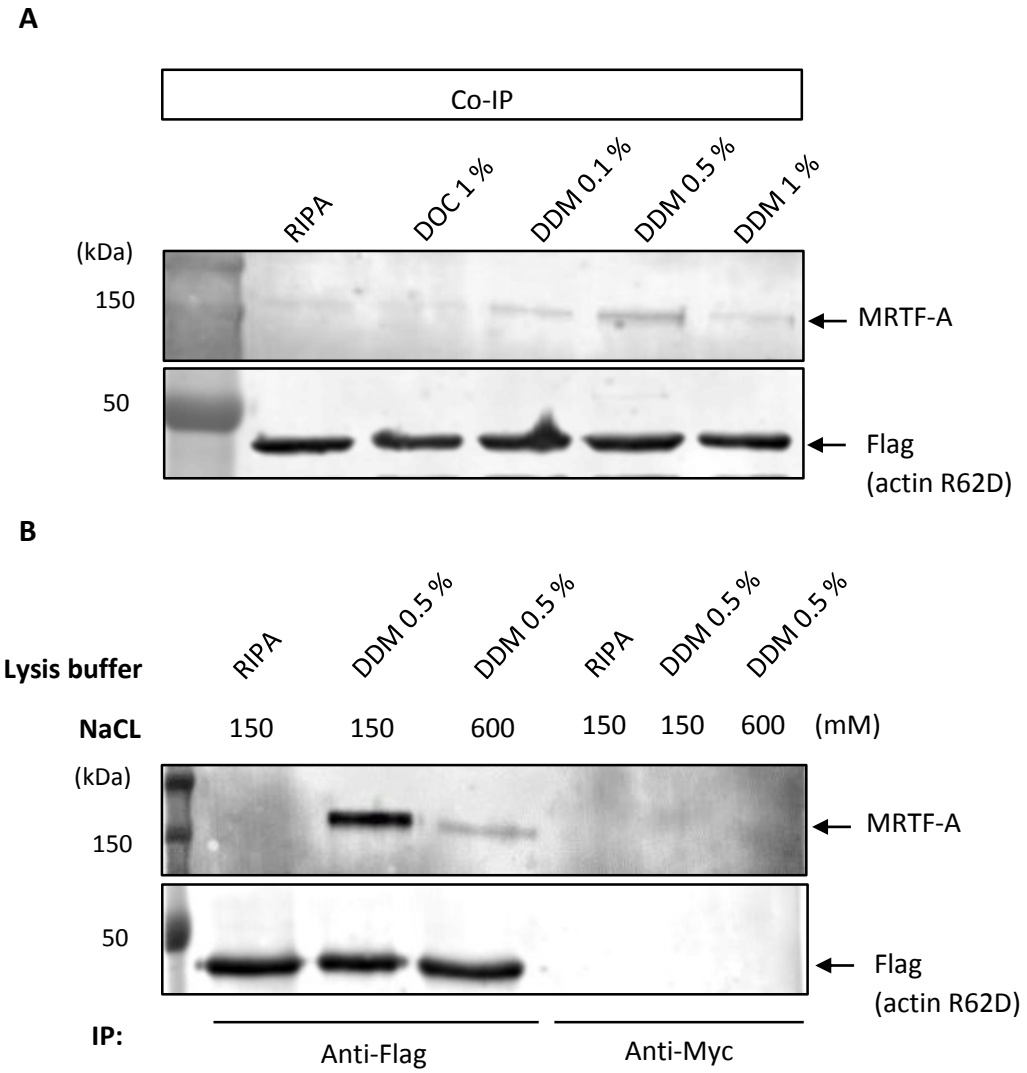

Figure 11: Optimization of Triton free lysis buffer. A) The standard RIPA buffer, DOC buffer and DDM buffer with increasing DDM concentration (0.1%, 0.5% and 1%) were compared for co-immunoprecipiteted MRTF-A amount with MRTF and FLAG immunoblots. B) NaCl 150 mM and 600 mM DDM 0.5% lysis buffers were tested in comparison to the standard RIPA buffer for the buffer optimization. As an additional control for the specificity of the signal band, magnetic beads anti-Myc were also used.

4.1.2.2. Optimization of FBS-stimulation time

In order to determine the optimal time for FBS-stimulation before conducting mass spectrometry analysis, a series of experiments were performed to investigate the effect of FBS on MRTF signal in Co-IPed samples. NIH 3T3 cells transiently expressing R62D were used. It was observed that there was a significant reduction in MRTF signal and MRTF:actin dissociation up to 2 hours after the addition of FBS (Miralles et al. 2003). However, for the purpose of capturing the initial response of MRTF to FBS stimulation, earlier time points after FBS addition were examined.

Co-IPed MRTF abundances were compared after 10, 20, and 30 minutes of FBS stimulation (Fig. 12A). The corresponding MRTF signals were then quantified by normalizing the MRTF/Flag-R62D

actin ratio to that of the unstimulated sample (Fig. 12B). Interestingly, over time, the MRTF signal increased slightly on the WB after Co-IP, indicating a gradual increase in the amount of MRTF re-binding to actin in an attempt to return to the original state.

Based on these findings, the 10-minute stimulation time was chosen as the optimal time point for further analysis to identify the MRTF competitors. This decision was based on the observation that the 10-minute stimulation time displayed a lower abundance of MRTF-R62D actin binding, suggesting that a higher amount of the MRTF competitor may be binding to actin when a lower amount of Co-IPed MRTF is detected (Fig. 12B). This selection of the optimal FBS-stimulation time for MS analysis will enable a more comprehensive investigation into the mechanism of MRTF-actin interaction and the potential involvement of the MRTF competitor in this process.

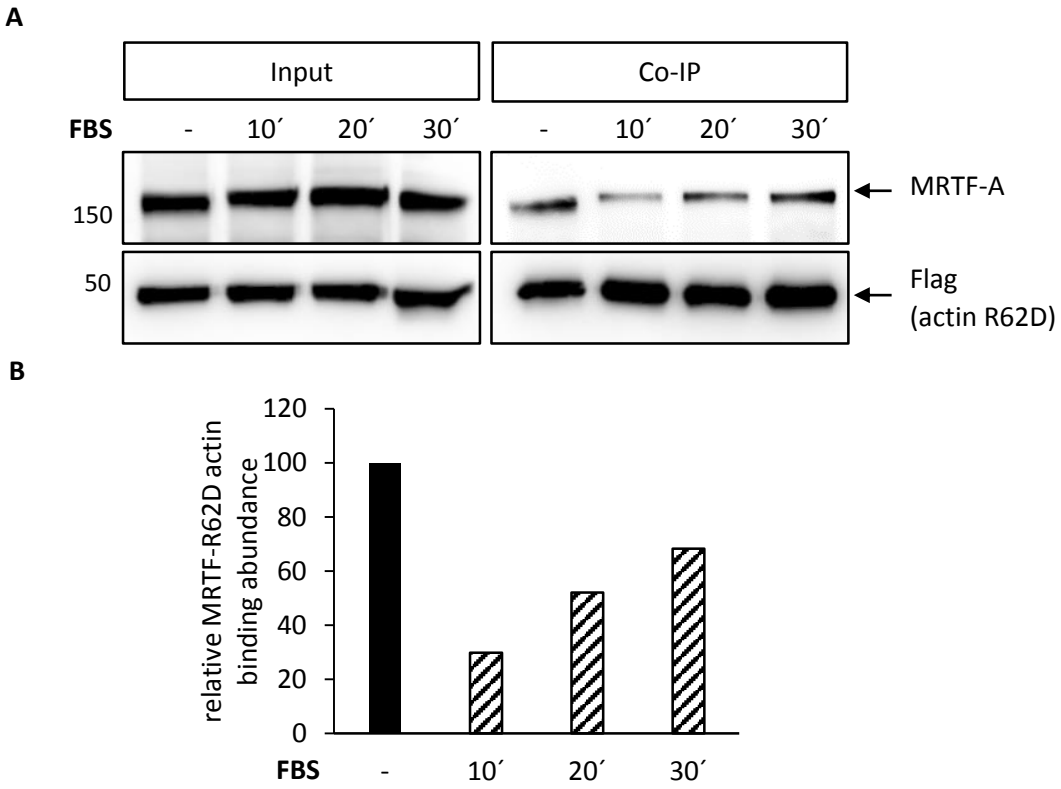

Figure 12: MRTF-actin binding was recovered with increased stimulation time. A) Different stimulation times (10', 20' and 30') showed differences in MRTF signal in the immunoblot after Co-IP (right panel). Additionally, a shift in molecular weight of MRTF-A was also observed after stimulation. B) Quantification of MRTF-A signal after Co-IP in the stimulation times.

4.1.3. Amine-reactive isobaric mass tag labeling

A sample multiplexing strategy was employed to reduce the run time in mass spectrometry. After establishing the Co-IP conditions, three biological replicates were collected to increase the reproducibility of finding MRTF competitor candidates. Both stable and transient induced expression systems for Flag-R62D actin were analysed. Each replicate consisted of four different samples, where two control samples (+/- FBS) with no induced Flag-R62D actin expression and two samples with Flag-R62D actin expression (+/- FBS) were compared.

To verify the reduced signal of MRTF after stimulation in all replicates after Co-IP and to preserve the rest of the sample for further analysis, WB was performed on 1/10 of the sample using the enhanced chemiluminescence (ECL) method (Fig. 13A). Previous attempts with fluorescent secondary antibody detection were unsuccessful due to lower sensitivity of this technique compared to ECL-based detection.

Using ECL WB with higher sensitivity, MRTF and Flag signals were detected using 1/10 of the sample, allowing visualization of MRTF and Flag signals in samples where Flag-tag R62D actin was induced after Co-IP. MRTF-FBS signal reduction was verified in all biological replicates (A, B and C) for both stable and transient expression systems. To reduce variability between samples, the lysis buffer was prepared with 1X complete protease inhibitor cocktail instead of individual protease addition at 1X concentration.

In the next step, all samples were processed for MS experiments using a TMT-10 plex labeling kit as a strategy to analyse all samples in only three runs in the Orbitrap mass spectrometer. The TMT labeling allowed for better comparison of protein amounts between the samples. However, due to the impossibility of protein concentration determination via BCA kit before TMT-10 plex labeling, human Alcohol dehydrogenase 1A (ADH1) was spiked-in with a defined amount (20pmol) for peptide normalization (O'Rourke et al. 2019). This allowed for comparison of protein abundances between different samples by adding the same known amount of the spike-in protein to all samples.

One biological replicate of the stable expressing system and one biological replicate of the transient expressing system were labeled, mixed, and ran in the Orbitrap Fusion Tribrid Mass Spectrometer together, enabling analysis of all samples in only three runs (see table 18). Additionally, each mix was ran three times for technical analysis, and evaluation of shared proteins between the technical replicates indicated good measurement reproducibility (Fig. 13B). For peptide and protein analysis Proteome Discoverer 2.3.0.305 was used. For protein identification, uniprot mouse database was applied and a False discovery rate (FDR) was set to 1%. Proteins were then normalized to ADH1 amount. The labeled peptides were used to quantify

the proteins in the samples by each tag channel (Table 19). Shared proteins between the biological replicates for both expression systems were found to be the majority, with replicate B exhibiting a higher number of exclusive proteins (Fig. 13C). Furthermore, an increase in β-actin abundance was observed when Flag-R62D actin was induced in all replicates, and similar abundance trends were found for already known actin binding proteins such as MRTF, Profilin, and Twinfilin (data not shown).

Despite the good reproducibility between biological replicates, different problems were encountered. Only MRTF-B was detected in a very low amount only in one biological replicate in both stable and transient expression systems. Additionally, the number of proteins obtained in the MS experiment was extremely low and very few ABPs were detected. Thus, the absence of known MRTF competitor candidates could be attributed to various factors, including: inefficient trypsin digestion, poor labeling efficiency, low sensitivity or low signal-to-noise ratio. Further analysis and optimization may be needed to identify potential MRTF competitor candidates.

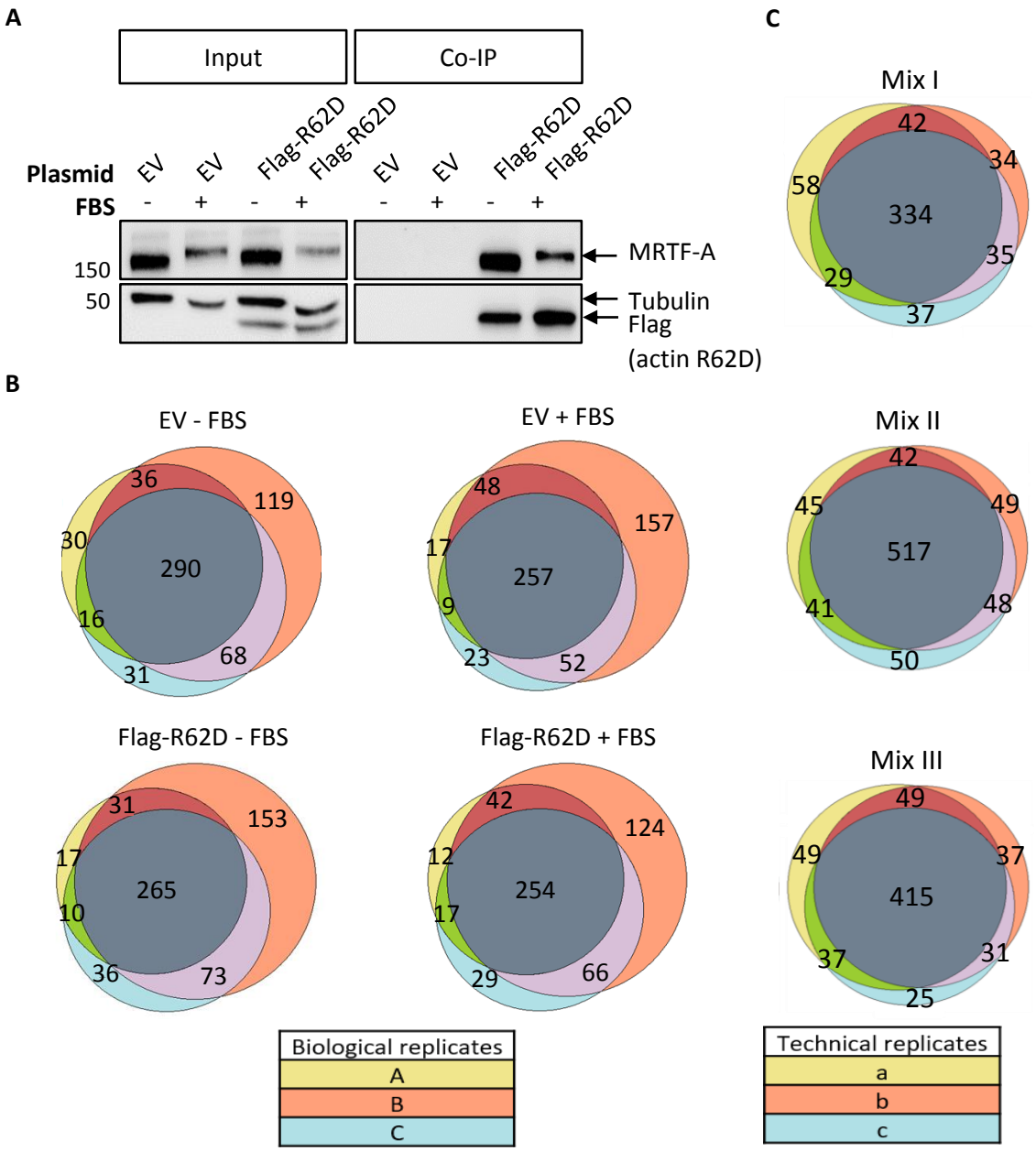

Figure 13: Analysis of all biological replicates indicate a good reproducibility. A) Validation of the MRTF-actin dissociation event and specificity of the pull-down via immunoblot. The graphic represents the WB of one biological sample where Flag-R62D expression was induced transiently as compared to the empty vector (EV), where Flag signal was not detected. Similar results were obtained for all replicates. B) Venn diagram of the shared number of proteins between the three technical replicates within each biological replicate. Similar results were obtained for all replicates. C) Number of proteins shared within each condition for the transient expression of Flag-R62D actin experiment between the three different replicates. Similar results were obtained for stable expression of Flag-R62D actin experiments.

4.1.4. Label-free mass spectrometry

Since TMT labeling did not yield a sufficient number of candidate proteins, an alternative strategy using label-free mass spectrometry was employed to identify MRTF competitor candidates. To achieve our goal, a stable expression system was utilized. In the mass spectrometry analysis, Co-IPed samples with or without FBS were compared with their

corresponding inputs, instead of non-expressing Flag-R62D actin samples, to determine enriched proteins after immunoprecipitation. Three biological replicates (named A, B, and C) were collected and analysed via WB as a quality control measure (Fig. 14A).

After trypsin digestion, peptides were loaded into the Orbitrap and were normalized to the total number of peptides obtained for each sample. Although the hetamap of the peptide quantification of each sample showed a different pattern of distribution in sample B, a higher number of proteins were identified (Data not shown). Both MRTF-A and β-actin abundances were compared between samples with or without FBS, and distinct patterns were observed (Fig. 14B). MRTF was found to be highly enriched in the starved Co-IPed samples, indicating a strong interaction with the β-actin under conditions of low serum. By contrast, the stimulated Co-IPed samples showed low abundance of MRTF, which suggests that the interaction between MRTF and the β-actin may be disrupted or reduced upon stimulation with FBS. On the other hand, β-actin was highly abundant in all inputs compared to the Co-IPs, possibly due to the presence of endogenous β-actin in addition to Flag-R62D actin in the inputs, which could explain the differential abundance observed.

As an additional quality control analysis, a comparison of the number of proteins enriched in the input versus the Co-IPed samples showed a higher number in the input, indicating that only a small portion of proteins were pulled down (data not shown). Further analysis of the Co-IPed samples revealed around 30 proteins that were successfully enriched after stimulation, as depicted in the volcano plot (Fig. 14C, right box). Among the top 10 proteins enriched in Co-IP + FBS samples, four proteins were selected as potential MRTF competitors for further experiments (Fig. 14C, red boxes).

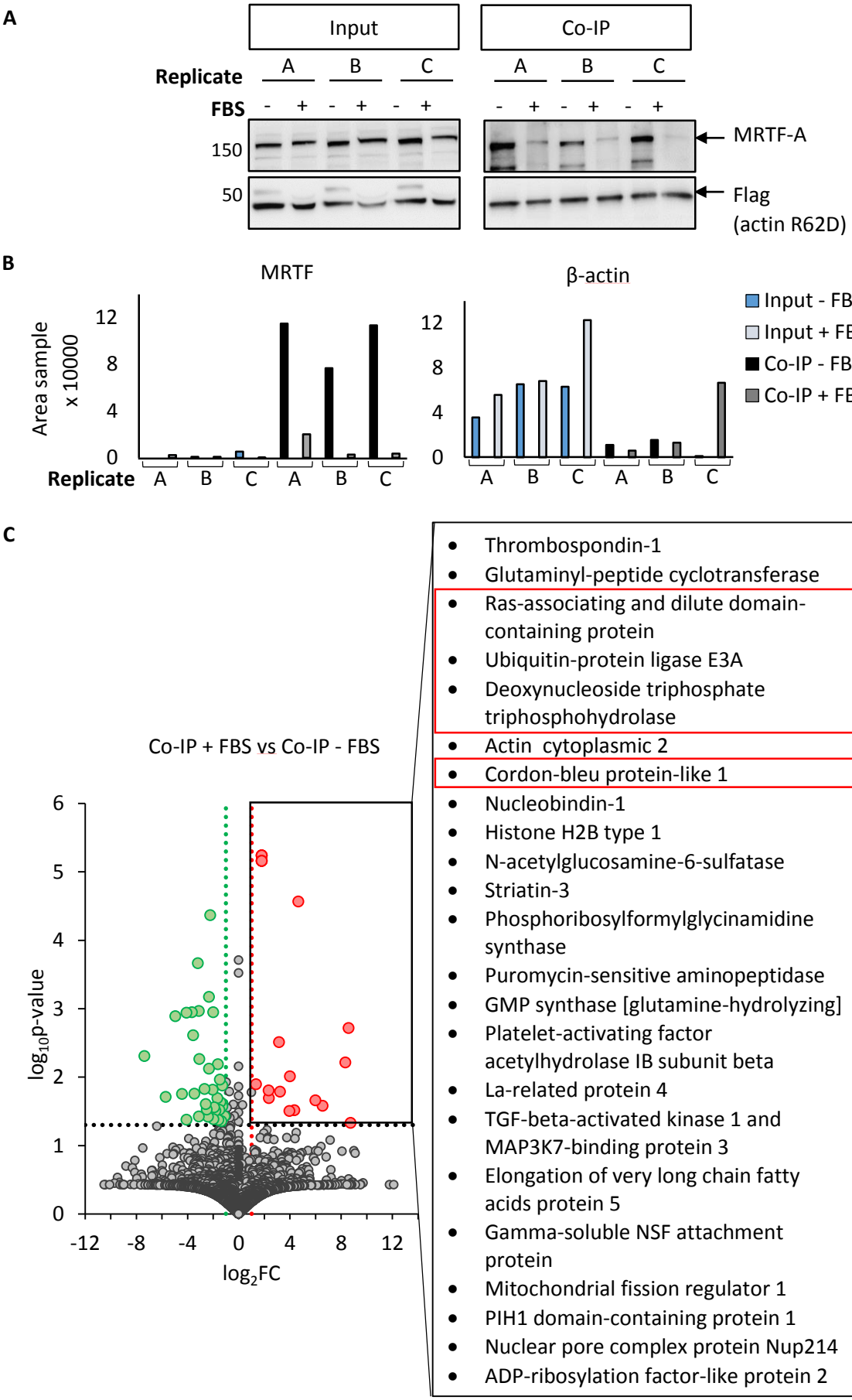
A
Input
Co-IP
Replicate
A B C A B C
FBS
- + - + - + - + - +
150
50
MRTF-A
Flag
(actin R62D)
B
MRTF
β-actin
Area sample
x 10000
12
8
4
0
Replicate
A B C A B C
Input - FBS
Input + FBS
Co-IP - FBS
Co-IP + FBS
C
Co-IP + FBS vs Co-IP - FBS
log10p-value
log2FC
6
5
4
3
2
1
0
-12 -8 -4 0 4 8 12
Thrombospondin-1
Glutaminyl-peptide cyclotransferase
Ras-associating and dilute domain-containing protein
Ubiquitin-protein ligase E3A
Deoxynucleoside triphosphate triphosphohydrolase
Actin cytoplasmic 2
Cordon-bleu protein-like 1
Nucleobindin-1
Histone H2B type 1
N-acetylglucosamine-6-sulfatase
Striatin-3
Phosphoribosylformylglycinamidine synthase
Puromycin-sensitive aminopeptidase
GMP synthase [glutamine-hydrolyzing]
Platelet-activating factor acetylhydrolase IB subunit beta
La-related protein 4
TGF-beta-activated kinase 1 and MAP3K7-binding protein 3
Elongation of very long chain fatty acids protein 5
Gamma-soluble NSF attachment protein
Mitochondrial fission regulator 1
PIH1 domain-containing protein 1
Nuclear pore complex protein Nup214
ADP-ribosylation factor-like protein 2

Figure 14: Identification of proteins up-regulated after FBS stimulation via label-free MS experiment. A) MRTF-R62D actin FBS dissociation event after Co-IP validated via WB (right panel) for all three biological replicates (A, B and C) compared to the input (left panel). B) MRTF and β-actin abundance plot obtained for all samples after label-free MS experiment. The abundances are indicated as Area sample, which is the sum of all the peaks obtained from the chromatogram of the different peptides assigned to the protein. C) Volcano plot displaying the up- and down-regulated proteins after stimulation (in red and green colours respectively). On the right panel, up-regulated proteins are listed. In the red boxes are highlighted proteins selected for further experiments. A protein up- or down-regulated was considered significant with a log_2FC of 1 or -1 respectively (x-axis) and with a P value of 0.05, which means a log_{10}p-value of 1.3 (y-axis).

4.1.5. Analysis of candidates for MRTF-competitive actin binding

In order to test the function of the potential MRTF competition from the candidates identified in the MS data, several experiments were conducted. Firstly, the binding of the candidates to monomeric actin was verified through WB analysis following Co-IP experiments (Fig. 15). Cobll1, Radil, and Samhd1 were found to bind to Flag-R62D actin, validating their interaction as potential MRTF competitors. However, Ube3a did not show binding to Flag-R62D actin, possibly due to its low abundance in the sample, which could also explain its low presence in the TMT-10 plex labeling experiment. Interestingly, Radil and Samhd1 were only detected in stimulated samples after Co-IP, indicating a specific interaction induced by FBS.

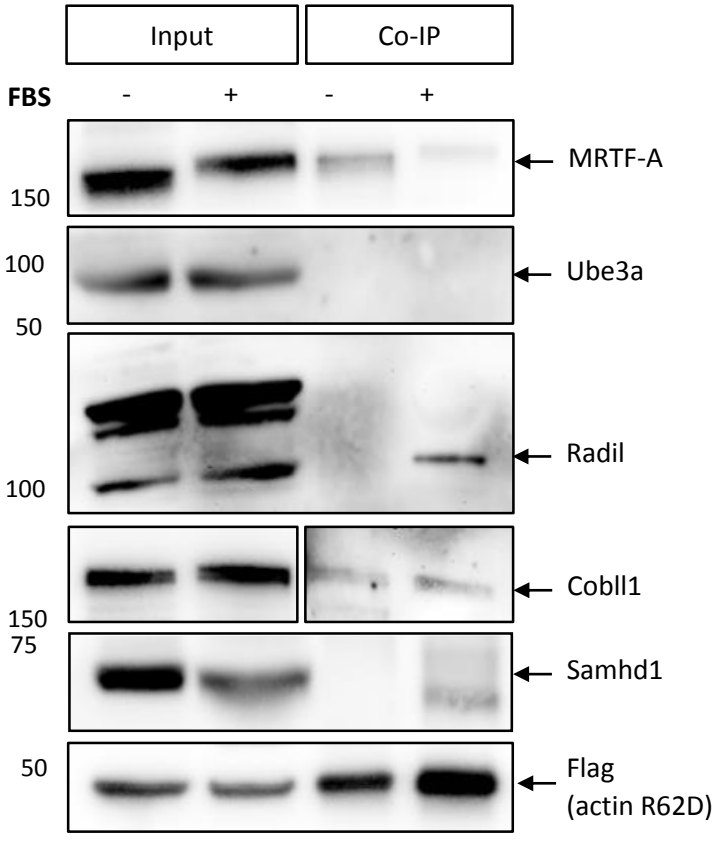

Figure 15: Validation of Flag-R62D binding after immunoprecipitation of MRTF-A competitor candidates. Protein abundance of Ube3a, Radil, Cobll1 and Samhd1 was analysed via western blot -/+ FBS.

As a next step, the influence of the candidates on MRTF activation was assessed through specific siRNA experiments (Fig. 16). With the silencing of the candidates, MRTF activation after FBS stimulation is expected to not be detected and, thus, a similar amount of MRTF should be found before and after stimuli. Single protein knockdown using specific siRNAs for each candidate was performed in both unstimulated and stimulated samples, and Co-IP was conducted to verify MRTF inactivation. Additionally, a quadruple knockdown targeting all candidates in one sample was performed to explore any potential synergistic effect on MRTF competition. A non-targeting siRNA was used as a control.

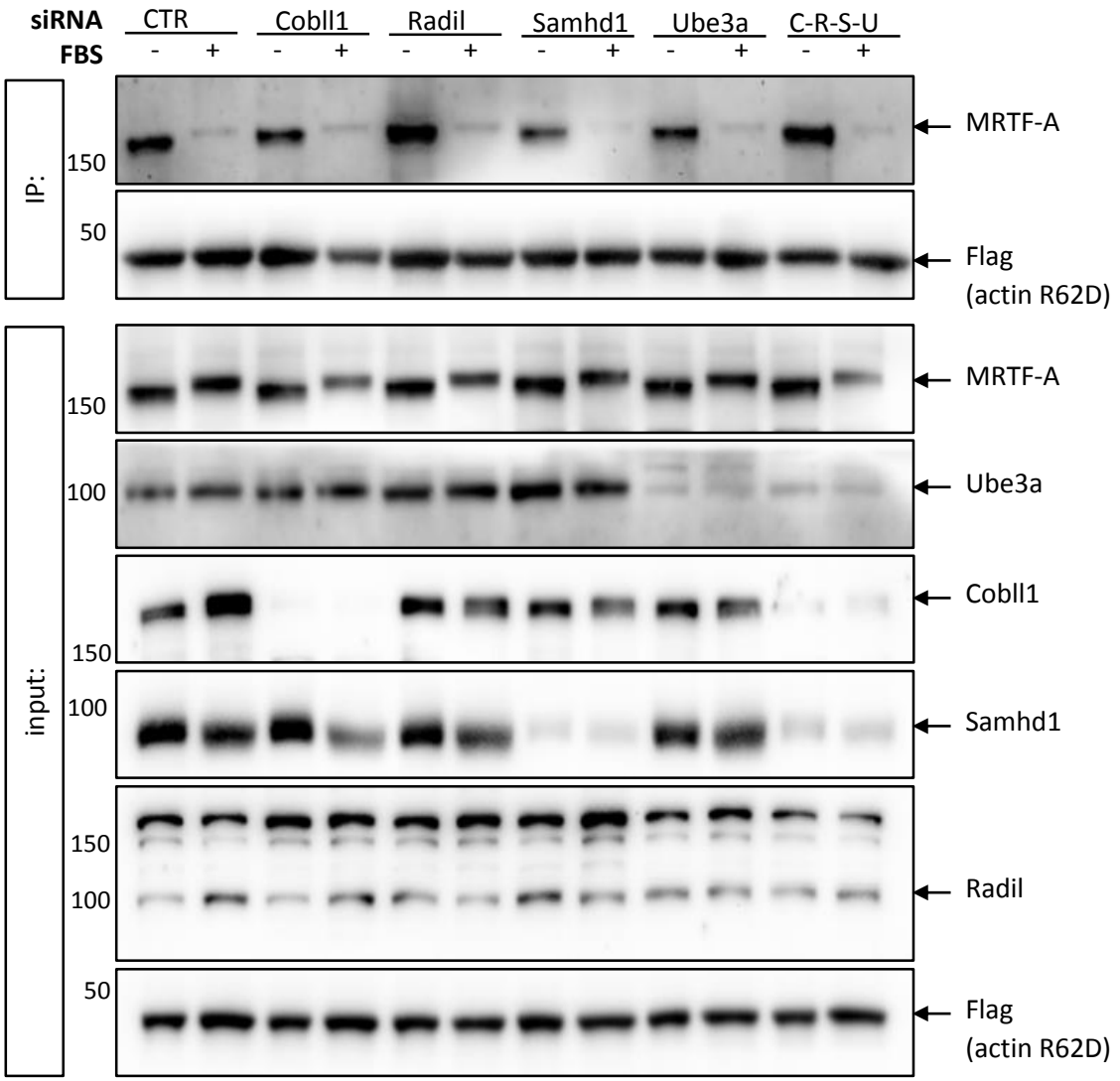

Figure 16: Validation of potential MRTF competitors. MRTF signal +/- FBS after Co-IP (IP panel) detected for the knockdowns targeting different candidates. Protein knockdowns were analysed in the inputs (input panel). In order to analyse a possible synergistic effect of combined siRNAs applications, protein knockdown of Cobll1, Radil, Samhd1 and Ube3a together were performed in the same sample. siRNA CTR was used as control.

The effectiveness of knockdown was evaluated in the input samples using specific antibodies for each protein, and knockdown was confirmed for all candidates except Radil (Fig. 16, IP blots). WB analysis of MRTF signals in Co-IPed samples revealed that all candidate knockdowns did not change the reduction in MRTF after FBS addition (Fig. 16, Co-IP blots). Therefore, no significant MRTF competitor function was observed for any of the candidates, indicating that none of them caused the dissociation of MRTF:actin complex upon FBS stimulation.

Although Radil's knockdown effect on MRTF:actin FBS dissociation could not be evaluated, these results collectively demonstrate that none of the candidate knockdowns had a noticeable impact on the dissociation of MRTF:actin complex in response to FBS stimulation.

4.2. RPEL:actin spatial and temporal interaction analysis

4.2.1. Creation and expression of new RPEL:actin FRET constructs

Another aspect of my PhD research work was to investigate when and where MRTF and actin dissociate within the cell upon stimulation. To address this question, FRET experiments (Förster resonance energy transfer or Fluorescence resonance energy transfer) were selected as the method of choice due to their sensitivity in probing spatio-temporal dynamics of protein interactions inside the cell. The investigation of MRTF:actin interaction dynamics was performed using FRET experiments.

A new FRET sensor was developed, which allowed for a detailed analysis of the spatial and temporal interactions between MRTF and actin (Fig. 17). The FRET sensor design included a 1:1 stoichiometry of the two proteins of interest, MRTF and actin, separated by the acceptor (mVenus) and the donor (Cerulean3) fluorophores within the same polypeptide. To prevent non-specific FRET signals, a ribosomal protein-based linker (L9Hx3) with α-helical repeats was used.

A key feature of the newly developed RPEL:actin FRET sensor is its reversibility, allowing for the investigation of both association and dissociation events in time. This makes it a powerful tool to study how different MRTF-interfering factors may influence the dynamics of the RPEL:actin complex in space and time. The design of the RPEL:actin FRET sensor was based on the previously developed Rho-ΔPKN FRET sensor obtained from Prof. Jaap van Buul, Department of Molecular Cell Biology, University of Amsterdam. The Rho-ΔPKN FRET sensor has been applied for interaction analysis of various proteins (Reinhard et al. 2016).

To create the FRET sensor, constructs containing different combinations of the proteins of interest were created to select the most suitable construct. The RPEL motif consists of three different RPEL sequences, each capable of binding a monomeric actin. Thus, the full RPEL motif and each individual RPEL sequence were cloned, along with both wild type (WT) and non-

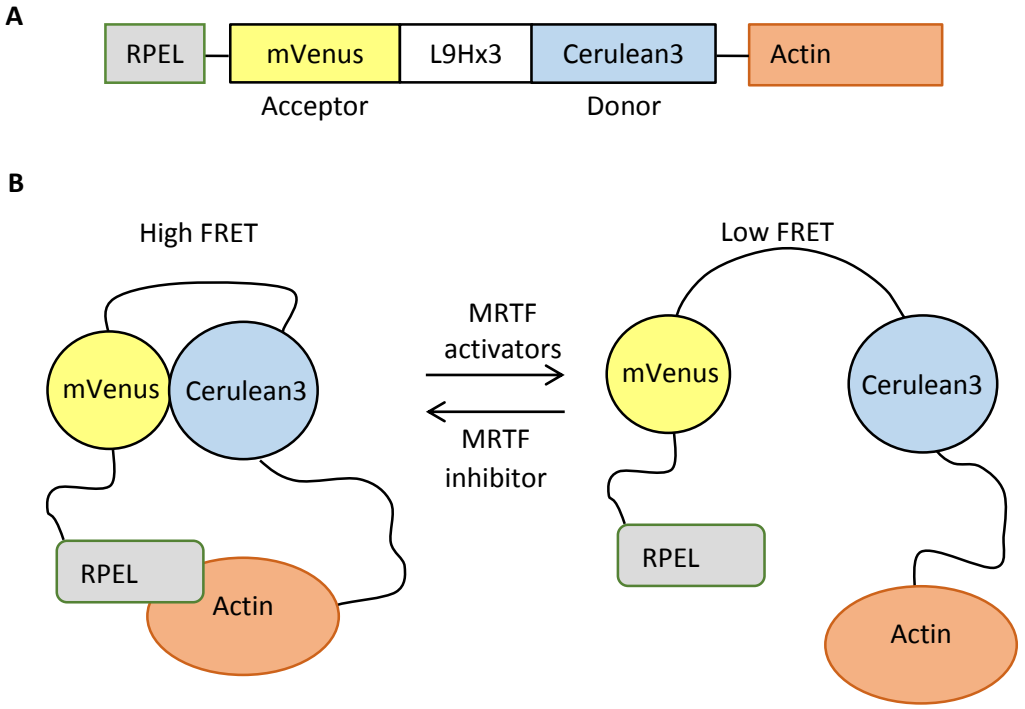

Figure 17: Schematic view of the FRET construct. A) Starting from the N-terminus, the FRET sensor is composed of: RPEL region, mVenus, a ribosomal protein-based linker (L9Hx3), mCerulean and actin. B) Representation of the intramolecular FRET energy transfer mechanism of the RPEL-actin FRET sensor inside the cell. A high FRET was yielded when RPEL and actin interaction was induced; vice versa, when RPEL:actin complex was dissociating after MRTF inhibitor addition, a low FRET was observed.

polymerizable actin mutant (R62D) as counterparts. The successful expression of all constructs in NIH 3T3 cells was verified using western blotting, confirming the expected molecular weights of the expressed proteins (Fig. 18).

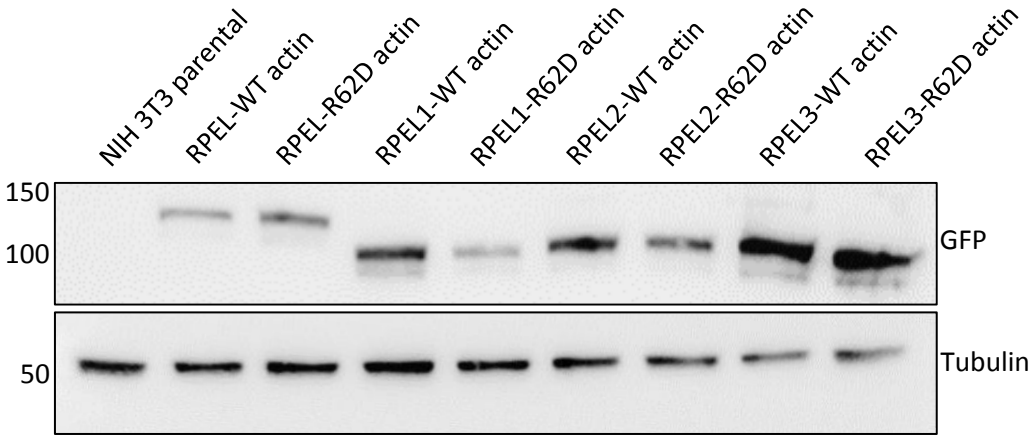

Figure 18: Expression of the new FRET constructs verified via western blot. Expression and protein size of 115 kDa and 104 kDa for the full RPEL constructs and for the single RPEL constructs respectively was investigated in NIH 3T3 cells performing a western blot using GFP antibody. Tubulin signal was used as loading control. The GFP signal specificity was compared to un-transfected NIH 3T3 parental cells.

4.2.2. FRET analysis on fixed and live cells

Subsequently, the localization and FRET analysis of the constructs were performed on fixed NIH 3T3 cells (Fig. 19A). Upon comparing the subcellular localization of all constructs, a notable difference was observed between the WT and R62D-expressing constructs, while no difference was observed for the different individual RPELs. All WT FRET sensor-expressing cells showed an inclusion of the sensor in the actin filaments, whereas all the R62D FRET sensors displayed a homogeneous distribution in the cytosol of the NIH 3T3 cells, indicating preserved actin structure and function in the sensor. As our goal was to analyse the interaction between G-actin and the RPEL motif, WT constructs were excluded from further experiments due to their inclusion into the actin filaments.

To select a construct for deeper analysis, FRET ratio changes before and after FBS stimulation in fixed NIH 3T3 cells were investigated (Fig. 19B). Here, FBS addition is expected to induce RPEL dissociation from the R62D actin through the Rho signalling pathway. For each construct, the FRET ratio of stimulated cells was normalized to the FRET ratio of all starved cells, which was then set to value 1. Among all the R62D constructs, only the RPEL2 sequence FRET sensor showed a reduction in the FRET ratio after FBS stimulation, whereas the RPEL1 and RPEL3 sequences displayed an increase in FRET ratio. This suggests that only the RPEL2 sequence was successfully dissociating from R62D actin, possibly due to different affinities of the RPEL sequences. RPEL1 has the strongest affinity to actin, whereas RPEL3 has the weakest affinity (Mouilleron et al. 2008). It is possible that RPEL1 did not dissociate in our construct due to the absence of other RPEL sequences, or RPEL3 did not bind to R62D actin, or the RPEL3:R62D actin interaction was too low to detect any dissociation after FBS. Additionally, the full-length RPEL motif displayed strong nuclear localization and did not show FRET reduction after FBS stimulation, and hence was excluded from further analysis.

Taken together, these results strongly show that the RPEL2-R62D FRET sensor is suitable for monitoring events leading to MRTF:actin dissociation.

Moreover, the events that induce MRTF dissociation are more likely to be due to actin-binding competition since no PTM event was so far found in the RPEL sequence after stimulation (Panayiotou et al. 2016).

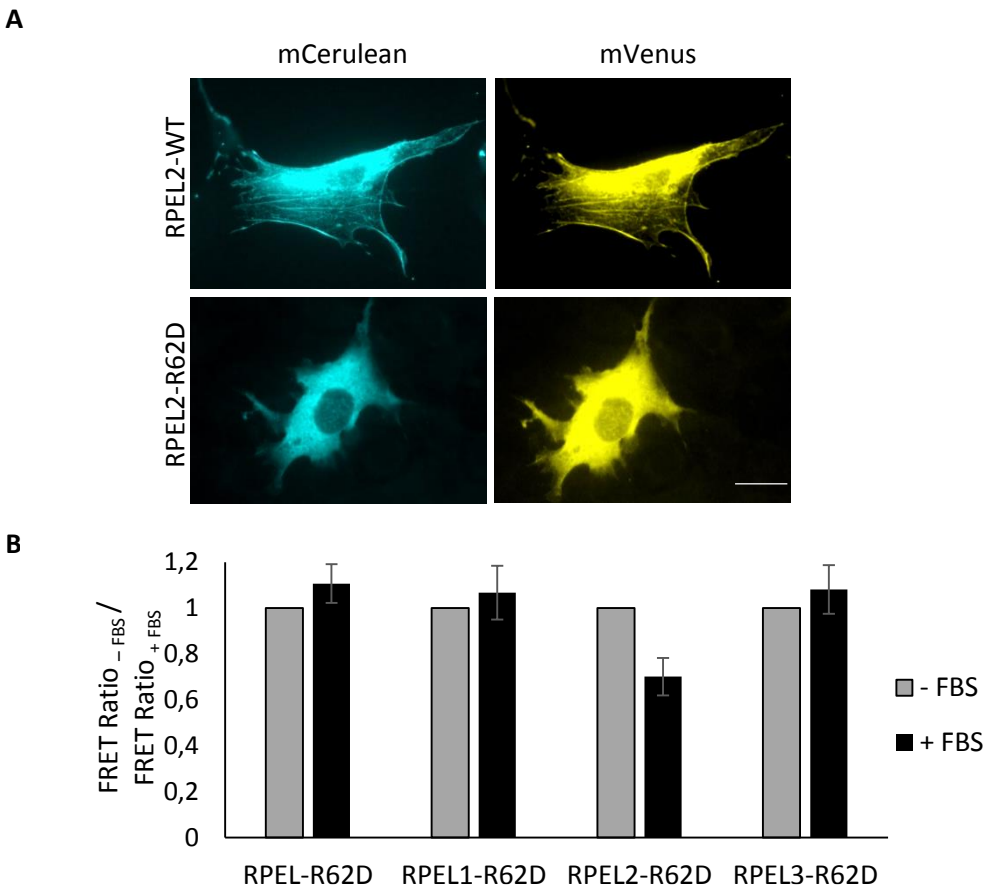

Figure 19: Constructs spatial and FRET ratio analysis in fixed cells. A) Visual localization of the RPEL2 FRET constructs inside fixed cells expressing the WT or the R62D actin. Donor (mCerulean) and acceptor (mVenus) fluorophores shown in blue and yellow respectively. Same construct localization was observed also for the other RPEL constructs. B) Comparison of the FRET ratio after FBS stimulation (+ FBS) normalized to starvation condition (- FBS) in fixed cells expressing R62D actin constructs. Three independent experiments were performed, each with a range of 3 to 18 cells analysed per condition. Error bars indicates SEM. Scale bar 20 µm.

4.2.3. Live imaging analysis

After having checked the dissociation of RPEL2:R62D actin complex in fixed cells, the dissociation of RPEL2:R62D actin complex after FBS addition was also confirmed through live imaging analysis (Fig. 20). To avoid interference during the measurements, a complete medium without phenol red was used (Trapani et al. 2012). The dissociation of RPEL2:R62D actin was monitored for 15 minutes, and the resulting FRET ratio was calculated at every minute. The normalized FRET ratio at 5, 10, and 15 minutes after FBS addition was compared to time 0 for the analysis of FRET ratio reduction. As a control, the normalized FRET ratio was also calculated for samples where PBS was added instead of FBS (Fig. 20, right graphic). Remarkably, a reduction in FRET ratio was observed only after FBS addition, which resembled MRTF activation.

To confirm that the observed FRET ratio reduction was sequence and stimulus related, a mutated RPEL2 sequence was analysed in both conditions (Fig. 20, left graphic). Specifically, a

substitution of alanine for the canonical proline in the RPEL sequence has been shown to disrupt MRTF:actin complex formation (Posern et al. 2004; Miralles et al. 2003). No FRET ratio reduction was observed in cells expressing the RPEL2 (P133A)-R62D construct after FBS or PBS addition, indicating that the RPEL2 (P133A):R62D complex was not formed due to the point mutation, and thus, no difference in FRET ratios could be detected.

Although the RPEL2-R62D construct exhibited a specific FBS-induced FRET ratio reduction that was maintained over time, ratiometric images for the analysis of FRET differences in space inside the cell could not be obtained using fluorescent microscope ZEISS Apotome. Consequently, in collaboration with the group of Prof. Dr. Ralf Anton Benndorf, further FRET experiments were conducted using a confocal laser scanning microscope (Nikon A1R) to obtain spatial information.

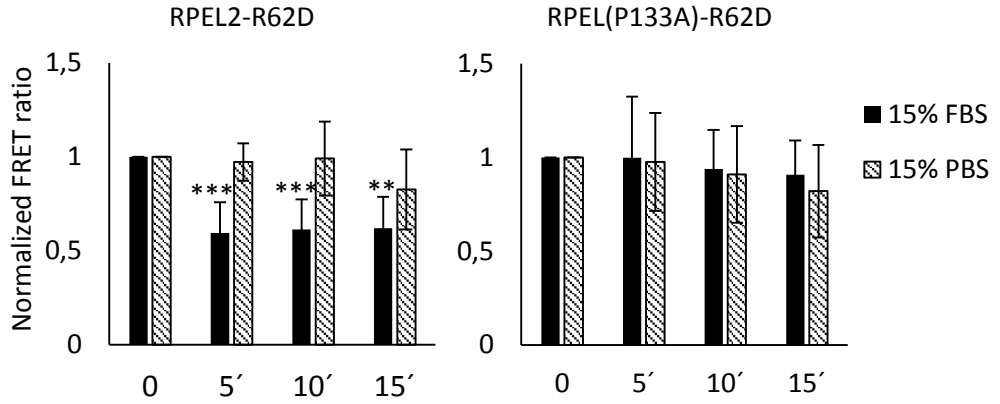

Figure 20: Temporal FRET ratio trend study. FRET ratio of the RPEL2-R62D sensor 5´, 10´ and 15´ after FBS/ PBS was normalized to t0 in starvation condition (left graphic). For RPEL2 sequence specific effect validation, RPEL(P133A)-R62D FRET sensor was analysed as negative control (right graphic). A minimum of 13 cells were analysed per condition recorded on three different days. Error bars indicates SEM; **p≤ 0.01, ***p≤0.001 significant change RPEL2-R62D + FBS compared with +PBS; unpaired one sample Student's t-test.

4.2.4. FRET experiments with confocal

4.2.4.1. FBS effect on RPEL2-R62D and RhoA sensors validated with confocal set up

To verify data reproducibility, FBS/PBS experiments were repeated using a confocal microscope in the lab of Ralf Benndorf, Institute of Pharmacy, MLU Halle (Hauke et al. 2022) (Fig. 21A). The FRET index was evaluated (Berney and Danuser 2003) and normalized to the FRET index of the baseline. FBS induces dissociation of RPEL2 from R62D inside the FRET sensor and, consequently, a detection of the reduction in FRET index is expected. Similar to previous experiments, a specific FBS-induced FRET index reduction was detected compared to PBS both added to the cells at time 0, indicating the dissociation of RPEL2 from R62D only after FBS addition (Fig. 21A, bottom). FRET index reduction after FBS was significant (p≤ 0.05). Additionally, images representing the FRET index in percentage were obtained by normalizing the corrected FRET image to the

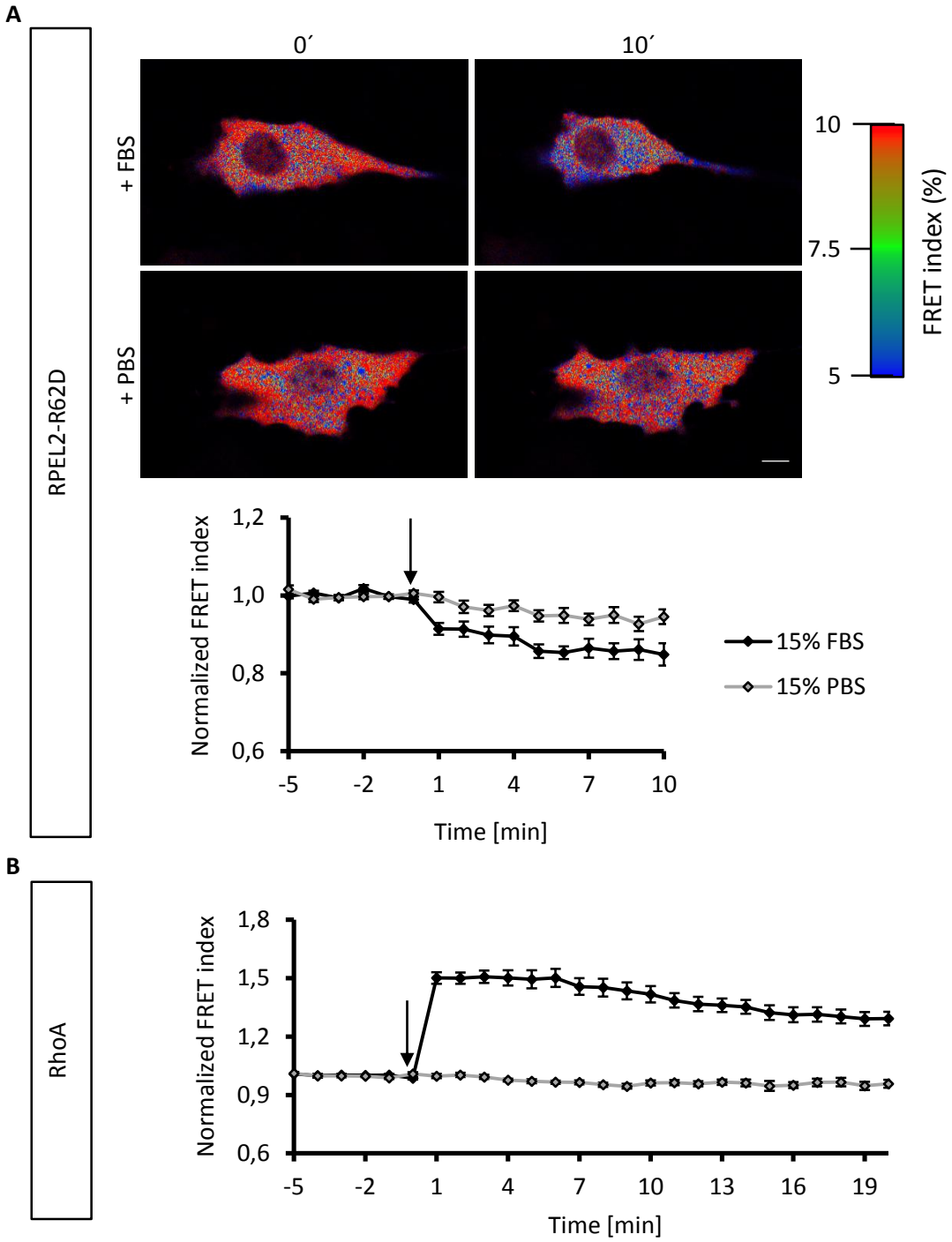

Figure 21: Validation of the RPEL2-R52D and Rho sensors for confocal experimental set up. A) Visualization of average baseline-normalized FRET index in time RPEL2-R62D (bottom). Interaction dynamics were detected with confocal microscope after FBS/PBS addition at t0 (black and grey lines respectively). Visualisation of corrected FRET images at time 0 and 10 +FBS/PBS (top). B) Rho-ΔPKN FRET sensor was tested +FBS/PBS for the set-up control. A minimum of 15 cells were analysed per condition on three different days. FRET index was normalized to averaged baseline. Error bars indicate SEM. Scale bar 10 µm.

intensity of the donor intensity (Fig. 21A, top). Since each corrected FRET image is normalized to the corresponding donor, it is not possible to compare the FRET index between different experiments. This is also due to the fact that the signal and the FRET reduction recorded are too

small for a direct comparison, thus it is essential to calculate the FRET index normalized to the baseline.

As an additional positive control, FBS action on the cells and RhoA activation after FBS addition were also investigated using a previously developed RhoA FRET sensor (Fig. 21B); data were significant with a p-value equal or lower to 0.001. The addition of FBS to the cells activates the Rho signaling pathway and thus, should activate the RhoA:ΔPKN FRET sensor and increas in FRET index after baseline normalization. As expected, FBS strongly increased FRET index of RhoA biosensor, indicating efficient RhoA activation. Moreover, the slow deactivation of RhoA was observed after 5 minutes (van Nieuw Amerongen et al. 2000; Zeidan et al. 2006).

In conclusion, our setups enabled us to detect changes in protein-protein interactions after FBS addition for both RhoA:ΔPKN and RPEL2:R62D complexes, indicating that our FRET sensor and confocal setups are suitable for investigating the dynamics of RPEL2:R62D interaction over time. Unfortunately, it was not possible to obtain spatial information; this could be due to the fact that this approach is not good enough for this kind of analysis or that the sensor needs further optimization.

4.2.4.2. Latrunculin B and Cytochalasin D

Many different actin drugs have been identified in nature that affect actin polymerization or depolymerization. Two examples are Latrunculin B (Lat B) and Cytochalasin D (Cyt D), produced by sponges and fungi, respectively. Lat B binds to monomeric actin, preventing actin polymerization, while Cyt D binds to the barbed end of actin, obstructing the sites for new monomeric actin insertion (Casella et al. 1981). Both of these actin drugs have been shown to affect not only actin polymerization, but also the actin:MRTF complex. Interestingly, Lat B and Cyt D have opposite effects on actin:MRTF complex; Lat B stabilizes actin:MRTF interaction, while Cyt D activates MRTF (Miralles et al. 2003; Sotiropoulos et al. 1999a). To further validate our sensor, the dynamics of RPEL2:R62D interaction were investigated in space and time using the RPEL2-R62D FRET sensor. To do so, NIH 3T3 cells were pre-treated with 0.1 µM Lat B for one hour, and then 15% FBS was added, and FRET measurements were recorded for 10 minutes (Fig. 22A). The derived FRET index revealed a significant increase in normalized FRET index after FBS addition in Lat B pre-treated cells compared to the pre-treated DMSO control cells ($p \leq 0.01$ at time 3 and 4; $p \leq 0.001$ after time 4). Additionally, it was observed that cell shape recovered after FBS addition from Lat B pre-treatment, which induced morphological changes to a spherical shape (Fig. 22A, right). For Cyt D analysis, the effect of 10 µM Cyt D on starved cells was compared for 20 minutes after its addition (Fig. 22B). In this case, Cyt D showed a direct effect

on RPEL2:R62D complex, inducing its dissociation, as indicated by the decreasing FRET index (Fig. 22B, left graphic), but with a lower rate compared to FBS (complessive p-value equal or lower to 0.05). Similar to Lat B, Cyt D induced morphological changes, showing cell retraction and arborization (Schliwa 1982; Loty et al. 1995)

In conclusion, using the newly developed RPEL2-R62D FRET sensor, it was possible to conduct a more in-depth analysis of the effects of Lat B and Cyt D on the complex. Although both drugs have a negative effect on actin polymerization, they showed opposite effects on RPEL2 affinity to actin.

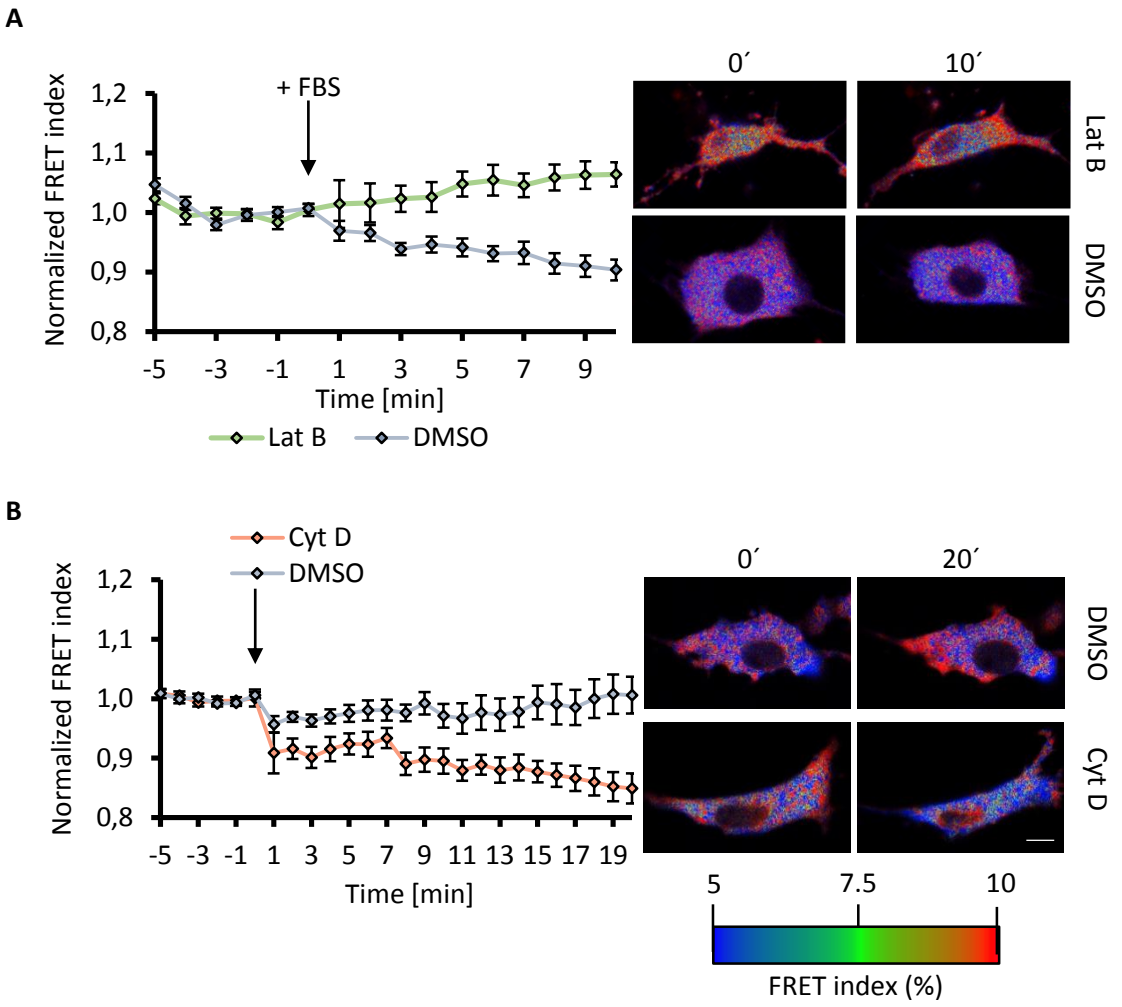

Figure 22: Investigation of RPEL-R62D sensor responses upon addition of different drugs. A) FBS was added to pre-treated cell with 0.1 µM Latrunculin B (LatB) or with DMSO as a control. Comparison of the FRET index effect (left) and cell morphology changes (right) after FBS addition is shown. (B) 10 µM CytD or DMSO were added at t0 in order to validate CytD MRTF-activation. CytD effect on the FRET index trend was followed up to 20 minutes (left graphic) and a strong effect at the morphology level were observed (FRET index figure on the right). The average baseline was used to normalize the FRET index. On three different days, a minimum of 15 cells were analysed per condition. Error bars indicate SEM. Scale bar 10 µm.

4.2.4.3. Analysis of MRTF:actin complex interfering factors

Continuing with the analysis of factors that interfere with the MRTF:actin complex, FRET experiments were conducted to gain a deeper understanding of their mechanism of action and their temporal and spatial influence. To investigate the effect of a ROCK inhibitor (Y-27632) on MRTF activation via the Rho signalling pathway, NIH 3T3 cells were pre-treated with either 10 µM Y-27632 or water as a control, and subsequently stimulated with FBS (Peh et al. 2015). Y-27632 inhibits the Rho-associated protein kinases (ROCKs) effectors, thereby blocking the transmission of the signal which should prevent FRET index reduction during stimulation. Normalized FRET index showed a decrease after FBS addition in cells pre-treated with water, while an increase was observed in Y-27632 pre-treated cells, suggesting an increase in RPEL2:R62D complex affinity (Fig. 23A).

Previous studies have shown that the WH2 region competes with MRTF for actin binding (Kluge et al. 2018). To analyse the effect of the WH2 region on our RPEL2-R62D FRET sensor, the sequence of the first WH2 region of JMY was cloned with the mCherry fluorophore (Fig. 23B). Since mCherry has a different excitation and emission wavelength than mVenus and Cerulean3, it was used for identifying cells co-expressing the RPEL2-R62D FRET sensor and the WH2-mCherry plasmid. In this case, cells co-expressing both mCherry-WH2 and RPEL2-R62D FRET sensor are expected to not display any effect after FBS addition. No reduction in FRET index was detected in mCherry-WH2 and RPEL2-R62D FRET sensor co-expression after FBS addition. To confirm the specificity of the WH2 effect, mCherry alone was co-transfected with the RPEL2-R62D FRET sensor, and its effect was compared to the mCherry-WH2 co-transfected cells. Here, the activation of RPEL2-R62D FRET sensor is expected to be recorded. As expected, mCherry co-expression did not interfere with the FBS response of the RPEL2-R62D FRET sensor. It is possible that the mCherry-WH2 induced RPEL2:R62D dissociation in the absence of FBS, thereby making the sensor less responsive to FBS, since a significant change was observed after only 9 minutes ($p \leq 0.01$). In this case, the FRET index in the baseline should be lower compared to the only mCherry co-transfected cells. As mentioned before, it is not possible to verify the differences between the two conditions by comparing the FRET indexes.

To verify our sensor's ability to detect inhibitory compounds that act on MRTF outside the RPLE motif, a second-generation inhibitor, CCG-203971, was tested (Fig. 23C) (Johnson et al. 2014; Melcher et al. 2022). Since the hypothesised inhibitory action of CCG-203971 on MRTF is its binding outside the RPEL sequence, the FRET index is expected to not be influenced by the presence of the CCG-203971. Cells were pre-treated with either 20 µM CCG-203971 or DMSO for 1 hour before FBS addition for inhibitor effect analysis. Interestingly, CCG-203971 had no

inhibitory effect on RPEL2-R62D dissociation and showed a reduction in FRET index ($p \leq 0.01$). Notably, CCG-203971 pre-treatments exhibited a stronger initial RPEL2:R62D dissociation compared to the DMSO control ($p \leq 0.01$ between time 1 and 12).

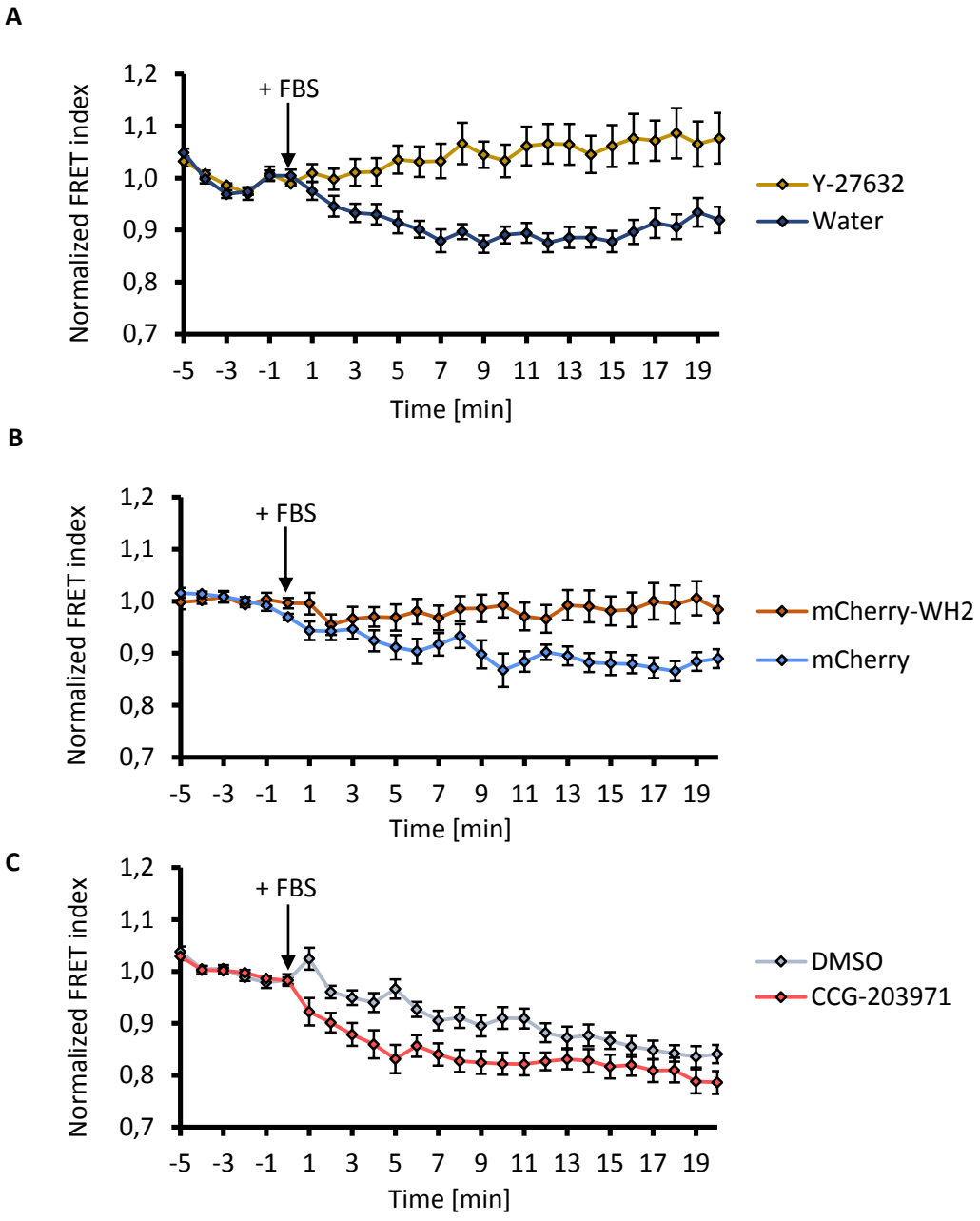

Figure 23: Analysis of effects of various MRTF-interfering factors on the RPEL2-R62D FRET sensor. A) NIH 3T3 cells were pre-treated for 1 hour with 10 µM Y-27632 ROCK inhibitor and FBS was then added at t0. To verify the specificity of the inhibitory effect of the Y-27632, FRET index trend was compared to cells pre-treated with water. B) FBS induced FRET index reduction was tested in cells co-expressing mCherry-WH2 construct with the RPEL2-R62D FRET sensor. Only mCherry construct co-expression experiments were carried out as control. C) Comparison of 20 µM CCG-203971 or DMSO pre-treated cells were stimulated with FBS at t0 normalized FRET index. For FRET index analysis, normalization to baseline FRET index was performed. A minimum of 15 cells were analysed per condition on three different days. Error bars indicate SEM.

Further, to verify the suitability of the RPEL2-R62D FRET sensor for long-term analysis, FRET measurements were performed for more than two hours in a study of the FBS reduction effect (Fig. 24A). To avoid phototoxicity from prolonged exposure time, measurements were taken for 20 minutes after FBS addition and then again after one and two hours. Unexpectedly, no recovery of FRET index was detected during this period of time, but instead, a constant decrease was observed up to two hours, after which it reached an apparent plateau (see section 4.1.2.2). To further investigate the recovery process, a Y-27632 ROCK inhibitor was added after 30 minutes of FBS stimulation for recovery analysis (Fig. 24B) (Eckenstaler et al. 2022). Interestingly, a tendency of normalized FRET index increment was detected after Y-27632 addition, indicating a direct influence of the Rho pathway on the dissociation of RPEL2:R62D actin complex. These findings shed light on the time-dependent dynamics of MRTF-actin interaction and provide valuable insights into the role of the Rho pathway in modulating this process.

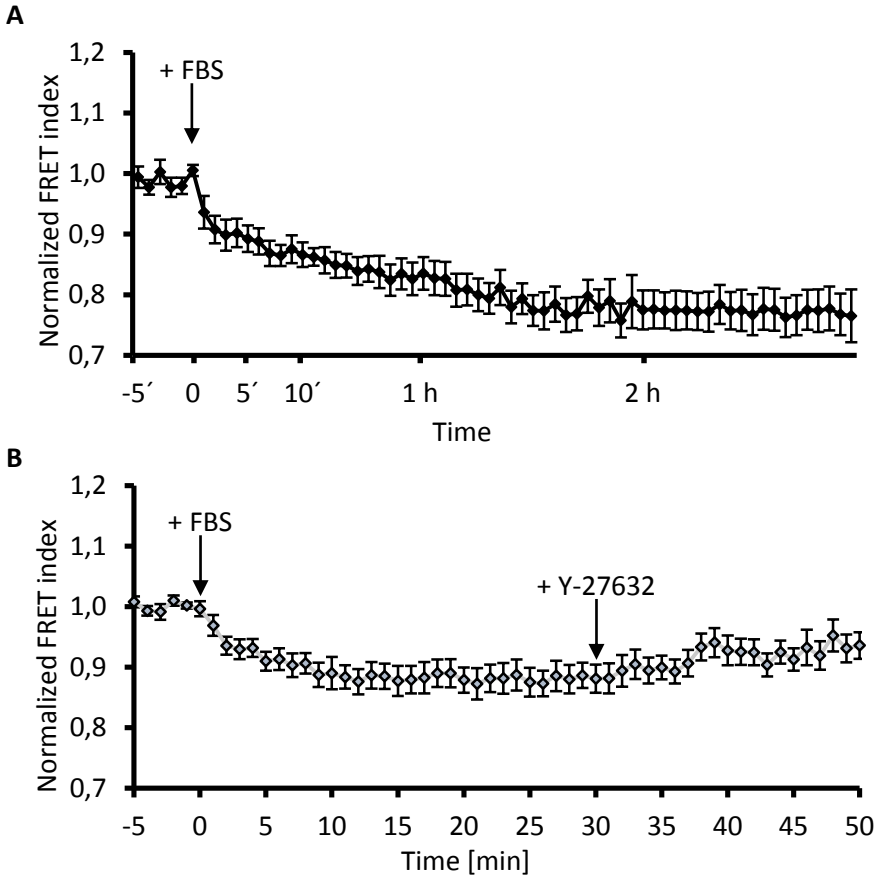

Figure 24: RPEL2-R62D FRET sensor is suitable for long-term analysis and for recovery experiments. A) RPEL2-R62D FRET sensor normalized FRET reduction was detected for more than 2h after FBS addition at time 0. B) Y-27632 ROCK inhibitor was added after 30 min FBS stimulation for the RPEL2:R62D re-association event analysis. RPEL2:R62D re-association was followed for 20 minutes after Y-27632 addition. For FRET index evaluation, normalization to baseline FRET index was performed. To obtain three different biological replicates, on three different days, a minimum of 15 cells per condition were recorded. Error bars indicate SEM.

4.2.4.4. Verification of FLIM experiments for RPEL2:R62D actin interaction

In addition to the sensitized emission FRET method, another FRET method used to verify the interaction between RPEL2 and R62D actin was FLIM (Fluorescence-lifetime imaging microscopy) (Fig. 25). FLIM allows for measurement of the fluorescence lifetime of the donor, also providing information about the FRET between the donor and acceptor molecules. A comparison was made between the fluorescence lifetime of the donor in the RPEL2-R62D FRET sensor and the negative control RPEL(P133A)-R62D FRET sensor for further validation.

A higher fluorescence lifetime of the donor was detected for the RPEL(P133A)-R62D negative control FRET sensor, indicating a greater distance (lower FRET) between the RPEL(P133A) and the R62D actin. In this configuration, the donor is further away from the acceptor, resulting in less quenching of the donor fluorescence by the acceptor and an increased lifetime of fluorescence decay. These results confirmed the specific interaction between RPEL2 and R62D actin, as detected in all previous experiments using the sensitized emission technique. FLIM was performed also in fixed and live cell experiments expressing the RPEL2-R62D actin FRET sensor comparing +/- FBS condition. In this case, no difference was observed between the two conditions within the same sample.

Nevertheless, the FLIM experiments provided additional evidence supporting the interaction between RPEL2 and R62D actin, although it was not possible to monitor the events which induce MRTF dissociation.

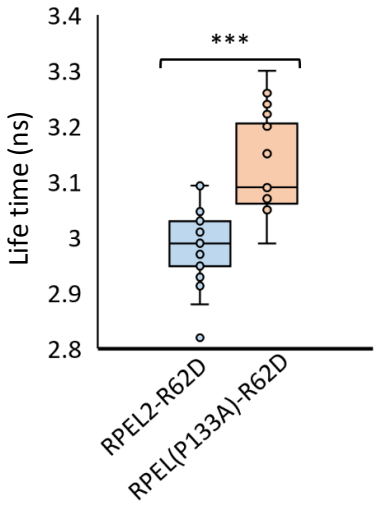

Figure 25: FLIM analysis of RPEL2-R62D and RPEL(P133A)-R62D FRET sensors. Box plot displaying the comparison of average lifetime of amplitude weighted donor in cells expressing the wild type RPEL2 sequence and the mutated RPEL2 sequence RPEL(P133A) for actin binding validation. For each sensor, a minimum of 16 cells were analysed on three different days; ***p≤0.001, error bars indicate SEM.

5. Discussion

Fibroblast recruitment in a wound is a physiological event for the recovery of an organ structure and its function after an injury or surgery. A dysregulation of fibroblast physiological function leads to the pathological condition of fibrosis, which can then bring about many complications, including organ failure. In order to prevent and cure fibrosis, many efforts have been made to elucidate the main causes and mechanisms that lead to fibrosis. MRTF dysregulation has been proven to be a major player in the formation of fibrosis in almost all organs. Many different factors and stimuli have been linked to MRTF regulation inside the cells, but it is still unclear how MRTF transcriptional activity is regulated. In this study, MRTF dissociation event from actin in the cytosol for MRTF activation is investigated. As a model, fibroblasts cell line isolated from embryonic mouse, called NIH 3T3 cell line, was used for the analysis. Furthermore, NIH 3T3 cell line has been widely used to study fibrosis *in vitro*.

Establishment of protein complex isolation and analysis

From previous experiments performed by Weissbach et al., a competition event between the RPEL domain of MRTF and WH2 region of other actin binding proteins (ABPs) has been hypothesized to take place during FBS stimulation (Weissbach et al. 2016). In order to identify possible MRTF competitor candidates, immunoprecipitation experiments were established (Miralles et al. 2003).

Posern et al. have analysed the biochemical properties of different mutant actins (Posern et al. 2002). They were able to identify different point mutations which had an impact on actin polymerization state. The mutants fell into two different groups: highly polymerizable (V159N and S14C mutants) and non-polymerizable actins (G13R, R62D, VP16 fusion protein in the C-terminal). Since MRTF binds specifically to actin monomers and the goal of this project is to identify monomeric actin binding proteins, R62D actin was expressed in NIH 3T3 cells. The switch from a negatively charged to a positively charged amino acid in position 62 prevents the formation of a salt bridge that is usually formed between subdomains 2 and 4 of actin. This non-polymerizable actin has been already used for the purification of ABPs by Weissbach et al. As a strategy to facilitate protein purification, a Flag tag was added to the N-terminus of the R62D actin sequence. Because the mutated actin allowed the pulldown of many known ABPs, it is possible to conclude that actin structure was preserved and the disruption of the salt bridge did not affect its folding or its binding ability (Miralles et al. 2003; Posern et al. 2004).

Different detergents have been applied in different lysis buffers depending on the system under analysis, the type of protein-protein interaction under investigation, and the kind of further

experiments that are planned. In fact, the choice of the detergent is essential for successful experiments. If the detergent used is too harsh, it may interfere with protein-protein interaction, reducing the detected interactome. On the other hand, if the detergent is too weak, unspecific proteins may not be washed away. For our purposes, a lysis buffer containing a MS-compatible detergent was compared to the standard RIPA buffer. The N-Dodecyl-beta-D-maltosid (DDM) detergent has already been proven to be a good alternative to other kinds of detergent and to not interfere with further MS analysis of the lysed sample (Stetsenko and Guskov 2017). DDM containing lysis buffer does not affect MRTF:actin complex in unstimulated cells in comparison to the standard RIPA buffer. Moreover, typical MRTF-actin dissociation after FBS addition was observed. Cytosolic MRFT:actin complex after FBS stimulation drastically decreases within one minute and after considerable time, only a small amount of MRTF re-locates from the nucleus to the cytoplasm. To verify the efficacy of the DDM detergent, MRTF binding to actin after FBS stimulation was visualized after 10, 20, and 30 minute intervals of post-stimulation, with slow actin binding recovery being observed over the respective times. This is due to the fact that free MRTF in the nucleus from SRF bound to actin, allowing the export of MRTF (Sidorenko and Vartiainen 2019). Since the goal of this project was to identify possible MRTF competitors, samples stimulated after 10 minutes were analysed under the assumption of having a higher amount of MRTF competitor bind to actin within a shorter stimulation time.

Co-immunoprecipitated sample analysis

For the identification of a possible MRTF competitor during FBS stimulation, different controls have been taken into account. As first, pulled down proteins in R62D expressing cells were compared to pulled down proteins in R62D non-expressing cells for specificity verification. As a second step, unstimulated and stimulated samples were analysed for proteins which were enriched in the stimulated condition. Moreover, MRTF competitor identification analysis was carried out in cells expressing R62D actin via two different forms of expression systems: transiently transfected and stably transfected NIH 3T3. The latter allowed for inducible expression by utilizing the TetON-system. This was done for two reasons: firstly, to increase biological replicates and have more solid results; secondly, to demonstrate that the results are reproducible in both expression systems, with the transient system typically having a higher expression of the exogenous protein compared to the stable system. For protein identification, one of the most sensitive and fastest techniques is mass spectrometry (MS). It has been widely used for many proteomics in both *in vitro* and *in vivo* experiments. For this reason, MS was selected for the analysis of co-immunoprecipitated samples. Given the high number of samples

(four samples per biological replicate for both expression systems, bringing a total of twenty-four samples), a MS-analysing strategy had to be applied. For this purpose, TMT-10 plex labeling kit was applied. With this technique, it is possible to combine and directly compare peptide and protein amounts between different samples in only one MS run. This reduces the variability due to sample injection and reduces the measurement time. Unfortunately, this led to different problems in both expression systems: i) a very low number of proteins were identified in all samples; ii) a similar amount of proteins were found in samples +/- R62D expression; iii) a very low amount of ABPs were identified; iv) no possible MRTF competitor was found. Even though the analysis of actin and other ABPs reflected the same trend and the results that were observed in the western blots previously to the MS-TMT analysis indicating a high reproducibility between the samples, new experiments had to be performed.

In order to reduce experiment complexity, further experiments were analysed in MS label-free condition. In this case, only stable Flag-R62D cell line was used to reduce R62D expression variation between the samples, and proteins enriched after immunoprecipitation were identified by comparing Co-immunoprecipitated samples with the corresponding input instead of the R62D non-expressing samples. As a last step, protein abundances between the Co-immunoprecipitated samples +/- FBS were compared to determine ABPs binding after FBS addition. Although the analysis of the peptides identified in each sample revealed that one biological replicate had a different peptide content, no strong difference was observed at the protein level between the biological replicates. Moreover, all of the previous complications faced with the TMT-10 plex experiment were overcome and it was possible to identify some proteins enriched after FBS stimulation.

Analysis of function of MRTF competition

Among the top 10 enriched proteins in the stimulated samples after immunoprecipitation, four proteins were then selected to be further analysed, namely Cobll1 (Cordon-bleu protein-like 1), Radil (Ras-associating and dilute domain-containing protein), Samhd1 (Deoxynucleoside triphosphate triphosphohydrolase) and Ube3a (Ubiquitin-protein ligase E3A). With the exception of Samhd1, the involvement of these proteins in cell signalling and actin rearrangement was proposed (Choi et al. 2021; Tonazzini et al. 2019; Winckler and Schafer 2007). As a next step, the binding ability of the four proteins was tested via western blot using specific antibodies for each protein and validated for Radil, Cobll1 and Samhd1; however, Ube3a was not detected after immunoprecipitation. This could be due to a very low presence of Ube3a in the Co-immunoprecipitated samples or to the high sensitivity of MS compared to WB (Timp

and Timp 2020; Ye et al. 2013). Furthermore, higher abundance of the proteins was detected after FBS stimulation. Afterward, specific knockdown for each specific candidate was performed to address their ability to dissociate MRTF from actin during stimulus. The knockdowns were performed by using a mixture of four small interfering RNAs (siRNAs) targeting the same gene of interest, and thereby increasing knockdown efficiency. The knockdown was validated for all the candidates with the exception of Radil. Because many different growth factors are contained in the FBS solution, it is also possible that different pathways synergistically activated and dissociated MRTF from actin; therefore, a quadruple knockdown with all siRNAs was also put under investigation. For each knockdown and combined knockdowns, immunoprecipitated MRTF amount was analysed in the western blot in both starved and stimulated cells. Unfortunately, none of the knockdown was observed to have an evident MRTF inhibition. It is possible that these proteins may dissociate a very low amount of MRTF and, thus, it is not possible to detect clearly the effects of the knockdown with western blot. Moreover, because Radil knockdown was not successful with the siRNA, its influence on MRTF:actin complex still needs to be analysed. In fact, Radil knockdown performed by Smolen et al. in zebrafish model has shown to impair cell adhesion and migration during neural crest development (Smolen et al. 2007). In addition, Ross et al. laboratory performed different knockdowns of various Rap effectors and, among all, Radil has been proven to be the only Rap effector to have a major impact in Rap signalling (Ross et al. 2011). In this case, Radil knockdown was analysed in lung epithelial cells where cell spreading was inhibited in the majority of cells (70%).

In conclusion, it was not possible to verify the involvement of Cobll1, Radil, Samhd1 and Ube3a in activating MRTF during stimulation with this specific approach. Therefore, further investigation is needed in order to conclude any influence on MRTF.

Analysis of formation of RPEL-actin complex and dissociation events

Protein-protein interaction (PPI) is crucial for regulation of cellular processes. For this reason, much effort has been put forth to clarify protein interaction dynamics and the nature of the interaction. This is highly important since many pathological conditions are due to dysregulation of PPI and protein function. Among the techniques that are currently in use for the analysis of PPI in space and in time, FRET technique is one of the most used (Xing et al. 2016). Thanks to its many advantages, FRET technique can be used not only for PPI studies, but also for studying cellular environments which may affect protein conformation and protein sublocalisation, among others. For the analysis of FRET in living cells, different kinds of biosensors have been recently developed, where the donor and the acceptor are expressed in the same polypeptide

together with the proteins of interest. In recent time, new Rho FRET biosensors have been developed and tested by Reinhard et al. (Reinhard et al. 2016). Thanks to these new FRET biosensors, Reinhard et al. were able to study the activity of Rho A, B and C in endothelial cell line in different conditions. Furthermore, they were also able to identify the subcellular region where the different Rho were activated.

Because our goal was to visualize the events which lead to the known MRTF:actin dissociation and association inside fibroblasts after the addition of different compounds and stimuli, a new FRET biosensor based on the Reinhard sensor was designed. Because the FRET sensor is completely independent of G-actin depletion and F-actin dynamics, the subsequent events will be restricted to the direct activation of the complex. As clarified in section 1.1.2., MRTF interacts with actin via its intrinsically disordered region called RPEL motif. For our purposes, we focused our attention on only RPEL motif sequences and actin. Thanks to the studies of the crystal structures done by Mouilleron et al., it was demonstrated that each RPEL sequence, together with the two spacers contained in the RPEL motif, are able to bind a monomeric actin to form either pentameric or trivalent complexes (Mouilleron et al. 2011). This indicates that other domains of the MRTF do not influence the binding of RPEL to actin and, for this reason, only the RPEL motif and each RPEL sequence were used for the development of a new FRET biosensor. Wild type (WT) and R62D actins were used for the design of the FRET sensor. Subsequently, the expression and function of the different constructs were investigated using a fluorescent microscope. All constructs were successfully expressed and no variation on the expected molecular weight was observed, indicating that the entire biosensor was expressed as a single polypeptide. In relation to the subcellular localization of the different biosensors, a major difference between the constructs was observed regardless of whether WT or R62D actin was expressed. In all cells expressing R62D actin sensors, signals from the fluorophores were detected throughout the cytosol. WT actin constructs were inserted into the actin filament in some cells. From this, it is possible to conclude that WT actin structure is not affected inside the sensor and was able to form actin filaments as the endogenous actin. Considering that the ultimate goal is to analyse the events in the cytosol that influence RPEL and the monomeric actin, all the constructs expressing WT actin were not considered for RPEL-actin interaction analysis. As a further step, energy transfer in R62D construct was checked and inspected in fixed cells. FRET ratio in stimulated cells was normalized to the corresponding unstimulated cells and the normalized FRET ratio after stimulation was compared between the RPELs constructs. After normalization, a decrease in FRET ratio to the corresponding unstimulated samples was

observed only in RPEL2-R62D FRET sensor. In this way, a decrease in FRET ratio indicates a higher distance between the proteins of interest and, in turn, the dissociation of RPEL from actin.

This can be explained by the different interaction affinity that each RPEL sequence has with actin. RPEL1 has the strongest interaction affinity to actin in comparison with the other RPEL sequences, probably due to its non-canonical RRxxxEL core sequence, whereas RPEL3 has the lowest interaction affinity. From crystal structure analysis of the structure of RPEL:actin complexes, it seems that RPEL2 is essential to the formation of both pentameric and the trivalent forms and is not fully structured in both complexes. This makes RPEL2 a major target for the disruption of the MRTF:actin complex. From this, it is possible to conclude that: i) RPEL2:actin dissociation is independent of other MRTF domains; ii) the only RPEL2 sequence is sufficient to resemble the events which induce MRTF activation; iii) R62D structure is not affected inside the biosensor and it maintains its functions; iv) because no phosphorylation within the RPEL2 sequence has been recorded after stimulation, it is more likely that RPEL2-R62D dissociation is due to protein competition (Panayiotou et al. 2016).

In order to prove that the ability of the RPEL2-R62D FRET sensor is able to respond to FBS stimulation in live cells, FRET ratio trend over time after FBS stimulus addition was followed. In order to be able to compare all of the different samples, FRET ratios were normalized to time 0 when cells were in unstimulated condition. A strong reduction of normalized FRET ratio was observed only after FBS addition, as compared to the PBS controls where no major changes were detected. In 2003 the Treisman group investigated how RPEL:actin complex is affected when the RPxxxEL core sequence is mutated (Miralles et al. 2003). In their research, the point mutation of the prolin to an alanine had drastically affected the ability of RPEL to bind actin in the cytosol, having as an effect a constitutive nuclear localization. Thus, as an extra control for the verification of the specificity of our sensor, the prolin of the RPxxxEL core sequence of RPEL2 sensor was mutated to alanine. As expected, the point mutation impaired the capability of RPEL2 to respond to FBS and no difference was noticed if PBS was instead added to the cells. This first step of functional validation of the RPEL2:R62D FRET sensor proved to be a powerful tool for the analysis of RPEL:actin interaction dynamics in living cells.

As discussed in section 1.1.3, MRTF transcriptional activity can be activated by many different factors, but a critical step is the release of MRTF from actin. For this reason, the newly developed RPEL2-R62D FRET sensor was used for the analysis of dissociation-association events that may occur inside the cells using different MRTF interfering compounds. Because, in the previous experiments, it was not possible to obtain ratio-metric images representing protein interaction inside the cells, all further analyses were performed with confocal microscope set-ups for better

outcomes. At first, validation of the set-ups were performed for the comparison of the results between the different microscopes. Here, FRET index trends, after the addition of compounds to the cells, were determined and normalized to the average of the baseline FRET index. In cells expressing RPEL2-R62D FRET sensor, the FBS addition induced a reduction in the normalized FRET index to the baseline compared to the PBS addition. Furthermore, the RhoA- ΔPKN FRET sensor was also tested for the comparison of our results with Reinhard et al. as an additional step of validation of our microscopy set-up and data analysis. RhoA activity drastically increased initially when FBS is added, and then its activity slowly reduced over time. This response was specifically induced by FBS, as no response was detected with PBS addition. This RhoA activation trend was comparable to the one seen by Reinhard et al., which indicates a good reproducibility of the data as well as the adaptability of the FRET sensors with different microscopes.

After validation and visualization of FBS dissociation with the RPEL2:R62D FRET sensor over time, we analysed how different compounds that interfere with physiological MRTF:actin interaction may affect our sensor. Different cytoskeletal drugs exist naturally and have been developed that affect either polymerization or depolymerisation. Two actin drugs have been widely used in scientific research that affect actin polymerization with different mechanisms, Latrunculin B (Lat B) and Cytochalasin D (Cyt D) (Morton et al. 2000). Lat B binds to actin monomers, preventing them from being inserted into new filaments, whereas Cyt D binds to the barbed end of actin filaments preventing binding of new actin monomers to the filament. It is hypothesised that the ABPs binding is prevented when Cyt D is bound to actin (Sotiropoulos et al. 1999b; Miralles et al. 2003; Posern et al. 2002). Due to their ability to bind only actin monomers, Lat B is widely used for structural analysis of actin, while Cyt D is used for the inhibition of migration, adhesion and other actin cellular function (Goodman 2008). Both drugs have been shown to also affect MRTF:actin interaction with opposites effects; Lat B increases the binding affinity of MRTF to the monomers, whereas Cyt D induces the dissociation of MRTF from actin. We investigated how these two drugs affect RPEL2:R62D in fibroblasts in comparison with the DMSO controls. For Lat B, transfected cells were either pre-treated for one hour with 0.1 µM Lat B or DMSO and FBS was added to the cells. Compared to the baseline of Lat B treated cells, normalized FRET index increased, indicating a stronger interaction between RPEL2 and R62D, an increase which was not observed in the DMSO control where the FRET index trend was comparable to the FBS experiment. In the other case, 10 µM Cyt D was added instead of the FBS. Interestingly, CytD-induced decreases in FRET efficiency occur at a slower rate when compared to FBS. This is a new powerful tool to have a better understanding of the mechanism of the action of different actin drugs.

As previously explained, MRTF is activated via the Rho signalling pathway, so we analysed the influence of the Rho signalling pathway inhibition to our biosensor. In research, a variety of inhibitors against specific targets have been developed and used for the analysis of protein-protein interaction and for the analysis of different pathways. Specifically, the effects of Y-27632 inhibiting the Rho-associated kinases (ROCKs) downstream targets of the Rho pathway was examined. In different studies, Y-27632 has been shown to have an anti-fibrotic effect and, in colonic myofibroblasts, it reduces the formation of both mature focal adhesion and actin stress fibers (Bourgier et al. 2005; Johnson et al. 2014). 10 µM Y-27632 treatment was carried out one hour before the addition of FBS to the cells for the analysis of RPEL2-R62D interaction dynamics. As compared to the water pre-treatment control, Y-27632 completely desensitized the complex from FBS and instead, an apparent increase in RPEL2-R62D interaction was observed. From this result, we can conclude that Y-27632 inhibits MRTF activation from interfering with RPEL2-actin interaction and that this is the main event required for MRTF to dissociate.

During stimulation, as discussed above and in section 1.1.3, a competition event has been hypothesised and, from the analysis of different ABPs, WH2 domain (WASP-Homology 2, or Wiskott-Aldrich homology 2) has been shown to be a possible MRTF competitor during stimulation. In fact, the influence of each WH2 region of JMY (Junction mediating and regulatory protein) on MRTF transcriptional activity was studied by Kluge et al. They were able to demonstrate that the overexpression of each single WH2 region was sufficient to inhibit the expression of MRTF target genes (Kluge et al. 2018). Thus, the first WH2 region isolated from JMY was used for competition analysis with the RPEL2 sequence with the R62D in the FRET biosensor. In order to visualize cells expressing both components, the WH2 region was expressed in the same polypeptide with mCherry fluorophore for identification of co-expressed cells. As a result, the sensor was insensitive to the FBS and no difference in normalized FRET index was observed when WH2 region was co-expressed. Any influence on the RPEL2:R62D complex due to the presence of the mCherry was excluded, since the sensor was able to respond to FBS when only mCherry was co-expressed. The working hypothesis is that the WH2 region competes with the RPEL2 sequence for the binding to the R62D actin already in the starvation condition and, thus, the addition of FBS does not have any further effect on the complex.

Many different MRTF inhibitors have been developed, but their exact mechanism of function is still under investigation. For example, Evelyn et al. identified CCG-1423 as a Rho/MRTF/SRF pathway inhibitor via a high-throughput screening in Rho-induced cancers. Although many efforts have been made for the clarification of CGG-1423 function, it was not possible to identify a molecular target or its molecular function. For the moment, it is assumed that CCG-1423 may

interfere with MRTF regulation in different ways, such as preventing its nuclear translocation by binding the NLS of MRTF or indirectly by binding to another regulating actin protein, MICAL-2 (Evelyn et al. 2007; Lisabeth et al. 2019). From here, other new CCG compounds have been developed for the MRTF inhibition in both cancer and fibrosis. Between these second-generation inhibitors, CCG-100602 and CCG-203971 have been tested by Johnson et al. in human colonic myofiroblasts (Johnson et al. 2014). Both compounds are the focus of new research, since they display a low toxicity compared to the CGG-1423 and a higher MRTF inhibition. Also in this case, the mechanism of action and the molecular target are not known and a similar mechanism as for CGG-1423 is hypothesised. In order to examine if these compounds inhibit MRTF by affecting RPEL:actin interaction, cells were pre-treated for one hour with 20 µM CCG-203971 and FBS response was then investigated. As expected, normalized FRET index decreased after FBS addition, but with the CCG-203971 pre-treatment a stronger reduction of the FRET index was observed compared to the DMSO control. As mentioned before, it is hypothesized that CCG compound blocks the translocation into the nucleus of MRTF interfering with the importin α/β1 binding (Sisson et al. 2015). It is possible that CCG-203971 has multiple targets inside the cell and that the inhibitory MRTF effect is due to the inhibition of MRTF translocation. Given the inconsistency of these results with the known CCG-203971 MRTF inhibitory effects, it is possible also that these results are not fully resembling their real effect on RPEL2-actin complex. In the future, further analyses need to be performed to test this hypothesis.

The dissociation of MRTF from actin after stimulation has been observed up to 2 hours with a slow recovery during this observation time. With our FRET sensor, it was possible to monitor the increase of dissociation for up to 2 hours before reaching a plateau. This may indicate a continuous dissociation event, which reached its peak around 2 hours, with the system being saturated and more stabilized to the FBS stimulus afterwards. From these results, it is possible to hypothesise that the regulation of the other MRTF domains, for example via PTMs, are essential for the control of MRTF-actin re-binding event. Because of the impossibility to visualize MRTF-actin recovery binding, 10 µM Y-27632 effect after 30 minutes from FBS stimulation was analysed. As expected, the addition of the ROCK inhibitor slowly reverted the effect of the FBS to the FRET sensor. This indicates that Rho inhibition has a direct effect on the cause of MRTF dissociation and is sustained in time by the constant activation of Rho signalling pathway. Taking into consideration the hypothesis of WH2 domain competition with RPEL for actin protein, proteins containing WH2 are activated via a variety of ways through different pathways (Lane et al. 2014). For instance, they can be activated through phosphorylation of tyrosin$_{291}$ by the

hematopoietic-specific Src family kinase, Hck (Cory et al. 2002); or with the tyrosin$_{256}$ phosphorylation being regulated by focal adhesion kinase (FAK) (Wu et al. 2004). Through the Rho signalling pathway, the WH2 regions are exposed after Cdc42 or phosphatidylinositol 4,5-bisphosphate (PIP2) binding, which disrupts the auto-inhibition conformation due to the interaction of the GBD (GTPase binding domain) to the VCA domain (verprolin; central, acidic domain) (Ngoenkam et al. 2021). To conclude, it is possible to hypothesise that FBS activates Rho signalling pathway, which in turn activates a competitor, possibly a WH2 containing protein, and its activation is sustained in time by the activity of Rho.

Comparison of RPEL2:R62D actin intensity-based FRET via an alternative FLIM-FRET method

Although all previous results had given new knowledge of the RPEL2:R62D actin complex dissociation event, there was a need to validate the RPEL2:R62D interaction inside the cell. In order to reach this goal, the validation of the FRET data is often performed with another FRET technique (Elder et al. 2009; Mueller et al. 2013; van Unen et al. 2015). FLIM (Fluorescence-lifetime imaging microscopy) is a powerful tool for the analysis of protein-protein interaction where only the donor lifetime is measured. In case the acceptor fluorophore is in close proximity (high FRET), it is possible to see the donor being quenched by the acceptor causing a reduction in fluorescence lifetime. The RPEL2:R62D lifetime is compared to the donor lifetime of the mutated non-actin-binding RPEL2 FRET sensor, the RPEL(P133A)-R62D. The RPEL(P133A)-R62D FRET sensor displayed a higher donor lifetime compared to the WT RPEL2 sequence, indicating a lower FRET by the lower distance between the two proteins of interest. This result validates the different affinity which the two sequences have for actin binding. Although FLIM is able to overcome many of the limitations of the sensitized emission, it was not possible to confirm a difference in the lifetime of the donor in the RPEL2-R62D FRET sensor between starvation and stimulation condition. This could be due to the fact that the difference in the lifetime of the donor before and after FBS addition to the cells is too small to be detected or that the signal-to-noise ratio is low (Leavesley and Rich 2016). Moreover, the lifetime of donor expressed without the acceptor was not achieved in our experiments, preventing corrections for the FLIM analysis. To conclude, thanks to the newly developed RPEL2-R62D FRET sensor, it was possible to analyse more closely the RPEL2:R62D dissociation event that occurs under different conditions. The RPEL2-R62D FRET sensor represents a powerful tool for future research investigating of the events which influence MRTF-actin interaction for a better understanding of MRTF regulation.

6. Bibliography

Al-Hetty H, Ismaeel GL, Mohammad WT, Toama MA, Kandeel M, Saleh MM, Turki Jalil A (2022) SRF/MRTF-A and liver cirrhosis: Pathologic associations. J Dig Dis 23 (11):614-619. doi:10.1111/1751-2980.13150

An J, Naruse TK, Hinohara K, Soejima Y, Sawabe M, Nakagawa Y, Kuwahara K, Kimura A (2019) MRTF-A regulates proliferation and survival properties of pro-atherogenic macrophages. J Mol Cell Cardiol 133:26-35. doi:10.1016/j.yjmcc.2019.05.015

Bajar BT, Wang ES, Zhang S, Lin MZ, Chu J (2016) A Guide to Fluorescent Protein FRET Pairs. Sensors (Basel) 16 (9). doi:10.3390/s16091488

Berney C, Danuser G (2003) FRET or no FRET: a quantitative comparison. Biophys J 84 (6):3992-4010. doi:10.1016/S0006-3495(03)75126-1

Bourgier C, Haydont V, Milliat F, Francois A, Holler V, Lasser P, Bourhis J, Mathe D, Vozenin-Brotons MC (2005) Inhibition of Rho kinase modulates radiation induced fibrogenic phenotype in intestinal smooth muscle cells through alteration of the cytoskeleton and connective tissue growth factor expression. Gut 54 (3):336-343. doi:10.1136/gut.2004.051169

Broussard JA, Green KJ (2017) Research Techniques Made Simple: Methodology and Applications of Forster Resonance Energy Transfer (FRET) Microscopy. J Invest Dermatol 137 (11):e185-e191. doi:10.1016/j.jid.2017.09.006

Casella JF, Flanagan MD, Lin S (1981) Cytochalasin D inhibits actin polymerization and induces depolymerization of actin filaments formed during platelet shape change. Nature 293 (5830):302-305. doi:10.1038/293302a0

Chen T, He B, Tao J, He Y, Deng H, Wang X, Zheng Y (2019) Application of Forster Resonance Energy Transfer (FRET) technique to elucidate intracellular and In Vivo biofate of nanomedicines. Adv Drug Deliv Rev 143:177-205. doi:10.1016/j.addr.2019.04.009

Choi BH, Kou ZY, Colon TM, Chen CH, Chen Y, Dai W (2021) Identification of Radil as a Ras binding partner and putative activator. Journal of Biological Chemistry 296. doi:10.1016/j.jbc.2021.100314

Cory GO, Garg R, Cramer R, Ridley AJ (2002) Phosphorylation of tyrosine 291 enhances the ability of WASp to stimulate actin polymerization and filopodium formation. Wiskott-Aldrich Syndrome protein. J Biol Chem 277 (47):45115-45121. doi:10.1074/jbc.M203346200

Crider BJ, Risinger GM, Jr., Haaksma CJ, Howard EW, Tomasek JJ (2011) Myocardin-related transcription factors A and B are key regulators of TGF-beta1-induced fibroblast to

myofibroblast differentiation. J Invest Dermatol 131 (12):2378-2385. doi:10.1038/jid.2011.219

Dorn T, Kornherr J, Parrotta EI, Zawada D, Ayetey H, Santamaria G, Iop L, Mastantuono E, Sinnecker D, Goedel A, Dirschinger RJ, My I, Laue S, Bozoglu T, Baarlink C, Ziegler T, Graf E, Hinkel R, Cuda G, Kaab S, Grace AA, Grosse R, Kupatt C, Meitinger T, Smith AG, Laugwitz KL, Moretti A (2018) Interplay of cell-cell contacts and RhoA/MRTF-A signaling regulates cardiomyocyte identity. EMBO J 37 (12). doi:10.15252/embj.201798133

Eckenstaler R, Ripperger A, Hauke M, Braun H, Ergun S, Schwedhelm E, Benndorf RA (2022) Thromboxane A(2) receptor activation via G(alpha13)-RhoA/C-ROCK-LIMK2-dependent signal transduction inhibits angiogenic sprouting of human endothelial cells. Biochem Pharmacol 201:115069. doi:10.1016/j.bcp.2022.115069

Elder AD, Domin A, Schierle GSK, Lindon C, Pines J, Esposito A, Kaminski CF (2009) A quantitative protocol for dynamic measurements of protein interactions by Forster resonance energy transfer-sensitized fluorescence emission. J R Soc Interface 6:S59-S81. doi:10.1098/rsif.2008.0381.focus

Esposito A, Gralle M, Dani MA, Lange D, Wouters FS (2008) pHlameleons: a family of FRET-based protein sensors for quantitative pH imaging. Biochemistry 47 (49):13115-13126. doi:10.1021/bi8009482

Evelyn CR, Wade SM, Wang Q, Wu M, Iniguez-Lluhi JA, Merajver SD, Neubig RR (2007) CCG-1423: a small-molecule inhibitor of RhoA transcriptional signaling. Mol Cancer Ther 6 (8):2249-2260. doi:10.1158/1535-7163.MCT-06-0782

Gau D, Roy P (2018) SRF'ing and SAP'ing - the role of MRTF proteins in cell migration. J Cell Sci 131 (19). doi:10.1242/jcs.218222

Goodman SR (2008) Cytoskeleton. Med. Cell Biol., Third ed. edn., Elsevier Inc. . doi:10.1016/B978-0-12-370458-0.50008-6

Gualdrini F, Esnault C, Horswell S, Stewart A, Matthews N, Treisman R (2016) SRF Co-factors Control the Balance between Cell Proliferation and Contractility. Mol Cell 64 (6):1048-1061. doi:10.1016/j.molcel.2016.10.016

Gupta M, Sonnett M, Ryazanova L, Presler M, Wuhr M (2018) Quantitative Proteomics of Xenopus Embryos I, Sample Preparation. Methods Mol Biol 1865:175-194. doi:10.1007/978-1-4939-8784-9_13

Hauke M, Eckenstaler R, Ripperger A, Ender A, Braun H, Benndorf RA (2022) Active RhoA Exerts an Inhibitory Effect on the Homeostasis and Angiogenic Capacity of Human Endothelial Cells. J Am Heart Assoc 11 (12):e025119. doi:10.1161/JAHA.121.025119

Heemskerk N, Schimmel L, Oort C, van Rijssel J, Yin T, Ma B, van Unen J, Pitter B, Huveneers S, Goedhart J, Wu Y, Montanez E, Woodfin A, van Buul JD (2016) F-actin-rich contractile endothelial pores prevent vascular leakage during leukocyte diapedesis through local RhoA signalling. Nat Commun 7:10493. doi:10.1038/ncomms10493

Holstein I, Singh AK, Pohl F, Misiak D, Braun J, Leitner L, Huttelmaier S, Posern G (2020) Post-transcriptional regulation of MRTF-A by miRNAs during myogenic differentiation of myoblasts. Nucleic Acids Res 48 (16):8927-8942. doi:10.1093/nar/gkaa596

Ito S, Hashimoto Y, Majima R, Nakao E, Aoki H, Nishihara M, Ohno-Urabe S, Furusho A, Hirakata S, Nishida N, Hayashi M, Kuwahara K, Fukumoto Y (2020) MRTF-A promotes angiotensin II-induced inflammatory response and aortic dissection in mice. PLoS One 15 (3):e0229888. doi:10.1371/journal.pone.0229888

Johnson LA, Rodansky ES, Haak AJ, Larsen SD, Neubig RR, Higgins PD (2014) Novel Rho/MRTF/SRF inhibitors block matrix-stiffness and TGF-beta-induced fibrogenesis in human colonic myofibroblasts. Inflamm Bowel Dis 20 (1):154-165. doi:10.1097/01.MIB.0000437615.98881.31

Kircher P, Hermanns C, Nossek M, Drexler MK, Grosse R, Fischer M, Sarikas A, Penkava J, Lewis T, Prywes R, Gudermann T, Muehlich S (2015) Filamin A interacts with the coactivator MKL1 to promote the activity of the transcription factor SRF and cell migration. Sci Signal 8 (402):ra112. doi:10.1126/scisignal.aad2959

Kluge F, Weissbach J, Weber A, Stradal T, Posern G (2018) Regulation of MRTF-A by JMY via a nucleation-independent mechanism. Cell Commun Signal 16 (1):86. doi:10.1186/s12964-018-0299-x

Knoll B (2011) Serum response factor mediated gene activity in physiological and pathological processes of neuronal motility. Front Mol Neurosci 4:49. doi:10.3389/fnmol.2011.00049

Komatsu N, Aoki K, Yamada M, Yukinaga H, Fujita Y, Kamioka Y, Matsuda M (2011) Development of an optimized backbone of FRET biosensors for kinases and GTPases. Mol Biol Cell 22 (23):4647-4656. doi:10.1091/mbc.E11-01-0072

Lai X, Wang L, Witzmann FA (2013) Issues and applications in label-free quantitative mass spectrometry. Int J Proteomics 2013:756039. doi:10.1155/2013/756039

Lane J, Martin T, Weeks HP, Jiang WG (2014) Structure and role of WASP and WAVE in Rho GTPase signalling in cancer. Cancer Genomics Proteomics 11 (3):155-165

Leavesley SJ, Rich TC (2016) Overcoming limitations of FRET measurements. Cytometry A 89 (4):325-327. doi:10.1002/cyto.a.22851

Li S, Chang S, Qi X, Richardson JA, Olson EN (2006) Requirement of a myocardin-related transcription factor for development of mammary myoepithelial cells. Mol Cell Biol 26 (15):5797-5808. doi:10.1128/MCB.00211-06

Lisabeth EM, Kahl D, Gopallawa I, Haynes SE, Misek SA, Campbell PL, Dexheimer TS, Khanna D, Fox DA, Jin X, Martin BR, Larsen SD, Neubig RR (2019) Identification of Pirin as a Molecular Target of the CCG-1423/CCG-203971 Series of Antifibrotic and Antimetastatic Compounds. ACS Pharmacol Transl Sci 2 (2):92-100. doi:10.1021/acsptsci.8b00048

Liu L, He F, Yu Y, Wang Y (2020) Application of FRET Biosensors in Mechanobiology and Mechanopharmacological Screening. Front Bioeng Biotechnol 8:595497. doi:10.3389/fbioe.2020.595497

Loty S, Forest N, Boulekbache H, Sautier JM (1995) Cytochalasin D induces changes in cell shape and promotes in vitro chondrogenesis: a morphological study. Biol Cell 83 (2-3):149-161. doi:10.1016/0248-4900(96)81303-7

Mank M, Reiff DF, Heim N, Friedrich MW, Borst A, Griesbeck O (2006) A FRET-based calcium biosensor with fast signal kinetics and high fluorescence change. Biophys J 90 (5):1790-1796. doi:10.1529/biophysj.105.073536

Melcher ML, Block I, Kropf K, Singh AK, Posern G (2022) Interplay of the transcription factor MRTF-A and matrix stiffness controls mammary acinar structure and protrusion formation. Cell Commun Signal 20 (1):158. doi:10.1186/s12964-022-00977-2

Minton K (2021) Mechanosurveillance of tumour metastasis. Nat Rev Cancer 21 (6):342-343. doi:10.1038/s41568-021-00360-2

Miralles F, Posern G, Zaromytidou AI, Treisman R (2003) Actin dynamics control SRF activity by regulation of its coactivator MAL. Cell 113 (3):329-342. doi:10.1016/s0092-8674(03)00278-2

Miranda MZ, Lichner Z, Szaszi K, Kapus A (2021) MRTF: Basic Biology and Role in Kidney Disease. Int J Mol Sci 22 (11). doi:10.3390/ijms22116040

Morton WM, Ayscough KR, McLaughlin PJ (2000) Latrunculin alters the actin-monomer subunit interface to prevent polymerization. Nat Cell Biol 2 (6):376-378. doi:10.1038/35014075

Mouilleron S, Guettler S, Langer CA, Treisman R, McDonald NQ (2008) Molecular basis for G-actin binding to RPEL motifs from the serum response factor coactivator MAL. EMBO J 27 (23):3198-3208. doi:10.1038/emboj.2008.235

Mouilleron S, Langer CA, Guettler S, McDonald NQ, Treisman R (2011) Structure of a pentavalent G-actin*MRTF-A complex reveals how G-actin controls nucleocytoplasmic shuttling of a transcriptional coactivator. Sci Signal 4 (177):ra40. doi:10.1126/scisignal.2001750

Mueller S, Galliardt H, Schneider J, Barisas BG, Seidel T (2013) Quantification of Forster resonance energy transfer by monitoring sensitized emission in living plant cells. Front Plant Sci 4. doi:10.3389/fpls.2013.00413

Ngoenkam J, Paensuwan P, Wipa P, Schamel WWA, Pongcharoen S (2021) Wiskott-Aldrich Syndrome Protein: Roles in Signal Transduction in T Cells. Front Cell Dev Biol 9:674572. doi:10.3389/fcell.2021.674572

O'Rourke MB, Town SEL, Dalla PV, Bicknell F, Koh Belic N, Violi JP, Steele JR, Padula MP (2019) What is Normalization? The Strategies Employed in Top-Down and Bottom-Up Proteome Analysis Workflows. Proteomes 7 (3). doi:10.3390/proteomes7030029

Panayiotou R, Miralles F, Pawlowski R, Diring J, Flynn HR, Skehel M, Treisman R (2016) Phosphorylation acts positively and negatively to regulate MRTF-A subcellular localisation and activity. Elife 5. doi:10.7554/eLife.15460

Patel VJ, Thalassinos K, Slade SE, Connolly JB, Crombie A, Murrell JC, Scrivens JH (2009) A comparison of labeling and label-free mass spectrometry-based proteomics approaches. J Proteome Res 8 (7):3752-3759. doi:10.1021/pr900080y

Pawlowski R, Rajakyla EK, Vartiainen MK, Treisman R (2010) An actin-regulated importin alpha/beta-dependent extended bipartite NLS directs nuclear import of MRTF-A. EMBO J 29 (20):3448-3458. doi:10.1038/emboj.2010.216

Peh GS, Adnan K, George BL, Ang HP, Seah XY, Tan DT, Mehta JS (2015) The effects of Rho-associated kinase inhibitor Y-27632 on primary human corneal endothelial cells propagated using a dual media approach. Sci Rep 5:9167. doi:10.1038/srep09167

Pertz O, Hodgson L, Klemke RL, Hahn KM (2006) Spatiotemporal dynamics of RhoA activity in migrating cells. Nature 440 (7087):1069-1072. doi:10.1038/nature04665

Posern G, Miralles F, Guettler S, Treisman R (2004) Mutant actins that stabilise F-actin use distinct mechanisms to activate the SRF coactivator MAL. EMBO J 23 (20):3973-3983. doi:10.1038/sj.emboj.7600404

Posern G, Sotiropoulos A, Treisman R (2002) Mutant actins demonstrate a role for unpolymerized actin in control of transcription by serum response factor. Molecular Biology of the Cell 13 (12):4167-4178. doi:10.1091/mbc.02-05-0068

Posern G, Treisman R (2006) Actin' together: serum response factor, its cofactors and the link to signal transduction. Trends Cell Biol 16 (11):588-596. doi:10.1016/j.tcb.2006.09.008

Reed F, Larsuel ST, Mayday MY, Scanlon V, Krause DS (2021) MRTFA: A critical protein in normal and malignant hematopoiesis and beyond. J Biol Chem 296:100543. doi:10.1016/j.jbc.2021.100543

Reinhard NR, van Helden SF, Anthony EC, Yin T, Wu YI, Goedhart J, Gadella TW, Hordijk PL (2016) Spatiotemporal analysis of RhoA/B/C activation in primary human endothelial cells. Sci Rep 6:25502. doi:10.1038/srep25502

Rejmontova P, Capakova Z, Mikusova N, Marakova N, Kasparkova V, Lehocky M, Humpolicek P (2016) Adhesion, Proliferation and Migration of NIH/3T3 Cells on Modified Polyaniline Surfaces. Int J Mol Sci 17 (9). doi:10.3390/ijms17091439

Ross SH, Post A, Raaijmakers JH, Verlaan I, Gloerich M, Bos JL (2011) Ezrin is required for efficient Rap1-induced cell spreading. Journal of Cell Science 124 (11):1808-1818. doi:10.1242/jcs.079830

Savaryn JP, Toby TK, Kelleher NL (2016) A researcher's guide to mass spectrometry-based proteomics. Proteomics 16 (18):2435-2443. doi:10.1002/pmic.201600113

Schliwa M (1982) Action of cytochalasin D on cytoskeletal networks. J Cell Biol 92 (1):79-91. doi:10.1083/jcb.92.1.79

Shaposhnikov D, Kuffer C, Storchova Z, Posern G (2013) Myocardin related transcription factors are required for coordinated cell cycle progression. Cell Cycle 12 (11):1762-1772. doi:10.4161/cc.24839

Shimada H, Ochi T, Imasato A, Morizane Y, Hori M, Ozaki H, Shinjo K (2010) Gene expression profiling and functional assays of activated hepatic stellate cells suggest that myocardin has a role in activation. Liver Int 30 (1):42-54. doi:10.1111/j.1478-3231.2009.02120.x

Sidorenko E, Vartiainen MK (2019) Nucleoskeletal regulation of transcription: Actin on MRTF. Exp Biol Med 244 (15):1372-1381. doi:10.1177/1535370219854669

Sisson TH, Ajayi IO, Subbotina N, Dodi AE, Rodansky ES, Chibucos LN, Kim KK, Keshamouni VG, White ES, Zhou Y, Higgins PD, Larsen SD, Neubig RR, Horowitz JC (2015) Inhibition of myocardin-related transcription factor/serum response factor signaling decreases lung

fibrosis and promotes mesenchymal cell apoptosis. Am J Pathol 185 (4):969-986. doi:10.1016/j.ajpath.2014.12.005

Small EM (2012) The actin-MRTF-SRF gene regulatory axis and myofibroblast differentiation. J Cardiovasc Transl Res 5 (6):794-804. doi:10.1007/s12265-012-9397-0

Small EM, Thatcher JE, Sutherland LB, Kinoshita H, Gerard RD, Richardson JA, Dimaio JM, Sadek H, Kuwahara K, Olson EN (2010) Myocardin-related transcription factor-a controls myofibroblast activation and fibrosis in response to myocardial infarction. Circ Res 107 (2):294-304. doi:10.1161/CIRCRESAHA.110.223172

Smolen GA, Schott BJ, Stewart RA, Diederichs S, Muir B, Provencher HL, Look AT, Sgroi DC, Peterson RT, Haber DA (2007) A Rap GTPase interactor, RADIL, mediates migration of neural crest precursors. Gene Dev 21 (17):2131-2136. doi:10.1101/gad.1561507

Sotiropoulos A, Gineitis D, Copeland J, Treisman R (1999a) Signal-regulated activation of serum response factor is mediated by changes in actin dynamics. Cell 98 (2):159-169. doi:10.1016/S0092-8674(00)81011-9

Sotiropoulos A, Gineitis D, Copeland J, Treisman R (1999b) Signal-regulated activation of serum response factor is mediated by changes in actin dynamics. Cell 98 (2):159-169. doi:10.1016/s0092-8674(00)81011-9

Stetsenko A, Guskov A (2017) An Overview of the Top Ten Detergents Used for Membrane Protein Crystallization. Crystals 7 (7). doi:10.3390/cryst7070197

Taylor M, Treisman R, Garrett N, Mohun T (1989) Muscle-specific (CArG) and serum-responsive (SRE) promoter elements are functionally interchangeable in Xenopus embryos and mouse fibroblasts. Development 106 (1):67-78. doi:10.1242/dev.106.1.67

Timp W, Timp G (2020) Beyond mass spectrometry, the next step in proteomics. Sci Adv 6 (2). doi:10.1126/sciadv.aax8978

Tonazzini I, Van Woerden GM, Masciullo C, Mientjes EJ, Elgersma Y, Cecchini M (2019) The role of ubiquitin ligase E3A in polarized contact guidance and rescue strategies in UBE3A-deficient hippocampal neurons. Mol Autism 10 (1). doi:10.1186/s13229-019-0293-1

Trapani V, Schweigel-Rontgen M, Cittadini A, Wolf FI (2012) Intracellular magnesium detection by fluorescent indicators. Methods Enzymol 505:421-444. doi:10.1016/B978-0-12-388448-0.00030-9

Treisman R (1986) Identification of a protein-binding site that mediates transcriptional response of the c-fos gene to serum factors. Cell 46 (4):567-574. doi:10.1016/0092-8674(86)90882-2

van Nieuw Amerongen GP, van Delft S, Vermeer MA, Collard JG, van Hinsbergh VW (2000) Activation of RhoA by thrombin in endothelial hyperpermeability: role of Rho kinase and protein tyrosine kinases. Circ Res 87 (4):335-340. doi:10.1161/01.res.87.4.335

van Unen J, Reinhard NR, Yin T, Wu YI, Postma M, Gadella TW, Goedhart J (2015) Plasma membrane restricted RhoGEF activity is sufficient for RhoA-mediated actin polymerization. Sci Rep 5:14693. doi:10.1038/srep14693

Vartiainen MK, Guettler S, Larijani B, Treisman R (2007) Nuclear actin regulates dynamic subcellular localization and activity of the SRF cofactor MAL. Science 316 (5832):1749-1752. doi:10.1126/science.1141084

Velasquez LS, Sutherland LB, Liu Z, Grinnell F, Kamm KE, Schneider JW, Olson EN, Small EM (2013) Activation of MRTF-A-dependent gene expression with a small molecule promotes myofibroblast differentiation and wound healing. Proc Natl Acad Sci U S A 110 (42):16850-16855. doi:10.1073/pnas.1316764110

Wakatsuki T, Schwab B, Thompson NC, Elson EL (2001) Effects of cytochalasin D and latrunculin B on mechanical properties of cells. J Cell Sci 114 (Pt 5):1025-1036. doi:10.1242/jcs.114.5.1025

Wei K, Che N, Chen F (2007) Myocardin-related transcription factor B is required for normal mouse vascular development and smooth muscle gene expression. Dev Dynam 236 (2):416-425. doi:10.1002/dvdy.21041

Weissbach J, Schikora F, Weber A, Kessels M, Posern G (2016) Myocardin-Related Transcription Factor A Activation by Competition with WH2 Domain Proteins for Actin Binding. Mol Cell Biol 36 (10):1526-1539. doi:10.1128/MCB.01097-15

Winckler B, Schafer DA (2007) Cordon-Bleu: A new taste in actin nucleation. Cell 131 (2):236-238. doi:10.1016/j.cell.2007.10.003

Wisniewski JR, Zougman A, Nagaraj N, Mann M (2009) Universal sample preparation method for proteome analysis. Nat Methods 6 (5):359-362. doi:10.1038/nmeth.1322

Wu X, Suetsugu S, Cooper LA, Takenawa T, Guan JL (2004) Focal adhesion kinase regulation of N-WASP subcellular localization and function. J Biol Chem 279 (10):9565-9576. doi:10.1074/jbc.M310739200

Wynn TA (2008) Cellular and molecular mechanisms of fibrosis. J Pathol 214 (2):199-210. doi:10.1002/path.2277

Xing SP, Wallmeroth N, Berendzen KW, Grefen C (2016) Techniques for the Analysis of Protein-Protein Interactions in Vivo. Plant Physiol 171 (2):727-758. doi:10.1104/pp.16.00470

Ye FM, Smith PB, Wu CF, Chiu DT (2013) Ultrasensitive Detection of Proteins on Western Blots with Semiconducting Polymer Dots. Macromol Rapid Comm 34 (9):785-790. doi:10.1002/marc.201200809

Yu-Wai-Man C, Spencer-Dene B, Lee RMH, Hutchings K, Lisabeth EM, Treisman R, Bailly M, Larsen SD, Neubig RR, Khaw PT (2017) Local delivery of novel MRTF/SRF inhibitors prevents scar tissue formation in a preclinical model of fibrosis. Sci Rep 7 (1):518. doi:10.1038/s41598-017-00212-w

Zadran S, Standley S, Wong K, Otiniano E, Amighi A, Baudry M (2012) Fluorescence resonance energy transfer (FRET)-based biosensors: visualizing cellular dynamics and bioenergetics. Appl Microbiol Biotechnol 96 (4):895-902. doi:10.1007/s00253-012-4449-6

Zeidan A, Javadov S, Karmazyn M (2006) Essential role of Rho/ROCK-dependent processes and actin dynamics in mediating leptin-induced hypertrophy in rat neonatal ventricular myocytes. Cardiovasc Res 72 (1):101-111. doi:10.1016/j.cardiores.2006.06.024

7. Theses

1. MRTF-dependent transcription in fibroblasts is activated after MRTF-actin dissociation in the cytosol during stimulus.
2. During stimulation, a competition event was previously hypothesised to cause the dissociation of MRTF from actin. For identification of possible MRTF-competitor candidates during stimulation, co-immuniprecipitation-mass spectrometry experiments were established.
3. Cobll1, Radil, Samhd1 and Ube3a were identified as possible MRTF-A competitors for actin binding.
4. A new RPEL2-R62D actin FRET sensor to visualize events leading to actin-MRTF-A dissociation was created and characterized.
5. Different actin drugs, such as LatB, which stabilise MRTF-actin complex, and CytD, which induce MRTF-actin dissociation, influenced the RPEL2-R62D FRET sensor.
6. Additional inhibitors and activators of MRTF-A were functionally analysed using the FRET sensor.

Declarations

1) I declare that I have not undergone or started a doctoral procedure at any other university at any other higher education institution or that I have begun a doctorate.
2) I declare that the information I have provided is true and that I have not submitted the academic work to any other academic institution for the purpose of obtaining an academic degree at any other academic institution for the purpose of obtaining an academic degree academic degree.
3) I declare in lieu of an oath that I have written the thesis independently and without outside help without outside help. All rules of good scientific practice have been observed; no sources other than those specified by me have been used sources and aids other than those indicated by me have been used. I have not used any sources or aids other than those indicated by me, and the passages taken verbatim or in terms of content from the works used have been identified as such.

Marina Abd el Malek

Halle,

Acknowledgements

Here I would like to express my gratitude to those individuals, without whom this project would not have been possible.

First, I would like to thank Prof. Dr. Guido Posern for his generous advice and support throughout the duration of this project, and for the opportunity to work in the Zell- und Mollekularbiologie group as well as the research training group (RTG) 2467.

I would also like to thank the Promotionskolleg Medizin Halle (HaPKoM) for their support.

Special thanks go to Prof. Dr. Andrea Sinz for collaboration on the mass spectrometry experiments, and to the following members of her group: Dr. Lolita Piersimoni, Dr. Christian Ihling, Daniele Ubbiali, Alessio Di Ianni, and Alan An Jung Wei.

I am also grateful to Prof. Dr. Ralf Anton Benndorf for his collaboration with the confocal microscope. Thanks, too, go to Dr. Robert Eckenstaler for teaching me how to work with the confocal miscroscope and for all of his advice and support.

I would like to extend my sincere thanks to Dr, Anurag Singh and Dr. Igor Kovačević for suggestions and support throughout the duration of my research. I would also like to thank Karo and Anja for their support with laboratory techniques. Thanks to Marie and Laurin for their friendship, and also to Jens, Ines Block, Ines Knipping, Anna, Dora, and George.

Special thanks go to my family for their love and support, and to Jim for detailed comments. Lastly, I thank my husband, John, for his unconditional love.